UNIVERSITY OF OKLAHOMA

GRADUATE COLLEGE

KINETIC AND ISOTOPE ANALYSES DURING ABIOTIC TRANSFORMATION OF CHLORINATED HYDROCARBONS BY IRON AND SULFUR MINERALS

A DISSERTATION

SUBMITTED TO THE GRADUATE FACULTY

in partial fulfillment of the requirements of the

Degree of

DOCTOR OF PHILOSOPHY

By

XIAOMING LIANG
Norman, Oklahoma
2009

KINETIC AND ISOTOPE ANALYSES DURING ABIOTIC TRANSFORMATION OF CHLORINATED HYDROCARBONS BY IRON AND SULFUR MINERALS

A DISSERTATION APPROVED FOR THE
SCHOOL OF CIVIL ENGINEERING AND ENVIRONMENTAL SCIENCE

BY

Dr. Elizabeth C. Butler

Dr. Lee R. Krumholz

Dr. Richard P. Philp

Dr. David A. Sabatini

Dr. Tohren C. G. Kibbey

©Copyright by XIAOMING LIANG 2009
All Rights Reserved.

ACKNOWLEDGEMENTS

First, I would like to thank my advisor, Dr. Elizabeth C. Butler, for her guidance, patience and financial support through my Ph.D. study. Her profound knowledge, insightful thoughts, and serious attitude to research would benefit me for my entire life. Thank you to Dr. Krumholz, Dr. Philp, Dr. Sabatini, and Dr. Kibbey for their time and useful input in this work.

Thanks to all the Krumholz and Philp lab members for their valuable collaboration. Thanks also to those friends who so kindly helped me and made this time so much fun and memorable: Xingdong Zhu, Xuebing Yang, Bin Chen, Yiran Dong, Yao Tan, Lixia Chen, Xiaoxu Jiang, Qiong Lei, Bin Yong, James Hoggan, Jessica Whittle, Darcy Lutes, and Chris Cope.

Thank Tomasz Kuder and Janel McMahon from the School of Geology and Geophysics at OU for help with isotope analyses. I am also grateful to Scott Christenson, Ernie Smith, and Jason Masoner from the U.S. Geological Survey in Oklahoma City, John Wilson group from USEPA, Ada, OK, as well as Tohren Kibbey, Xingdong Zhu, and Hongbo Shao from OU CEES for their assistance in sampling.

I appreciate the support by the U.S. Department of Defense, through the Strategic Environmental Research and Development Program (SERDP). I also thank the Graduate College at the University of Oklahoma for a Robberson Research Grant.

Special thanks are extended to my parents, my sister, and my brother-in-law for their encouragement and understanding. Without their consistent support, it would be impossible for me to achieve my Ph.D in the U.S. Finally, I thank my soul mate Jiayi for her love and sacrifice throughout this period of our lives.

TABLE OF CONTENTS

LIST OF TABLES

APPENDICES

LIST OF FIGURES

APPENDICES

ABSTRACT

Abiotic reductive dechlorination of tetrachloroethylene (PCE), trichloroethylene (TCE), and carbon tetrachloride (CT) by naturally occurring minerals was investigated in this study. The kinetics and in some cases stable carbon isotope fractionation associated with abiotic reductive dechlorination of PCE and TCE by model Fe(II)-bearing minerals present in anaerobic soils were measured. The minerals studied were FeS, chloride green rust (GR-Cl), sulfate green rust (GR-SO_4), pyrite, magnetite, and adsorbed Fe(II) or FeS formed at the surface of goethite by treatment with dissolved Fe(II) or S(-II). Significant carbon isotope fractionation was observed during PCE dechlorination by FeS and TCE transformation by FeS, GR-Cl and pyrite. Bulk enrichment factors (ε_{bulk}) (in ‰) for PCE dechlorination by FeS were -30.2 ± 4.3 ‰ (pH 7), -29.54 ± 0.83 ‰ (pH 8), and -24.6 ± 1.1 ‰ (pH 9). ε_{bulk} values for TCE transformation were -33.4 ± 1.5 ‰ for FeS at pH 8, -27.9 ± 1.3 ‰ for FeS at pH 9, -23.0 ± 1.8 ‰ for GR-Cl at pH 8, and -21.7 ± 1.0 ‰ for pyrite at pH 8. ε_{bulk} values for abiotic PCE and TCE transformation are generally more negative than those for microbial dechlorination of PCE and TCE. For monitored natural attenuation, very large negative ε_{bulk} values for abiotic PCE and TCE transformation in this research can provide one line of evidence that abiotic degradation of PCE and TCE takes place at field sites. Other lines of evidence (e.g., identification and isotope analysis of reaction products) are also needed in order to make the better assessment of contaminant fate.

Abiotic reductive dechlorination of PCE and TCE was dominant under the iron-reducing condition at pH 8.2 for Duck Pond microcosm and for Landfill microcosm, which may be due to the inactivity of dechlorinating bacteria. Comparable abiotic and

biotic transformation was observed in five microcosms, including Duck Pond microcosm under methanogenic condition at pH 8.2, Landfill microcosms at pH 8.2 under iron-reducing and methanogenic conditions, and Landfill microcosms under sulfate-reducing condition at both pH 7.2 and 8.2. Four of these microcosms were conducted at pH 8.2 while only one microcosm was set up at pH 7.2. This provides additional evidence that at least in some cases high pH (8.2) may inhibit the growth of dechlorinating bacteria. In addition, no abiotic reaction products were detected in the three microcosms (Duck Pond and Landfill microcosms under methanogenic condition at pH 7.2, and unamended Landfill microcosms at pH 7.2), which typically had lower concentrations of Fe(II) or S(-II) species than did microcosms preincubated under iron or sulfate reducing conditions.

Widespread natural organic matter (NOM) may significantly influence the fate of contaminants in subsurface environment. In this study, a series of model NOM compounds were selected that have functional groups common to actual NOM in order to study NOM adsorption and its effects on the degradation of carbon tetrachloride by GR-Cl. The amount of NOM adsorbed on the mineral surface were found to depend on the number and positions of functional groups present in NOM. Strong adsorption was found for NOM with multiple carboxylic or phenolic groups on ortho- positions. Adsorption of NOM on GR-Cl was successfully modeled by using Langmuir equation, and adsorption equilibrium constants (*K*) and maximum adsorption capacity values ($q_{max\text{-}Langmuir}$) were derived from Langmuir isotherms. *K* values varied from 218 ± 127 L/mmole to 0.58 ± 0.13 L/mmole, suggesting that different affinity of GR-Cl for selected 10 NOM model compounds. We calculated the theoretical maximum amounts of NOM compounds ($q_{max\text{-}BET}$) that can be adsorbed on the external surface of GR-Cl using BET surface area of the

mineral and the occupation area of NOM anions. Comparisons between $q_{max\text{-}Langmuir}$ and $q_{max\text{-}BET}$ values for selected NOM compounds suggest the possibility that both ligand-exchange and anion intercalation are responsible for the adsorption of NOM on GR-Cl. Effects of NOM adsorption on the reduction of CT are compound-dependent. Although most NOM compounds significantly slowed CT degradation by GR-Cl due to competitive adsorption on reactive sites, caffeic acid greatly increased the CT reduction rate, which may be due to the generation of new Fe (II) sites associated with GR-Cl surface. High chloroform yields (in %) (> 70%) were observed for CT reduction by GR-Cl (both alone and with the addition of NOM).

Key words: reductive dechlorination, abiotic degradation, natural attenuation, stable carbon isotope fractionation, tetrachloroethylene, trichloroethylene, carbon tetrachloride, natural organic matter.

CHAPTER 1

Introduction

A number of remediation technologies have been developed for the treatment of chlorinated contaminants in groundwater and soil. However, conventional clean-up methods, such as pump-and-treat systems, often fail to meet remediation goals (NRC, 1994). Since the early 1990s, natural attenuation has drawn considerable interest due to its effectiveness and low cost on the removal of groundwater contaminants (Wiedemeier et al., 1999; Ferrey and Norris, 2003; Alvarez and Illmann, 2006). In order to better apply natural attenuation as a promising remediation approach, the natural degradation processes that determine the fate of contaminants need to be understood and quantified. This dissertation focuses on the role of naturally occurring minerals in the abiotic natural degradation of chlorinated hydrocarbons. This chapter is organized into four sections: (1) natural attenuation of chlorinated hydrocarbons; (2) significance of natural organic matter; (3) stable carbon isotope analysis; (4) overview of this work.

1.1. Natural Attenuation of Chlorinated Hydrocarbons

Chlorinated hydrocarbons have been produced, and used as solvents, degreaser, and dry-cleaning agents over the past several decades (Doherty, 2000; Hunkeler et al, 2002; Moran et al., 2007). They are frequently detected in groundwater due to accidental spills and improper disposal or storage (Vogel et al., 1987; Pankow and Cherry, 1996). Tetrachloroethylene (PCE) and trichloroethylene (TCE) are two of the top three groundwater pollutants that are most commonly found at contaminated sites (Masters, 1998). Although the industrial application of carbon

tetrachloride (CT) was completely banned in 2000, CT is still often detected at hazardous waste sites (Zou et al., 2000) and on the Volatile Target Compound list (U.S. EPA, 2008) due to its massive production in history (Doherty, 2000). In addition, all three chlorinated hydrocarbons are potential carcinogens (Rechnagel et al., 1989; Chu et al., 2004) and the maximum contaminant level (MCL) in drinking water is 5 μg/L for all three chemicals. Since PCE, TCE, and CT are immiscible with water, they are often present as non-aqueous-phase liquids (NAPLs). In addition, they tend to sink to the bottom of the aquifer due to their higher specific gravities relative to water (Alvarez and Illmann, 2006). Site remediation of these contaminants therefore can be a real challenge due to their persistent nature and relative inaccessibility.

Pump-and-treat, the most frequently applied groundwater remediation tool, has difficulties in cleanup of chlorinated hydrocarbons due to the following factors (Wiedemeier et al., 1999): (1) movement of contaminants to inaccessible regions (e.g., clays or small pores in aggregates; (2) sorption of contaminants to soil and sediments; (3) presence of NAPLs, a continuing source of contaminants in groundwater. Performance limitations of traditional remediation technologies motivated the consideration of natural attenuation as a potential alternative for groundwater remediation. Natural attenuation can occur via the following processes: sorption, dispersion, dilution, volatilization, chemical transformation and biodegradation (U.S.EPA, 1997). However, only chemical transformation and biodegradation can result in the destruction of the contaminants.

Under anaerobic conditions, CT, PCE, and TCE can undergo reductive dechlorination leading to less chlorinated compounds through two major pathways: (1) hydrogenolysis, or replacement of a chlorine by a hydrogen in sequence to produce

chloroform (CF), dichloromethane, chloromethane, and methane for CT, *cis*-DCE, VC and ethylene for PCE and TCE; (2) dichloroelimination that forms carbon monoxide and formate with dichlorocarbene as an intermediate for CT degradation, and acetylene via the short-lived intermediate chloroacetylene for PCE and TCE transformation (Criddle and McCarty, 1991; Kriegman-King and Reinhard, 1992; Roberts et al., 1996; Butler and Hayes, 1999, 2000; Pecher et al., 2002; Elsner et al., 2004; Lee and Batchelor, 2002a, 2002b; Shao and Butler, 2007).

CT can be microbially degraded under denitrifying conditions (Criddle et al., 1990; Bouwer and McCarty, 1983; Skeen et al., 1995), sulfate reducing conditions (Egli and Leisinger, 1988; Bouwer and Wright, 1988; Cobb and Bouwer, 1991), and methanogenic conditions (Van Eekert et al., 1998; Krone et al., 1989; Novak et al., 1998). Both hydrogenolysis and dichloroelimination pathways can take place for microbial degradation of CT, and reaction products include CF, dichloromethane, chloromethane, carbon dioxide, carbon monoxide, and methane (Zou et al., 2000). In contrast, sequential hydrogenolysis is the only pathway observed for the biodegradation of PCE and TCE under sulfate-reducing condition (Bagley and Gossett, 1990), iron-reducing condition (Bjerg et al., 1999; Boopathy and Peters, 2001), and methanogenic conditions (Bjerg et al., 1999). Microbial degradation of PCE and TCE often results in incomplete dechlorination with some toxic intermediates, which are more toxic than their parent compounds. For example, VC is a common intermediate during microbial reductive dechlorination of PCE and TCE, and the MCL of VC is 2μg/L (Middeldorp et al., 1999; Arnold and Roberts, 2000).

Chlorinated hydrocarbons can be effectively degraded via both hydrogenolysis and dichloroelimination pathways by some naturally occurring iron and sulfide minerals including pyrite (Lee and Batchelor, 2002a; Weerasooriya and Dharmasena,

2001; Carlson et al., 2003), FeS (Butler and Hayes, 1998, 1999, 2000; Liu et al., 2003), magnetite (Lee and Batchelor, 2002a), and green rusts (Lee and Batchelor, 2002b; Maithreepala and Doong, 2005). Mineral mediated dechlorination of PCE and TCE leads mainly to accumulation of an environmental benign product, acetylene (Butler and Hayes, 2000; Arnold and Roberts, 2000). Iron minerals are abundant in subsurface environments since the average iron content of soils is approximately 3.8% (Lindsay, 1979). Natural occurrence of Fe(II)- bearing minerals involves a number of biogeochemical reactions. Briefly, considerable amount of Fe(II) are produced through microbial reduction of iron oxides by iron-reducing bacteria (Lovely et al., 1991), and biogenic Fe (II) species can be adsorbed on the surface of iron oxides, released to the aqueous solution, or form mixed Fe (II-III) minerals such as magnetite (McCormick et al., 2002, McCormick and Adriaens, 2004) and green rust (Fredrickson, et al., 1998; Parmar et al., 2001; Glasauer et al., 2002; Ona-Nguema et al., 2002; Berthelin et al., 2006, O'Loughlin et al., 2007). In addition, bisulfide (HS^-) resulting from microbial reduction of sulfate can react with either dissolved or adsorbed Fe(II) and form FeS (Devlin and Muller, 1999; Neal et al., 2001; Hofstetter et al., 2003), which can be further oxidized to more thermodynamically stable minerals like pyrite (FeS_2) and greigite (Fe_3S_4) (Berner, 1967; Richard, 1969; Luther, 1991; Wang and Morse, 1996; Benning, 2000).

1.2. Significance of Natural Organic Matter

Natural organic matter (NOM) is organic matter originating from decaying plants and animals as well as living organisms. NOM is widespread in groundwater and soil environments (Larson and Weber, 1994; Kappler and Haderlein, 2003). The dominant fraction of NOM is referred to as humic substances. Chemical oxidation

methods, nuclear magnetic resonance spectroscopy, and pyrolysis have been used to explore the molecular structure of NOM, and a basic unit of NOM is an aromatic ring substituted with COOH and OH functional groups as well as various aliphatic groups attached to the ring, as shown in Figure 1.1 (Hayes and Swift, 1978; Parsons, 1989; Simpson, 2001; Chefetz et al., 2002; Page et al., 2002).

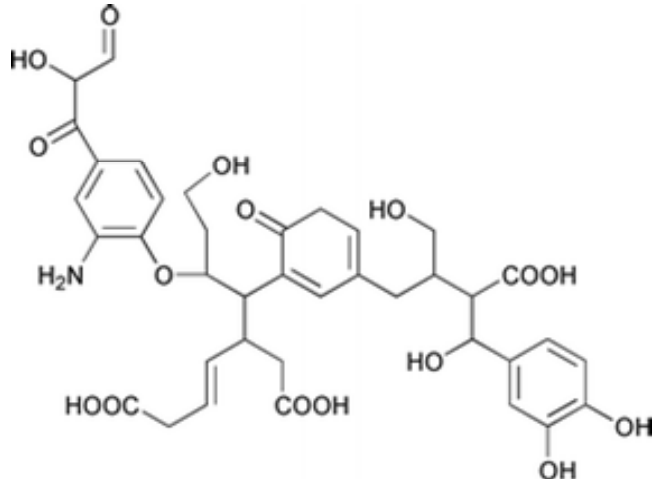

Figure 1.1. Building block of NOM. Figure copied from Steelink (1985) and von Wandruszka (2000).

NOM can adsorb on the surface of soil and clay minerals (Tipping, 1981; Davis, 1982; McKnight et al., 1992; Gu et al., 1995; Kappler and Haderlein, 2003; Marconetto et al., 2005). The type of functional groups and the steric arrangement of these groups may contribute to the adsorption behavior of NOM on the surface of iron oxides (Gu et al., 1995). Benjamin et al. (1993) observed that NOM with higher carboxylic acid content was preferentially adsorbed on the surface of oxides over the one with lower carboxylic acid content. By contrast, Davis (1982) reported that phenolic groups greatly contributed to the formation of a surface complex between NOM and hydroxide surface, whereas carboxylic groups were not related to the adsorption.

Sorbed NOM can significantly affect the fate and transport of contaminants. On the one hand, NOM can serve as an electron transfer mediator to catalyze the reduction of contaminants (Schwarzenbach et al., 1990; Dunnivant et al.., 1992; Curtis and Reinhard, 1994; Perlinger et al., 1996; Kim and Picardal, 1999; Fredrickson et al., 2000; Lloyd et al., 2000; Assaf-Anid and Lin, 2002; Kappler and Haderlein, 2003). Schwarzenbach et al. (1990) reported that NOM enhanced the reduction of CT by FeS. Similarly, increased reaction rates of hexachloroethane and CT were observed in the aqueous solution of Fe^{2+} and HS^- with the addition of NOM as an electron shuttle (Curtis and Reinhard, 1994; Perlinger et al., 1996). The ability of NOM to serve as an electron transfer mediator is mainly attributed to quinone moieties (Curtis and Reinhard, 1994; Perlinger et al., 1998). On the other hand, the adsorbed NOM can block surface reactive sites where the reduction of contaminants takes place (Tratnyek et al., 2001; Marconetto et al., 2005). Tratnyek et al. (2001) observed that the reduction of CT and TCE by zero-valent iron was inhibited in the presence of NOM. The degradation rate of TCE decreased significantly in the presence of NOM because competitive adsorption existed between TCE and NOM on the surface of granular iron (Marconetto et al., 2005). In addition, NOM can enhance the sorption of contaminants on the surface of minerals (Burris and Antworth, 1992; Murphy et al., 1990; Sheng et al., 1996). For example, increasing quantities of sorbed humic substances on hematite and kaolinite increased the sorption of anthracene, dibenzothiophene, and carbazole (Murphy et al., 1990).

1.3. Stable Carbon Isotope Analysis

Application of natural attenuation needs to understand the mechanism responsible for the loss of contaminant (Bekins et al., 2001). A traditional method for

monitoring natural attenuation is measurement of contaminant concentrations along with a depletion of electron acceptors (Lu et al., 1999; Wiedemeier et al., 1999). However, the disappearance of groundwater contaminants can be caused by several processes such as adsorption, dispersion, dilution, chemical transformation and biodegradation. Compared to other processes, chemical transformation and biodegradation are the only ones that can degrade contaminants to other products. Since carbon isotope fractionation is primarily caused by abiotic and microbial transformation reactions, and not by physical transport processes such as dilution, evaporation, and adsorption (Beneteau et al., 1999; Poulson and Drever, 1999; Slater et al., 1999, 2000; Hunkeler et al., 2001), stable carbon isotope analysis has become a promising alternative to identify and even quantify *in-situ* degradation of chlorinated hydrocarbons (Dayan et al., 1999; Hunkeler et al., 1999, 2002; Sherwood Lollar et al., 1999; Bloom et al., 2000; Slater et al., 2001, 2002, 2003; Barth et al., 2002; Brungard et al., 2003; Kirtland et al., 2003; Schüth et al., 2003; Vieth et al., 2003; Chu et al., 2004; Hirschorn et al., 2004; Meckenstock et al., 2004; VanStone et al., 2004; Zwank, 2005; Chartrand et al., 2005; Elsner et al., 2005, 2007, 2008; Nijenhuis et al., 2005; VanStone et al., 2008).

In natural environments, carbon has two stable isotopes ^{12}C and ^{13}C with the relative natural abundances of approximately 98.89% and 1.11%, respectively (Hoefs, 1997). The carbon isotope ratio ($^{13}C/\ ^{12}C$) of a given compound is determined by gas chromatography isotope ratio mass spectrometry (GCIRMS), normalized to an external standard, and expressed as $\delta^{13}C$ (Equation 1):

$$\delta^{13}C = \frac{\left(\frac{^{13}C}{^{12}C}\right)_{sample} - \left(\frac{^{13}C}{^{12}C}\right)_{std}}{\left(\frac{^{13}C}{^{12}C}\right)_{std}} \times 1{,}000‰ \qquad (1.1)$$

Vienna Peedee Belemnite is commonly used as an international standard for carbon isotope ratio calculation (Schmidt et al., 2004). Because the reaction rate of bonds containing ^{12}C is generally greater than that of bonds containing ^{13}C, the remaining parent compound would be enriched with ^{13}C during reaction process. If the rate limiting step involves the bond cleavage, strong isotope fractionation would be observed. On the other hand, if reaction steps such as transport to reactive sites and adsorption to reactive surfaces are rate-limiting in the overall process, isotope fractionation may hardly be manifested. The extent of isotope fractionation can be described by the bulk enrichment factor, ε_{bulk}, derived from the Rayleigh model (Equation 2) (Mariotti et al., 1981):

$$R_p = R_{p,o} f^{\left(\frac{\varepsilon_{bulk}}{1000}\right)} \qquad (1.2)$$

where R_p is the isotope ratio of the parent compound at any time, $R_{p,0}$ is its isotopic ratio at time zero, f is the fraction of parent compound remaining at a given time (i.e., C/C_0) (measured by gas chromatography), and ε_{bulk} is the bulk enrichment factor. ε_{bulk} values can be obtained by nonlinear regression using experimentally measured values of $\delta^{13}C$ and f.

Numerous ε_{bulk} values have been reported for the transformation of chlorinated hydrocarbons at a variety of experimental conditions. Substantial changes in ε_{bulk} values may indicate that different reaction mechanisms could be involved during dechlorination reactions. For example, ε_{bulk} values for microbial reductive dechlorination of PCE and TCE are generally smaller in magnitude than those for abiotic reductants like zero-valent iron, FeS, pyrite, and green rusts (Hunkeler et al., 1999; Sherwood Lollar et al., 1999; VanStone et al., 2004; Slater et al., 2003; Schüth et al., 2003; Zwank, 2004; Elsner et al., 2008). Microbial enzyme-catalyzed reactions

involve a sequence of steps below (Hunkeler and Aravena, 2000; Zwank, 2004; Nijenhuis et al., 2005):

$$S_{out} \underset{(1)}{\rightleftharpoons} S_{in} + E \underset{(2)}{\rightleftharpoons} E{\cdot}S_{in} \xrightarrow[(3)]{} E{\cdot}P_{in} \underset{(4)}{\rightleftharpoons} E + P_{in} \underset{(5)}{\rightleftharpoons} P_{out} \qquad (1.3)$$

where the numbers refer to: (1) transport of the substrate (S) from outside (S_{out}) to inside (S_{in}) the cell; (2) formation of the enzyme (E)-substrate complex; (3) bond cleavage and formation of enzyme-product (P) complex; (4) dissociation of enzyme-product complex; and (5) transport of the product from inside (P_{in}) to outside (P_{out}) the cell. Similar schemes involving mass transport of solutes to a mineral surface (step 1), surface complex formation (step 2), electron transfer (step 3), surface complex dissociation (step 4), and mass transport of solutes away from a mineral surface (step 5) have also been proposed for abiotic redox reactions (Stone, 1986); thus Equation 1.3 could apply to abiotic reactions as well. Step 3 is the only step in either scheme involving bond cleavage and consequently only step 3 can lead to isotope fractionation (Nijenhuis et al., 2005). Step 3 could, however consist of a series of elementary reaction steps related to bond cleavage, some of which, e.g., reduction of a reactive metal center in a dehalogenase enzyme, do not involve C-Cl cleavage. If such a sub-step were rate limiting, then no isotope fractionation would be observed. In addition, if steps 1, 2, 4, or 5 were rate limiting, little or no isotope fractionation would occur. Nijenhuis et al. (2005) observed an increase in isotope fractionation with a decrease in cell integrity during reductive dechlorination of PCE by *Sulfurospirillum multivorans* and *Desulfitobacterium sp*. Strain PCE-S, which suggests that transport of PCE into the cell (e.g., step 1 in equation 1.3) is the rate limiting step in dechlorination by these bacteria.

1.4. Overview of This Work

Previous studies have examined both degradation kinetics and carbon isotope fractionation during abiotic reductive dechlorination of PCE, TCE, and CT by zero-valent iron metal (Dayan et al., 1999; Slater et al., 2002; Schüth et al., 2003; VanStone et al., 2004; Elsner et al., 2008), Zn (0) (VanStone et al., 2008); Vitamin B_{12}(Slater et al., 2003) , FeS (Zwank, 2004, 2005), and surface associated Fe (II) (Elsner et al., 2004). Little information, however, exists on (1) carbon isotope fractionation during abiotic transformation of PCE and TCE by Fe(II)-bearing minerals; (2) assessment of simultaneous abiotic and biotic degradation of PCE and TCE in well-defined microcosms. In addition, to our knowledge, no papers study the effects of NOM on CT degradation by green rust. This research gap also needs to be filled since NOM may influence the degradation rate of CT and thus affect the contribution of mineral mediated dechlorination to natural attenuation of CT at field sites. The overall objective of this research was to investigate degradation kinetics and carbon isotope fractionation during abiotic and microbial reductive dechlorination of CT, PCE, and TCE by iron and sulfide minerals. Specific research objectives were: (1) to evaluate whether stable carbon isotope analysis can be used to distinguish between abiotic and biotic reductive dechlorination of PCE and TCE; (2) to quantify the relative contributions of abiotic and biotic processes on reductive dechlorination of PCE and TCE in anaerobic microcosms; (3) to examine the effects of NOM adsorption on CT degradation rate and production distribution by green rust. Our research findings could facilitate the application of stable isotope analysis to monitor natural attenuation of PCE and TCE, and provide the more accurate assessment of the fate of CT at contaminated sites.

This dissertation consists of three main chapters. In Chapter 2, kinetic and isotope analyses were performed during abiotic transformation of PCE and TCE by

model Fe(II)-bearing minerals. Reaction rate constants were measured, and ε_{bulk} values were determined and compared to those associated with microbial degradation. Chapter 3 addresses the relative importance of abiotic and microbial reductive dechlorination in anaerobic microcosms and geochemical conditions which are in favor of abiotic degradation. Chapter 4 focuses on the effects of NOM on the degradation of CT by green rust. Model NOM compounds were selected to study the adsorption behavior on the mineral surface, and degradation rates were measured for NOM-amended CT degradation by green rust.

In the end, our research findings and conclusions are summarized in Chapter 5. Potential applications of this work and directions of future research are also discussed.

CHAPTER 2*

Kinetic and Isotope Analyses of Tetrachloroethylene and Trichloroethylene Degradation by Model Fe(II)-Bearing Minerals

2.1. Introduction

There is growing interest in remediation technologies that utilize abiotic minerals for reductive transformation of ground water contaminants such as tetrachloroethylene (PCE) and trichloroethylene (TCE) (Everett et al., 2006; Shen and Wilson, 2007). One advantage of mineral over microbially mediated transformation of PCE and TCE is generation of acetylene and/or ethylene as the primary reaction products (Brown et al., 2006), rather than lesser chlorinated ethenes that are typical of microbial transformation (Haggblom and Bossert, 2003). Many current remediation technologies involve reactive minerals; for example permeable reactive barriers that contain plant derived mulch generate FeS and FeS_2 in a process that begins with microbial sulfate reduction (Shen and Wilson, 2007; He et al. 2008). In addition, the surface of zero valent iron used in permeable reactive barriers is oxidized to minerals such as green rusts (Refait et al., 1998) that contribute to contaminant dechlorination. Many reactive minerals also occur naturally and can contribute to the natural

---

* This chapter consists of half of paper by Liang et al. (2007) that was related with abiotic degradation and isotope analyses of PCE and TCE, and the entire paper by Liang et al. (2009). Half of the first paper was reproduced with permission from "Environmental Science & Technology 41, Liang, X.; Dong, Y.; Kuder, T.; Krumholz, L.R.; Philp, R.P.; Butler, E.C. Distinguishing abiotic and biotic transformation of tetrachloroethylene and trichloroethylene by stable carbon isotope fractionation, 7094-7100, Copyright (2007) American Chemical Society". The entire second paper was reprinted from Chemosphere, 75, Liang. X.; Philp, R.P.; Butler, E.C. Kinetic and isotope analysis of tetrachloroethylene and trichloroethylene degradation by model Fe(II)-bearing minerals, 63-69, Copyright (2009), with permission from Elsevier.

attenuation of ground water contaminants. For example, green rusts, pyrite, and magnetite have all been shown to degrade PCE and TCE (Sivavec and Horney, 1997; Weerasooriya and Dharmasena, 2001; Lee and Batchelor, 2002a,2000b; Maithreepala and Doong, 2005). Goethite, the most common iron oxide in soil and sediments (Rickard, 1974), reacts with dissolved Fe (II) to form surface associated Fe(II) that has been shown to degrade carbon tetrachloride and hexachloroethane (Elsner et al., 2004; Shao and Butler, 2007). Reaction of goethite with S(-II) produced by sulfate reducing bacteria results in Fe(III) reductive dissolution followed by precipitation of FeS (Pyzik and Sommer, 1981) that is capable of degrading carbon tetrachloride (Shao and Butler, 2007). To effectively design and monitor remediation processes involving reactive minerals (i.e., to determine the residence time and/or required mass of reagents) we need accurate data on the reactivity of different minerals with contaminants such as PCE and TCE.

Compound specific isotope analysis (CSIA) for carbon is a new tool to monitor in situ remediation technologies, and is reviewed in detail elsewhere (Elsner et al., 2005). Because chemical bonds containing ^{12}C are broken more easily than those containing the stable isotope ^{13}C, reactions in which bond cleavage is the rate limiting step will tend to result in enrichment of the unreacted parent compound with ^{13}C. The magnitude of this isotope fractionation can be described by the bulk enrichment factor, ε_{bulk} (Elsner et al., 2005). With isotope data, one can use the Rayleigh equation (Mariotti et al., 1981) to estimate the amount of parent compound (e.g., PCE or TCE) degraded (Elsner et al., 2005). Previous studies have shown that ε_{bulk} values for PCE or TCE transformation by different abiotic reductants vary significantly (Slater et al., 2002; Zwank, 2004). In order to accurately use isotope analysis to estimate the extent of abiotic degradation, it is critical to know accurate

ε_{bulk} values for different mineral that can react with PCE or TCE.

The first objective of this research was to measure ε_{bulk} values for transformation of PCE and TCE by Fe(II) minerals that could be used in subsurface remediation technologies and that have been shown to transform chlorinated aliphatic pollutants. To do this, we needed to measure concentration of PCE or TCE versus time in the presence of these minerals. Our second objective was to use this kinetic data to identify mineral species with the greatest reactivity toward PCE and TCE to aid in choosing remediation technologies. To meet our objectives, a series of batch experiments were carried out with the following minerals: FeS, chloride green rust (GR-Cl), sulfate green rust (GR-SO_4), pyrite, magnetite, and Fe(II) or S(-II) treated goethite.

2.2. Materials and Methods

2.2.1. Chemicals

The following chemicals were from Sigma-Aldrich (St. Louis, MO): sodium sulfide nonahydrate, sodium acetate, $FeCl_2 \cdot 4H_2O$ (99%), PCE (99%), TCE (99.5%), *cis* 1,2-dichlorethylene (*cis*-DCE), and N-(2-hydroxyethyl)-piperazine-N'-3-propanesulfonic acid (HEPES). Methanol, acetaldehyde, and sodium hydroxide were from Fisher Scientific (Pittsburgh, PA). Ethane (1018 ppm in N_2), ethylene (1026 ppm in N_2), acetylene (1001 ppm in N_2), and vinyl chloride (VC) (1019 ppm in N_2) were from Scott Specialty Gases (Houston, TX). Ethanol was from AAPER Alcohol and Chemical Co. (Shelbyville, KY). All aqueous solutions were prepared with Nanopure water (18.0 MΩ cm resistivity, Barnstead Ultrapure Water System, IA).

2.2.2. Preparation and Characterization of Minerals

FeS was synthesized using the method described by Rickard (1969). Pyrite from Zacatecas, Mexico was purchased from Ward's (Rochester, NY) and processed for 30 minutes in a Shatterbox Laboratory Mill (Model 8500, Spex Industries Inc., Metuchen, NJ), then immediately transferred to an anaerobic chamber with an atmosphere of approximately 96% N_2/4% H_2 and a catalytic O_2 removal system (Coy Products, Grass Lake, MI). Crushed pyrite was then washed with 1 M N_2-sparged HCl and air-dried in the anaerobic chamber. GR-Cl was synthesized by partial oxidation of ferrous hydroxide according to Refait et al. (1998) except that 1 M NaOH and 0.7 M $FeCl_2$ were used for synthesis of the ferrous hydroxide. The resulting blue-green precipitate was freeze-dried with a custom vacuum valve to exclude oxygen. GR-SO_4 was synthesized by the method of O'Loughlin et al. (2003). Magnetite was prepared using the method of Kang et al. (1996). Goethite was prepared as described in Atkinson et al. (1967).

All iron minerals were characterized by X-ray diffraction (XRD) (Rigaku DMAX X-ray Diffractometer) after freeze-drying. To prevent oxidation during XRD analysis, GR-Cl and GR-SO_4 samples were prepared in the anaerobic chamber by mixing them with petroleum jelly. Other mineral samples were stable with respect to oxidation during the period of XRD analysis. The peak patterns of mineral samples were consistent with those in the Powder Diffraction File (PDF) (Joint Committee on Powder Diffraction Standards (JCPDS), 1990). All minerals were poorly crystalline. Figure A1-A5 in Appendix A shows XRD patterns for all the minerals prepared in this work. The specific surface areas of FeS, GR-Cl, GR-SO_4, pyrite, magnetite, and goethite were (in $m^2\ g^{-1}$) 2.0, 21, 3.7, 7.5, 90, and 74, respectively, determined by BET surface analysis (Autosorb-1, Quantachrome Instruments, Boynton Beach, FL).

2.2.3. Experimental Procedures

Batch kinetic experiments were conducted at pH 8 (HEPES, 50 mM) in 5 mL flame sealed glass ampules. For FeS, batch experiments were also performed at pH 7 (HEPES, 50 mM) and 9 (CHES, 50 mM) in order to study the effects of pH on kinetics and isotope fractionation of PCE and TCE. In each ampule, the aqueous phase volume was 6.5 mL and the gas phase volume was approximately 1.25 mL. The ionic strength in all experiments was adjusted to 0.06 M by adding NaCl. Mineral mass loadings were (in g L^{-1}): FeS: 10; GR-Cl: 10; GR-SO_4: 25; pyrite: 77; magnetite: 20; and goethite: 4. Surface area loadings are reported in Tables 2.1 and 2.2. High surface area loadings for pyrite and magnetite (Tables 2.1 and 2.2) were chosen based on previous studies that reported slow transformation of PCE and TCE by these minerals (Lee and Batchelor, 2002a). Experiments with Fe(II)- or S(-II)-treated goethite used 4 mM $FeCl_2$ or 1 mM Na_2S, which were concentrations similar to previous experiments (Shao and Butler 2007) in which rapid transformation of carbon tetrachloride was observed. Assuming a site density of 2.3 sites per nm^2 (Davis and Kent, 1990), we estimated that the surface site concentration of a 4 g L^{-1} goethite slurry was approximately 1 mM. Thus, the added concentrations of $FeCl_2$ and Na_2S were in theory sufficient to react with available surface Fe(III) atoms in experiments with Fe(II)- and S(-II)-treated goethite. For TCE transformation by pyrite, we conducted a separate batch experiment at a significantly higher initial concentration of TCE (approximately 7.5 mM) in order to quantify additional reaction products. For this experiment, the mass loading of pyrite was 400 g/L and the surface area loading was 3000 m^2/L (Table 2.2).

Ampules were prepared in an anaerobic chamber containing approximately 96% N_2 and 4% H_2, with a catalytic O_2 removal system (Coy Products, Grass Lake,

MI). After preparation, ampules were temporarily covered with polyvinylidene chloride film (Saran^{TM} Wrap) that was secured with a short piece of plastic tubing (Barbash and Reinhard, 1989), then taken out of the chamber and spiked with a PCE or TCE stock solution prepared in N_2-sparged methanol to obtain an initial concentration of approximately 30 μM PCE or TCE, except for experiments with magnetite, where the initial concentration was approximately 15 μM in order to increase the molar ratio of reactive surface sites to PCE and TCE. Ampules were then immediately sealed using a methane/oxygen flame while kept anaerobic with the Saran^{TM} Wrap cover, and placed in a constant temperature chamber at 25 ^{o}C in the dark on a rocking platform shaker (Labquake, Cole Parmer Instrument Company). At regular intervals, ampules were centrifuged, broken open, and sampled.

2.2.4. Analytical Methods

For PCE and TCE analysis in abiotic experiments, a 250 μL aliquot of the supernatant was added to 750 μL isooctane in a 2 mL autosampler vial and 1 μL of the isooctane phase analyzed using a Shimadzu GC-17A gas chromatograph (GC) with an Agilent J&W DB-624 capillary column (30 m × 0.53 mm × 3 μm) and electron capture detector (ECD). The injector temperature was 250 °C and the detector temperature was 275 °C. The oven temperature was initially 70 °C, immediately ramped from 70 °C to 90 °C at 5 °C/min, isothermal at 90 °C for 2 min, ramped to 110 °C at 10 °C/min, isothermal at 110 °C for 1 min, and ramped to 140 °C at 15 °C/min. External calibration standards for GC/ECD analysis were prepared in isooctane. Relative standard deviations for duplicate injections using this method were typically less than 1 %. Each GC vial was analyzed in duplicate and the peak areas averaged. Relative standard deviations for PCE and TCE between duplicate

ampules (measured for selected samples only) were typically less than 1%, which was considered acceptable.

For analysis of *cis*-DCE, VC, and non-chlorinated transformation products (acetylene, ethylene, and ethane) in abiotic experiments, two-2 mL aliquots of supernatant from each ampule were transferred to separate 22 mL vials that were quickly sealed with Teflon-coated septa and aluminum crimp seals for analysis by Tamar 7000 headspace autosampler interfaced with a Shimadzu GC-17A/flame ionization detector (FID) and an Agilent GS-GASPRO capillary column (30 m × 0.32 mm). The GC injector temperature was 250 °C and the detector temperature was 275 °C. The oven temperature was isothermal at 35 °C for 3 min, ramped at 20 °C/min to 110 °C, isothermal at 110 °C for 6 min, ramped at 40 °C/min to 220 °C, and isothermal at 220 °C for 14.5 min. Headspace autosampler settings were: sample loop size: 1 mL; loop fill time: 0.25 min; loop, platen, and transfer line temperature: 70 °C; sample equilibrium time: 30 min; and inject time: 0.5 min. All standards and samples were run in duplicate. Five point external calibration curves were run daily. Relative standard deviations for duplicate analyses using this method were typically less than 3 %.

For the experiment using high initial TCE with pyrite, reaction products included acetate, ethanol, and acetaldehyde beside *cis*-DCE. Acetate was measured by ion chromatography using the same instrumental setup as in Zhu et al. (2005). Ethanol and acetaldehyde were analyzed by a HP 6890 GC with an Agilent J&W DB-624 capillary column (30 m × 0.53mm × 3 μm) and flame ionization detector (FID). The GC injector temperature was 250 ^{o}C and the detector temperature was 280 ^{o}C. The oven temperature was isothermal at 60 ^{o}C for 6.5 min.

Isotope ratios of samples were analyzed by gas chromatography/isotope ratio

mass spectrometry (GC/IRMS) using previously reported methods (Kuder et al., 2005). Briefly, isotope fractionation was determined by purge and trap concentration of aqueous samples using a Vocarb 3000 or Tenax-silica gel-charcoal trap interfaced with a Varian 3400 GC with a J&W DB-MTBE column (60 m x 0.32 mm x 1.8 μm). The GC program was 4 min isothermal at 40 ^{o}C, followed by a 6 ^{o}C min^{-1} ramp up to the elution of PCE or TCE. The GC oven was kept at 220 ^{o}C after each analytical run. Following chromatographic separation, PCE or TCE was combusted in an alumina tube at 980 ^{o}C followed by isotope separation and quantification using a Finnigan MAT 252 mass spectrometer in the $^{13}C/^{12}C$ configuration. Isotope ratios were measured against a CO_2 standard. The maximum standard deviations of the lowest and the highest $\delta^{13}C$ of any standard run for a specific sample set did not exceed 0.5 ‰, with most values not exceeding 0.2 ‰. Select samples were analyzed in duplicate with the typical standard deviation less than 0.3 ‰.

2.2.5. Treatment of Kinetic and Isotope Data

As discussed below, only certain experimental conditions showed significant transformation of PCE or TCE in the time scale of our experiments. In these cases, we fit data for aqueous concentration of PCE or TCE versus time to a pseudo-first-order rate model, adjusted the resulting rate constants to those that would be measured in a headspace-free system (Burris et al. 1996), then divided them by surface area concentration. Mass recoveries of PCE or TCE reaction products (Tables 2.1 and 2.2) were calculated as follows:

$$\text{Mass Recovery (\%)} = \frac{M_{\text{p, aq, t}} + M_{\text{p, g, t}}}{M_{\text{r, aq, 0}} + M_{\text{r, g, 0}}} \times 100\% \qquad (2.1)$$

where $M_{\text{p, aq, t}}$ and $M_{\text{p, g, t}}$ equal the moles of a product in the aqueous and gas phases at

the last sampling time (given in Tables 2.1 and 2.2), and $M_{r,\,aq,\,0}$ and $M_{r,\,g,\,0}$ equal the moles of reactant (PCE or TCE) in the aqueous and gas phases at time zero. The same approach was used to calculate mass recoveries of unreacted PCE and TCE. Dimensionless Henry's Law constants (PCE: 0.612; TCE: 0.404; *cis*-DCE: 0.221; acetylene: 0.932; ethylene: 9.013; acetaldehyde: 0.00322; ethanol: 0.000204) were used to convert measured aqueous concentrations to masses, based on the aqueous and gas phase volumes. These values (for 25 ^{o}C) were obtained by averaging data from Nirmalakhandan and Speece (1988), Howard and Meylan (1997), and Bierwagen and Keller (2001). Acetate was assumed to be nonvolatile. The aqueous phase volume was 6.5 mL and the gas phase volume was approximately 1.25 mL. Bulk enrichment factors (ε_{bulk} values) were calculated by nonlinear regression using the Rayleigh equation (Mariotti et al., 1981) and experimentally measured values of stable carbon isotope ratios ($\delta^{13}C$) and fraction of TCE remaining (f or C/C_0).

2.3. Results and Discussion

2.3.1. Abiotic Reductive Degradation of PCE and TCE by Fe(II)-bearing Minerals

Plots of concentration versus time for transformation of PCE and TCE by FeS, GR-Cl, pyrite, GR-SO_4, and magnetite at pH 8 are shown in Figures 2.1 (PCE and TCE), 2.2 (PCE) and 2.3 (TCE). Degradation of PCE and TCE followed pseudo first order kinetics at pH 8 in the presence of FeS, GR-Cl, and pyrite (Figures 2.1, 2.2 and 2.3). Surface area normalized rate constants were calculated only in cases where sufficient transformation of PCE or TCE (at least 15-20%) had occurred by the end of the experiment (Tables 2.1 and 2.2). Mass recoveries of reactants and products and, in some cases, surface area normalized pseudo first order rate constants, are given in

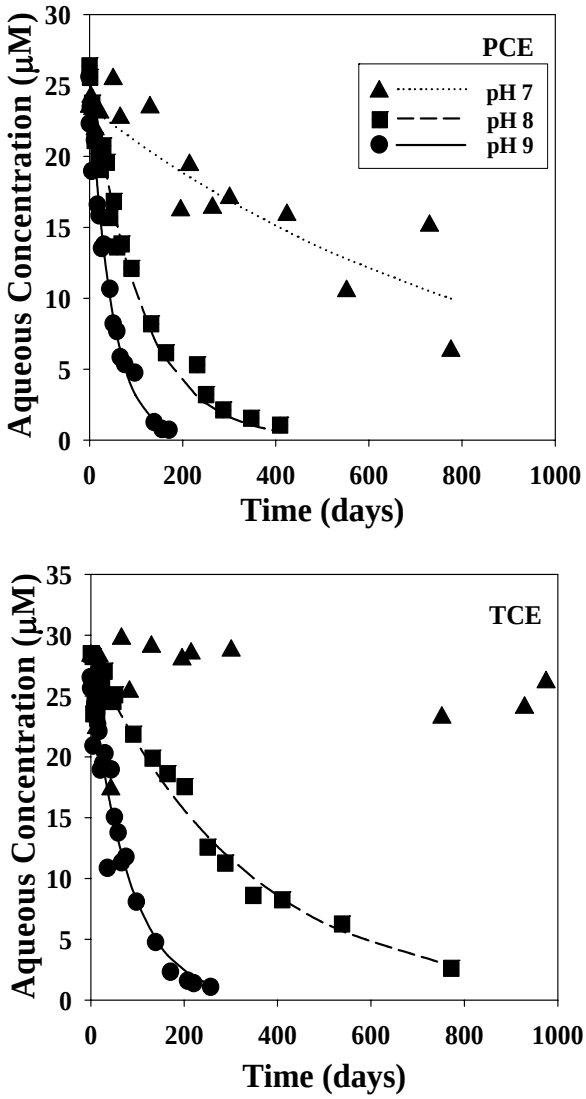

Figure 2.1. Abiotic reductive degradation of PCE and TCE in the presence of FeS at different pH values. Lines represent a pseudo first-order model fit.

Tables 2.1(PCE) and 2.2 (TCE). Relatively long half lives for the reactions discussed here (tens to hundreds of days) provide the evidence that surface electron transfer instead of mass transport (e.g., diffusion of contaminants to the surface, complexation with the surface, or diffusion of products away from the surface) limited the overall rate of PCE and TCE transformation.

There was little transformation of either PCE or TCE by Fe(II) and S(-II)-

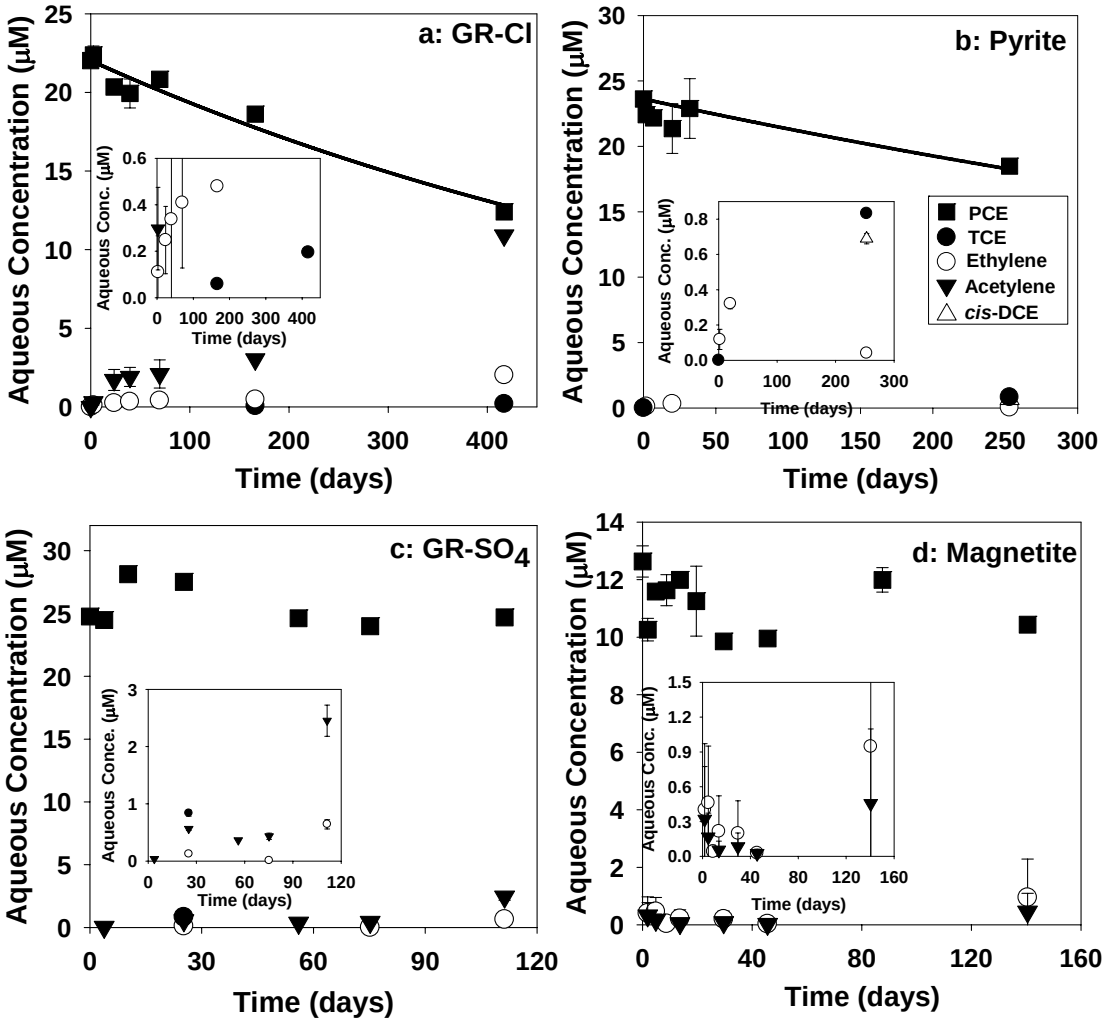

Figure 2.2. Abiotic transformation of PCE in the presence of (a) chloride green rust (GR-Cl), (b) pyrite, (c) sulfate green rust (GR-SO_4), and (d) magnetite at pH 8. Lines represent a pseudo-first-order model fit. The insets show reaction products with low concentrations.

treated goethite over 7-8 months (Tables 2.1 and 2.2); therefore these reactions are not illustrated in Figures 2.2 and 2.3. Even for reactions that were too slow to calculate rate constants, appearance of reaction products (Tables 2.1 and 2.2) is evidence that some reductive dechlorination of PCE and TCE took place in the presence of all mineral systems that were studied. Among all the minerals we studied, FeS is the most reactive mineral for the reaction with both PCE and TCE at pH 8 (Tables 2.1 and 2.2). The observed reactivities of PCE and TCE with GR-Cl are similar to those reported by Maithreepala and Doong (2005), who found 67% of PCE and 79% of

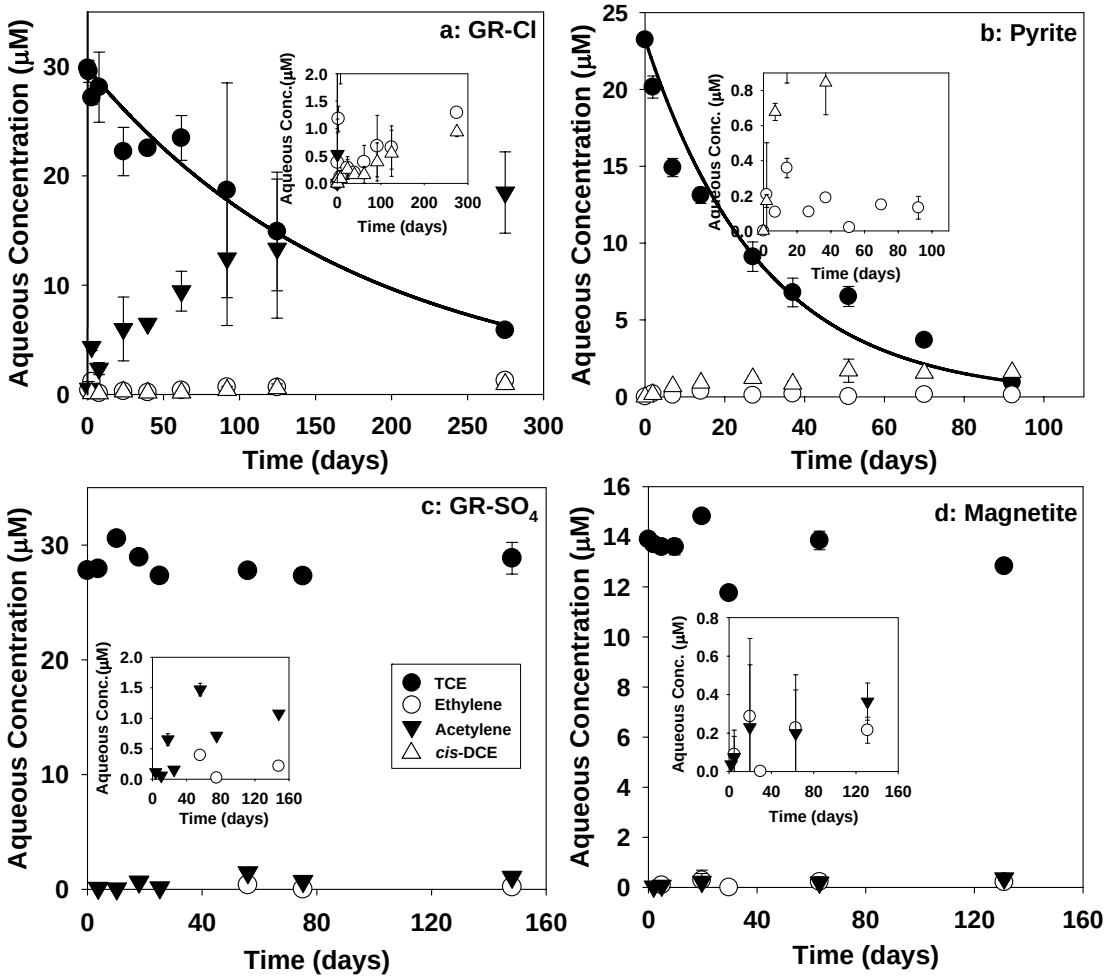

Figure 2.3. Abiotic transformation of TCE in the presence of chloride green rust (GR-Cl), pyrite, sulfate green rust (GR-SO_4), and magnetite at pH 8. Lines represent a pseudo-first-order model fit. The insets show reaction products with low concentrations.

TCE remaining after reaction with GR-Cl for 35 days (the GR-Cl surface area loading was not reported), although the relative reactivity reported by Maithreepala and Doong (2005) (PCE>TCE) differs from the results reported here (Figures 2.2 and 2.3; Tables 2.1 and 2.2). Small differences in surface composition may affect the relative rates of PCE and TCE transformation by different minerals.

Like this study, Lee and Batchelor (2002a) also found that TCE was transformed faster than PCE by pyrite, although their reported surface area

Table 2.1. Surface area normalized pseudo-first-order rate constants, products, and mass recoveries, for PCE transformation by FeS, chloride green rust (GR-Cl), pyrite, sulfate green rust (GR-SO_4), magnetite, Fe(II)-treated goethite, and S(-II)-treated goethite.

Mineral/pH (Surface area loading)	Time (days)	k_{SA} (L m^{-2} d^{-1})[a]	Products	Mass Recovery (%)[b]
FeS/pH 7 (20 m^2 L^{-1})	776	$(6.3 \pm 1.6) \times 10^{-5}$	acetylene	ND[c]
			TCE	26
			PCE remaining	27
			Total	ND
FeS/pH 8 (20 m^2 L^{-1})	409	$(5.30 \pm 0.51) \times 10^{-4}$	acetylene	ND
			TCE	2
			PCE remaining	4
			Total	ND
FeS/pH 9 (20 m^2 L^{-1})	172	$(1.21 \pm 0.12) \times 10^{-3}$	acetylene	ND
			TCE	3
			PCE remaining	3
			Total	ND
GR-Cl/ pH 8 (210 m^2 L^{-1})	417	$(5.6 \pm 1.4) \times 10^{-6}$	acetylene	52
			ethylene	23
			TCE	1
			PCE remaining	56
			Total	132
Pyrite/pH 8 (578 m^2 L^{-1})	253	$(1.6 \pm 1.0) \times 10^{-6}$	ethylene	0.4
			cis-DCE	3
			TCE	3
			PCE remaining	78
			Total	85
GR-SO_4/pH 8 (93 m^2 L^{-1})	111	NC[d]	acetylene	11
			ethylene	6
			PCE remaining	100
			Total	117
Magnetite/pH 8 (1800 m^2 L^{-1})	141	NC	acetylene	4
			ethylene	18
			PCE remaining	83
			Total	104
Fe(II)-treated goethite /pH 8 (296 m^2 L^{-1})	222	NC	acetylene	0.2
			ethylene	1
			PCE remaining	95
			Total	96
S(-II)-treated goethite /pH 8 (296 m^2 L^{-1})	233	NC	acetylene	0.03
			ethylene	1
			PCE remaining	100
			Total	101

[a] Uncertainties are 95% confidence intervals calculated by propagation of error; [b] See Appendix C for discussion of uncertainties; [c] ND: not determined due to analysis problems with acetylene; [d] NC: not calculated due to slow reaction.

Table 2.2. Surface area normalized pseudo-first-order rate constants, products, and mass recoveries, for TCE transformation by FeS, chloride green rust (GR-Cl), pyrite, sulfate green rust (GR-SO_4), magnetite, Fe(II)-treated goethite, and S(-II)-treated goethite.

Mineral (Surface area loading)	Time (days)	k_{SA} (L m^{-2} d^{-1}) [a]	Products	Mass Recovery (%)[b]
FeS/pH 7 (20 m^2 L^{-1})	974	NC [c]	acetylene	ND [d]
			cis-DCE	7
			TCE remaining	94
			total	ND
FeS/pH 8 (20 m^2 L^{-1})	772	$(1.61 \pm 0.19) \times 10^{-4}$	acetylene	ND
			cis-DCE	18
			TCE remaining	9
			total	ND
FeS/pH 9 (20 m^2 L^{-1})	258	$(6.40 \pm 0.81) \times 10^{-4}$	acetylene	ND
			cis-DCE	4
			TCE remaining	6
			total	ND
GR-Cl/pH 8 (210 m^2 L^{-1})	275	$(2.92 \pm 0.61) \times 10^{-5}$	acetylene	68
			ethylene	11
			cis-DCE	3
			TCE remaining	20
			total	101
Pyrite/low $[TCE]_0$ /pH 8 [e] (578 m^2 L^{-1})	92	$(6.4 \pm 1.5) \times 10^{-5}$	ethylene	1
			cis-DCE	7
			TCE remaining	4
			total	12
Pyrite/high $[TCE]_0$ /pH 8 [f] (3000 m^2 L^{-1})	18	NC	ethylene	0.01
			cis-DCE	1
			acetaldehyde	0.2
			ethanol	1
			acetate	11
			TCE remaining	84
			total	97
GR-SO_4/pH 8 (93 m^2 L^{-1})	148	NC	acetylene	4
			ethylene	2
			TCE remaining	104
			total	110
Magnetite/pH 8 (1800 m^2 L^{-1})	131	NC	acetylene	3
			ethylene	4
			TCE remaining	92
			total	99
Fe(II)-treated goethite /pH 8 (296 m^2 L^{-1})	222	NC	acetylene	0.01
			ethylene	1
			TCE remaining	104
			total	105
S(-II)-treated goethite /pH 8 (296 m^2 L^{-1})	233	NC	acetylene	0.2
			ethylene	1
			TCE remaining	107
			total	108

[a] Uncertainties are 95% confidence intervals calculated by propagation of error; [b] See Appendix C for discussion of uncertainties; [c] NC: not calculated due to slow reaction; [d] ND: not determined due to analysis problem with acetylene; [e] $[TCE]_0$ = 30 μM; [f] $[TCE]_0$ = 7.5 mM.

normalized rate constants for PCE and TCE are closer together than those reported here (Tables 2.1 and 2.2). In their experiments, the pyrite surface area loadings and initial concentrations of PCE and TCE may have resulted in a limitation of reactive surface sites (Lee and Batchelor, 2002a) that could have limited the reaction rate for PCE, TCE, or both.

Weerasooriya and Dharmasena (2001) reported much faster transformation of TCE than in this study (their data indicate a TCE half life of approximately 1 day at pH 8 for 2 m^2 L^{-1} pyrite (Weerasooriya and Dharmasena, 2001)). Their more rapid TCE transformation may have been caused by different impurities in the pyrite used for TCE transformation, since transition metal impurities in pyrite can catalyze contaminant transformation reactions (Carlson et al. 2003).

Although the reactions of PCE and TCE with GR-SO_4, magnetite, and Fe(II)- and S(-II)-treated goethite were too slow to calculate rate constants (Tables 2.1 and 2.2), mass recovery data for these experiments can in some cases be used to compare the reactivities of the different minerals with PCE and TCE, since amount of PCE or TCE removed and the yields of reaction products are proportional to rates. For GR-SO_4, total product yields were approximately 17% for PCE after 111 days and approximately 6% for TCE after 148 days. (Product yields were calculated by summing the mass recoveries of reaction products in Tables 2.1 and 2.2) Lee and Batchelor (2002b) found a greater extent of PCE and TCE disappearance in the presence of GR-SO_4 (30-40% over approximately two months) than in this study. The difference might be explained by a higher GR-SO_4 surface area loading (604 m^2/L in Lee and Batchelor (2002b) compared to 92 m^2/L used in these experiments). Comparing the total product yields for PCE and TCE transformation by GR-SO_4 (Tables 2.1 and 2.2) suggests that, unlike our results for GR-Cl and pyrite, PCE was

more reactive with GR-SO_4 than was TCE. Lee and Batchelor (2002b) also found significantly faster transformation of PCE than TCE by GR-SO_4. Comparing the intrinsic reactivity of GR-SO_4 with GR-Cl and pyrite is not possible since we could not calculate a surface area normalized rate constant for reaction of PCE and TCE with GR-SO_4 due to the slow reaction. It is likely that faster rates of PCE and TCE transformation would be observed at higher GR-SO_4 surface area loadings; thus the surface area normalized rate constants for PCE and TCE transformation by GR-SO_4 could be similar to those for GR-Cl and pyrite.

The extent of PCE and TCE transformed by magnetite over approximately 3 months was similar to that reported by Lee and Batchelor (2002a), but TCE disappearance in this study was significantly slower than that found by Sivavec and Horney (1997), who reported a half life for TCE reaction with magnetite of 19 days. This difference may be due to different magnetite synthesis methods, which Sivavec and Horney do not report. As was the case for pyrite, Lee and Batchelor (2002a) report a slightly larger rate constant for PCE versus TCE transformation by magnetite. In this study, we also found more PCE than TCE was transformed by magnetite over 141-148 days (i.e., less unreacted PCE versus TCE remained after that time) (Tables 2.1 and 2.2), suggesting greater reactivity of magnetite with PCE versus TCE. Unlike for GR-SO_4, however, quantitative comparison of product yields for PCE and TCE is not possible due to uncertainties in trace product measurements (Tables 2.1and 2.2). As with GR-SO_4, we could not calculate surface area normalized rate constants for reaction of PCE and TCE with magnetite, so we cannot compare the intrinsic reactivity of magnetite to that of GR-Cl, pyrite, or GR-SO_4. Considering the very high surface area loadings used for magnetite experiments (Tables 2.1 and 2.2), however, it is unlikely that surface area limited the reaction rate, and magnetite

appears to be significantly less reactive with PCE and TCE than the other minerals discussed so far.

There was no significant difference in the amount of PCE or TCE removed or total product yields (<2%) for Fe(II)- and S(-II) treated goethite after 222-233 days (Tables 2.1 and 2.2). This slow PCE or TCE transformation is in contrast to the high reactivity of Fe(II)-treated goethite with carbon tetrachloride and hexachloroethane reported under similar conditions (Elsner et al., 2004; Shao and Butler, 2007). For S(-II)-treated goethite, the estimated quantity of FeS formed (approximately 0.06 g L^{-1} based on the reaction stoichiometry for Fe(III) oxide reductive dissolution and FeS formation (Pyzik and Sommer 1981)), was significantly lower than in previous studies at similar pH values where mass loading was reported (Butler and Hayes, 1999; Liang et al., 2007) and was probably inadequate to cause significant transformation of PCE and TCE in the time scale of these experiments.

The particularly low total mass recovery for TCE transformation by pyrite (Table 2.2) led us to hypothesize that additional non-volatile or water soluble reaction products, such as acetate, ethanol, and acetaldehyde (Glod et al., 1997), had formed in this experimental system. In order to identify these products and improve the total mass recovery, an additional batch experiment was performed using a much higher initial TCE concentration (7.5 mM) to make it possible to detect these products using analytical methods with significantly higher detection limits. In this experiment, after 18 days, approximately 16 % of TCE had disappeared, and the following products were detected (in decreasing order of concentration): acetate, *cis*-DCE, ethanol, acetaldehyde, and ethylene (Table 2.2). Although the reaction did not proceed to a great extent for the higher initial concentration of TCE (high $[TCE]_0$) (probably due to the much higher ratio of TCE to pyrite surface area for the high $[TCE]_0$ experiment

(Table 2.2)), the total mass recovery was much higher (Table 2.2), indicating that the newly detected reaction products (acetate, ethanol, and acetaldehyde) likely account for the missing mass in the pyrite/low $[TCE]_0$ experiment (Table 2.2). In addition to hydrogenation to ethylene, acetylene produced by reductive β-elimination can be oxidized to acetaldehyde and acetic acid in the presence of some transition metals (Moggi and Albanesi, 1991) and aldehydes such as acetaldehyde can be reduced to the corresponding alcohol (which, for acetaldehyde, is ethanol) by catalytic hydrogenation or chemical reductants (Morrison and Boyd, 1983). Thus, the products detected in the pyrite/high $[TCE]_0$ experiment (Table 2.2) are consistent with initial reductive β-elimination of TCE to acetylene (*cis*-DCE, which comes from TCE hydrogenolysis, was a minor product.). It is possible that similar products could form during the transformation of PCE by pyrite (Table 2.1), but this must be confirmed experimentally.

We also studied abiotic transformation of PCE and TCE by FeS at pH 7 and pH 9, and results are shown in Figure 2.1. Surface area normalized pseudo first order rate constants (k_{SA} values) and mass recoveries are reported in Tables 2.1 and 2.2. For TCE at pH 7, degradation was too slow to calculate a rate constant, so no value of k_{SA} is reported in Table 2.2 and no line showing a pseudo first order fit is shown in Figure 2.1. Mass recoveries of acetylene for FeS reactions with PCE and TCE are not reported in Tables 2.1 and 2.2 due to analysis problems. Dechlorination of PCE and TCE by FeS was strongly pH-dependent with faster rates at higher pH values (Figure 2.1), in agreement with previously reported results (Butler and Hayes, 2001).

Although trends with respect to pH were similar, rate constants for TCE degradation by FeS were considerably lower than previously reported values at similar pH (Butler and Hayes, 2001). This may be due to use of different pH buffers

(tris(hydroxymethyl)aminomethane (Tris) in Butler and Hayes (2001) versus HEPES (pH 7 and 8) or CHES (pH 9) in this study). Addition of 0.01 M Tris to a magnetite/CCl_4 slurry increased the rate constant for CCl_4 reductive dechlorination by a factor of 3 at pH 8.9, compared to the case when no pH buffer was present (Danielsen et al., 2005). Differences in surface properties of the FeS samples used in this study versus previous study (Butler and Hayes, 2001) could also be responsible for differences in rate constants.

2.3.2. Stable Carbon Isotope Fractionation during Abiotic Transformation of PCE and TCE

Figure 2.4 shows that pH also affected isotope fractionation for PCE and TCE transformation by FeS, illustrated by the change in $\delta^{13}C$ with the fraction remaining of parent compound (*f*) and quantified by the difference in ε_{bulk} values (Table 2.3). The magnitude of isotope fractionation decreased (i.e., ε_{bulk} values became less negative) with increasing pH for both PCE and TCE. Acid/conjugate pairs such as $\equiv FeOH_2^+/\equiv FeOH$ (Butler and Hayes, 1998) and $\equiv Fe^{III}OFe^{II+}/\equiv Fe^{III}OFe^{II}OH^0$ (Charlet et al., 1998; Liger et al., 1999; Danielsen and Hayes, 2004) have been proposed to exist at reactive mineral surfaces. As discussed in greater detail elsewhere (Huskey, 1991; Elsner et al., 2005), the susceptibility of a bond containing a particular isotope to cleavage (and therefore fractionation) depends in part on its molecular vibrations in the transition state. Assuming the transition state consists of an activated complex between the mineral surface and PCE or TCE, pH-dependent changes in the chemical composition of the mineral surface could affect the transition state structure, molecular vibrations, and isotope fractionation. By "transition state structure" we mean the lengths and angles of partially broken and partially formed bonds in the

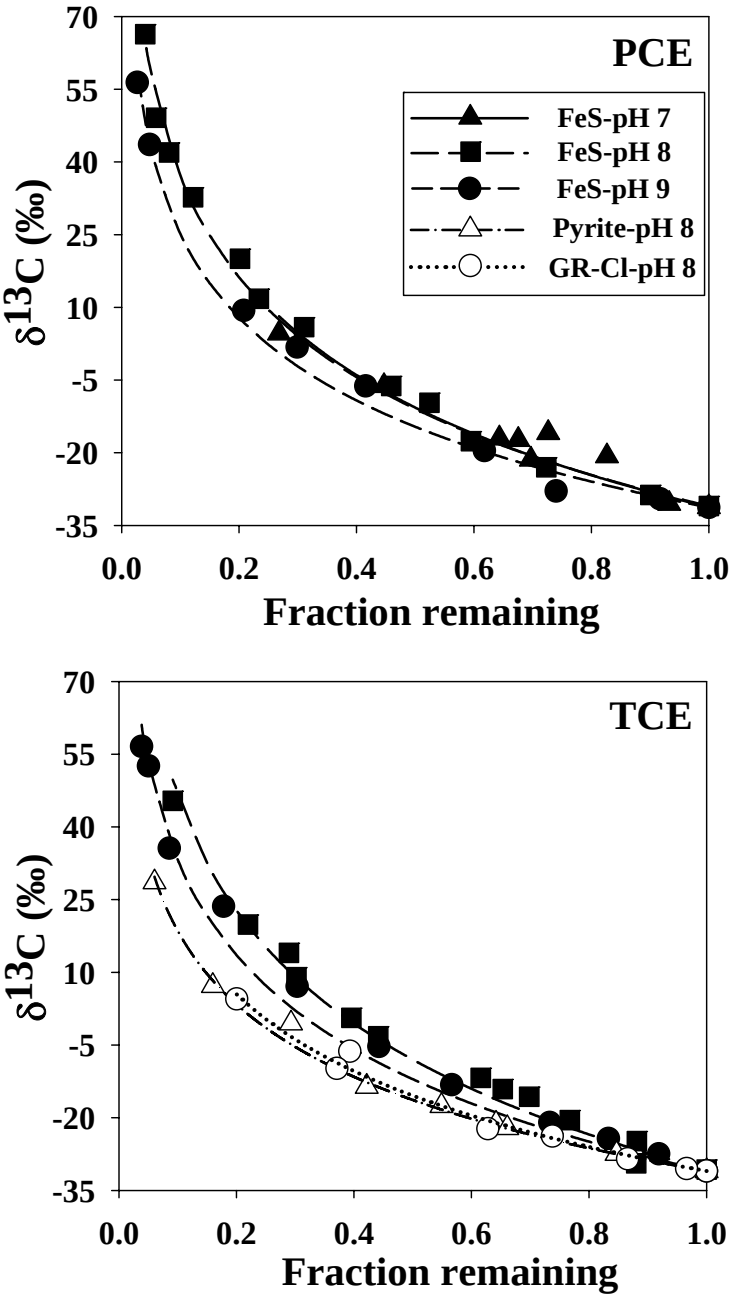

Figure 2.4. Carbon isotope fractionation during abiotic reductive dechlorination of PCE and TCE by FeS, pyrite, and chloride green rust (GR-Cl). Lines represent a Rayleigh model fit.

transition state.

Our ε_{bulk} value for PCE dechlorination by FeS at pH 7 (-30.2 ± 4.3 ‰) is not comparable to that measured by Zwank (2004) for an initial pH of 7.3 (-14.7 ‰), perhaps due to the presence of 4 mM dissolved Fe(II) (added as $FeCl_2$) in Zwank's

experiments. Addition of dissolved Fe(II) would tend to increase non-sulfide Fe(II) at the FeS surface, both weakly bound (i.e., $MgCl_2$ extractable) and strongly bound (i.e., 0.5 N HCl extractable) (Shao and Butler, 2007), which could influence ε_{bulk} values. The different ε_{bulk} values could also be due to the presence of HEPES buffer in our experiments, compared to Zwank's unbuffered experiments.

Table 2.3. Experimentally determined values of ε_{bulk} and calculated values of apparent kinetic isotope effect for carbon ($AKIE_C$)

	Conditions	ε_{bulk} (‰)[a]	Mechanism of Reductive β-Elimination[b]	n[b]	x[b]	z[b]	$AKIE_C$[c]
PCE	FeS, pH 7	-30.2 ± 4.3	1	2	2	2	1.0644 ± 0.0097
			2	2	2	1	1.0312 ± 0.0045
	FeS, pH 8	-29.54 ± 0.83	1	2	2	2	1.0628 ± 0.0019
			2	2	2	1	1.03044 ± 000088
	FeS, pH 9	-24.6 ± 1.1	1	2	2	2	1.0517 ± 0.0025
			2	2	2	1	1.0252 ± 0.0012
TCE	FeS, pH 8	-33.4 ± 1.5	1	2	1	1	1.0715 ± 0.0034
			2	2	2	1	1.0345 ± 0.0016
	FeS, pH 9	-27.9 ± 1.3	1	2	1	1	1.0592 ± 0.0030
			2	2	2	1	1.0287 ± 0.0014
	Pyrite, pH 8	-21.7 ± 1.0	1	2	1	1	1.0454 ± 0.0022
			2	2	2	1	1.0222 ± 0.0010
	GR-Cl, pH 8	-23.0 ± 1.8	1	2	1	1	1.0482 ± 0.0040
			2	2	2	1	1.0235 ± 0.0019

[a]Uncertainties are 95% confidence intervals calculated from non-linear regression. [b]See text discussion
[c]Uncertainties are 95% confidence intervals calculated by propagation of error.

Zwank (2004) found more isotope fractionation for PCE versus TCE dechlorination by FeS, which he attributed to different transition state compositions for PCE and TCE. Our experiments showed the same trend at pH 9, but the opposite trend at pH 8, although ε_{bulk} values for PCE and TCE at pH 8 and 9 are similar (Table 2.3). Figure 2.4 demonstrates that isotope fractionation for TCE dechlorination by FeS was significantly stronger than for TCE reaction with pyrite or GR-Cl at pH 8, and the difference in ε_{bulk} was greater than 10 ‰ (Table 2.3). ε_{bulk} values could not be reported for other experimental systems because reactions proceeded too slowly to

measure an ε_{bulk} value due to transformation of the parent compound to accurately calculate ε_{bulk} values. According to Zwank et al. (2005), assuming rate limitation by surface electron transfer and not mass transport to reactive surface sites, a more negative ε_{bulk} value suggests a greater extent of C-Cl bond cleavage in the transition state. Thus, we conclude that the less negative ε_{bulk} values for TCE transformation by GR-Cl and pyrite (Table 2.3) compared to that for TCE transformation by FeS under the same conditions is due to a smaller extent of bond cleavage in the transition state. Different transition state structures for TCE transformation by GR-Cl, pyrite, and FeS could result from different modes of interaction between TCE and the mineral surfaces (Zwank et al. 2005). For example, TCE could coordinate with surface iron atoms (Arnold and Roberts, 2000), with the disulfide groups in pyrite (as has been postulated for carbon tetrachloride transformation by pyrite (Kriegman-King and Reinhard, 1994)), or with no surface atoms (i.e., no covalent bonding between TCE and the mineral surface) in the case of outer-sphere electron transfer.

2.3.3. Use of Isotope Data to Determine Rate-limiting Steps in the Overall Abiotic Reactions

While ε_{bulk} values represent the overall isotope fractionation for an entire molecule, the kinetic isotope effect for carbon (KIE_C) equals the rate constant for cleavage of a ^{12}C-Cl bond divided by that for a ^{13}C-Cl bond (i.e., $^{12}k/^{13}k$), and thus represents isotope effects resulting from C-Cl bond cleavage. To determine rate-limiting steps in the overall abiotic reactions of PCE and TCE, we calculated the values of the "apparent" kinetic isotope effect for carbon ($AKIE_C$) from ε_{bulk} values using the approach described in Elsner et al. (2005) and Zwank et al. (2005). This approach considers two factors: (1) the presence of C atoms at positions in a molecule

that are non-reactive (i.e., C atoms with no potential for bond cleavage) and (2) the presence of different isotopes at more than one equally reactive position in a molecule (intra-molecular competition). These two factors can result in dilution or enhancement of the $AKIE_C$ and can be accounted for using the following equation (Zwank et al., 2005):

$$\frac{1}{AKIE_C} = \frac{z \cdot n \cdot \varepsilon_{bulk}}{x \cdot 1000} + 1 \qquad (2.2)$$

where n is the number of C atoms in the molecule, x is the number of C atoms with the potential for bond cleavage, and z is the number of C atoms having equal reactivity.

We then compared our calculated $AKIE_C$ values with theoretical KIE_C values for C-Cl bond cleavage to determine whether the rate limiting processes in the overall transformation reaction involved bond cleavage or other steps (e.g., transport of solutes to mineral surfaces, surface complex formation, and surface complex dissociation). Assuming bond cleavage is rate limiting, the $AKIE_C$ and KIE_C values should be the same (Elsner et al., 2005). We used a KIE_C value of 1.03, estimated by Semiclassical Streitwieser limits (Huskey, 1991) and assuming 50% bond cleavage in the transition state (Elsner et al., 2004, 2005). The term "semiclassical" means this parameter was calculated using a combination of classical and quantum mechanical assumptions (Huskey, 1991). While the extent of bond cleavage in the transition state is not known, this value provides a consistent basis for comparison of our abiotic experiments. The lower and upper limits of the KIE_C using Semiclassical Streitwieser limits are 1.00 (for 0% bond cleavage in the transition state) and ~1.057 (for 100% bond cleavage in the transition state) (Elsner et al., 2004).

Since reductive β-elimination is the major pathway for abiotic transformation of PCE and TCE in this study (see discussion in Section 3.1), we assume that

observed isotope fractionation mainly results from reductive β-elimination. Two mechanisms are possible for this pathway, each with different x and z values for equation 2.2. (Regardless of pathway or mechanism, n=2 for both PCE and TCE.) One previous study proposed that reductive β-elimination of PCE and TCE by FeS involves an initial rate limiting C-Cl cleavage step (Butler and Hayes, 1999). We refer to this as "mechanism 1" below. Another mechanism involving simultaneous carbon-halogen bond cleavage and C-C bond formation, referred to below as "mechanism 2", is also well known for nucleophiles like sulfide (Ramasamy et al., 1978; Baciocchi, 1983; Curtis and Reinhard, 1994; Perlinger et al., 1996; Miller et al., 1998). For reductive β-elimination by mechanism 1, x and z for PCE and TCE are identical to those for hydrogenolysis. For mechanism 2, x=2 for PCE and TCE since both C-Cl bonds are broken in the rate limiting step, and z=1, since there is no intramolecular competition (Zwank et al., 2005). $AKIE_C$ values for reductive β-elimination were calculated first assuming mechanism 1, then mechanism 2. All values of n, x, and z and the resulting values of $AKIE_C$ are summarized in Table 2.3.

Most $AKIE_C$ values for abiotic PCE and TCE reductive β-elimination calculated assuming mechanism 1 are near the top or outside the theoretical range of KIE_C values for C-Cl bond cleavage calculated using Semiclassical Streitwieser limits (Elsner et al., 2004) (i.e., 1.00-1.057). While $AKIE_C$ values calculated assuming mechanism 2 are within this range (Table 2.3), comparison of these values to the theoretical KIE_C for single C-Cl cleavage is not valid since other bond breaking and formation steps are also involved in a concerted mechanism like mechanism 2. Specifically, the strong driving force for formation of an additional C-C bond (i.e., the triple bond in the reactive chloro- and dichloroacetylene intermediates that yield acetylene), likely influences the theoretical KIE_C for mechanism 2, since atomic mass

(i.e., ^{12}C or ^{13}C) affects the driving force for bond formation as well as bond cleavage. Despite uncertainty about the mechanism of reductive β-elimination of PCE and TCE, the $AKIE_C$ values for PCE and TCE transformation by this pathway probably lie between those calculated assuming mechanisms 1 and 2.

2.4. Conclusions and Environmental Implications

These results confirm previous studies that show that FeS, green rusts, pyrite, and magnetite have the potential to contribute to the transformation of PCE and TCE at contaminated sites—either when these minerals occur naturally under iron or sulfate reducing conditions, or when they are exploited in engineered remediation technologies. Fe(II) adsorbed to the surface of goethite was far less reactive with PCE and TCE than it is reported to be with carbon tetrachloride and hexachloroethane (Elsner et al., 2004; Shao and Butler, 2007). It was also far less reactive with PCE and TCE than were the other minerals tested here. From this we conclude that Fe(II) adsorbed to iron oxides probably does not contribute significantly to PCE or TCE transformation in natural or engineered systems.

ε_{bulk} values for PCE and TCE transformation by FeS, GR-Cl and pyrite were very negative, which is typical of slow abiotic contaminant transformation reactions not controlled by mass transport (Zwank et al., 2005). These ε_{bulk} values can be used to assess the extent of PCE and TCE transformation using in situ remediation technologies that involve FeS, GR-Cl or pyrite. Another application of these results involves use of stable C isotope fractionation to distinguish PCE and TCE reductive dechlorination from non-fractionating processes such as advection, dispersion, and sorption (Beneteau et al., 1999; Poulson and Drever, 1999; Slater et al., 2000; Sherwood Lollar et al., 2001*)*. Use of an erroneously small (i.e., less negative) ε_{bulk}

value for this purpose would result in overestimation of contaminant degradation. Our reported ε_{bulk} values for abiotic PCE and TCE degradation are more negative than those for previously studied systems and should be considered when evaluating the performance of remediation technologies (including natural attenuation) that may involve abiotic transformation of PCE and TCE by FeS.

In addition, to our knowledge, the ε_{bulk} values of PCE and TCE in Table 2.3 are more negative than reported values for microbial PCE and TCE transformation, suggesting that measurement of such ε_{bulk} values can provide one line of evidence for mineral mediated transformation of TCE at contaminated sites. We emphasize that other lines of evidence must be also considered in any assessment of the relative contributions of abiotic versus microbial reductive dechlorination, since very negative ε_{bulk} values have also been reported for microbial degradation of TCE (e.g., -18.7 ± 4.2 ‰ (Cichocka et al., 2007)). Other lines of evidence that should be considered include identification of reaction products to determine if TCE reductive dechlorination occurred primarily by reductive β-elimination (mainly an abiotic pathway) or hydrogenolysis (mainly a microbial pathway), and measurement and analysis of isotope ratios in selected reaction products (Elsner et al. 2008). Also, while dispersion at field sites may result in "dilution" or underestimation of ε_{bulk} values (Abe and Hunkeler, 2006), this problem can be addressed by using an open system Rayleigh equation, which assesses both degradation and dispersion/dilution contributions to natural attenuation of contaminants (van Breukelen, 2007).

STATEMENT OF THE CONTRIBUTIONS OF AUTHORS TO CHAPTER 3 AND APPENDIX B

Research work in Chapter 3 and Appendix B was carried out by both Yiran Dong (Y. D.) and Xiaoming Liang (X. L.) with close collaboration, and was published in *Environmental Science and Technology* (2009). Both Y. D. and X. L. reprint it in full in their dissertations. Experimental data would be incomplete and could not produce an integrated paper with convincing conclusions if Y. D. and X. L. divided it up. This statement defines the contributions each student coauthor made to this work.

Experiments were designed by Y. D., and carried out by her and X. L. On the whole, Y. D. was in charge of setup and measurements of all PCE samples while X. L. took care of all TCE samples. For geochemical analyses, Y. D. measured the concentrations of weakly bound Fe (II) and strongly bound Fe(II) as well as TOC in solid phase. In contrast, X. L. determined the concentrations of FeS, Cr (II) reduced sulfur, and TOC in aqueous phase. In addition, Y.D. performed experiments for Figures B1and B4 as well as Table B4. X. L did the Hanawalt search/match XRD analysis in the appendix. Yiran Dong took the lead in writing this chapter and related Appendix B.

CHAPTER 3*

The Relative Contributions of Abiotic and Microbial Processes to the Transformation of Tetrachloroethylene and Trichloroethylene in Anaerobic Microcosms

3.1. Introduction

Ground water contamination by chlorinated aliphatic contaminants such as tetrachloroethylene (PCE) and trichloroethylene (TCE) is a widespread problem in the United States (Moran et al., 2007). PCE and TCE can be transformed abiotically by reactive Fe(II) and S(-II) minerals (Sivavec and Horney, 1996, 1997; Butler et al., 1999, 2001; Lee and Batchelor et al., 2002a, 2002b) that are typically formed during microbial reduction of Fe(III) oxides and sulfate (Morse et al., 1987; Fredrickson et al., 1998). Bacteria can also directly degrade PCE or TCE by dehalorespiration or cometabolism (Holliger et al., 1997; Bradley, 2003; Bhatt et al., 2007). Abiotic reductive dechlorination of PCE and TCE typically takes place by reductive β-elimination that results in accumulation of acetylene and other completely dechlorinated products (Sivavec and Horney, 1996, 1997; Butler et al., 1999, 2001; Lee and Batchelor et al., 2002a, 2002b), while microbial reductive dechlorination occurs via sequential hydrogenolysis that results in accumulation of lesser chlorinated ethenes along the sequence TCE, dichloroethylenes (DCEs), vinyl chloride (VC), and ethene (Brown et al., 2006). The distinct reaction products for abiotic versus microbial PCE and TCE reductive dechlorination can help identify the predominant

* Reproduced with permission from "Environmental Science & Technology 43, Dong, Y.; Liang, X.; Krumholz. L.R.; Philp, R.P.; Butler, E.C. The relative importance of abiotic and microbial transformation during remediation of tetrachloroethylene and trichloroethylene, 690-697, Copyright (2009) American Chemical Society".

process in a given environmental system.

Despite knowledge gained from the laboratory (Pasakarnis et al., 2006; Shen and Wilson, 2007) and field (Brown et al., 2006, Kennedy et al., 2006a, 2006b), the relative contributions of abiotic and microbial processes to the natural transformation of PCE and TCE is currently a subject of debate. Furthermore, while PCE and TCE transformation by pure mineral species has been well studied in the lab (Liang et al., 2007), the influence of readily measurable subsurface geochemical parameters, such as weakly and strongly bound Fe(II), acid soluble sulfur, and chromium extractable sulfur (CrES), on PCE and TCE transformation kinetics has not yet been reported. The objectives of this research were to: (1) assess the relative importance of microbial versus abiotic PCE and TCE reductive dechlorination under a variety of geochemical conditions and (2) identify the geochemical conditions for which abiotic PCE and TCE reductive dechlorination are most important. Microcosm studies were conducted using aquifer solids from three locations that were amended to generate iron reducing, sulfate reducing, and methanogenic conditions. We assessed the importance of abiotic and microbial reductive dechlorination in the microcosms by analysis of reaction products and kinetics, utilization of abiotic (killed) controls, comparison of observed half lives to those of laboratory studies using pure minerals, and stable carbon isotope analysis.

3.2. Materials and Methods

The specifications and sources of all chemical reagents are given in Appendix B. Solid and liquid samples were collected from three sites, including an anaerobic zone of an aquifer located adjacent to the closed landfill at the Norman Landfill Environmental Research Site (U.S. Geological Survey Toxic Substances Hydrology

Research Program), Norman, OK (Norman Landfill or L), a pond in Brandt Park, Norman, OK (Duck Pond or DP), and two permeable reactive barriers containing mulch ("biowalls") at Altus Air Force Base, Altus, OK (AAFB). There have been no reports of PCE or TCE contamination at the first two sites, while the sampling areas at AAFB intersect TCE plumes (Kennedy et al., 2006b; Liu et al., 2007). Two AAFB samples (AAFB 12 and AAFB 14) were from a biowall section that had been modified by addition of magnetite to promote formation of FeS upon microbial sulfate reduction (Parsons Corporation, 2006). Additional details about the sampling locations and procedures are given in Appendix B.

Microcosms were prepared in an anaerobic chamber (Coy Laboratory Products Inc., MI). Buffered site water (100 mL containing 25 mM HEPES (pH 7.2) or TAPS (pH 8.2)) and 20 g wet sediment or solids were added to 160 mL serum bottles. Experiments were done at pH 7.2 and 8.2 to include the range of pH values found in natural waters. HEPES and TAPS are generally considered suitable for biological systems, and we are not aware of any reports of HEPES or TAPS acting as electron donors for bacteria or exhibiting side effects such as toxicity to dehalogenating bacteria. Strict pH control was required since pH can strongly affect the rates of abiotic reductive dechlorination of PCE and TCE (Hwang and Batchelor et al., 2000; Maithreepala and Doong, 2005). Microcosms were either "unamended" (U), which were not preincubated with electron donors or acceptors before spiking with PCE or TCE and represented baseline geochemical conditions; "amended" (A), which were preincubated with electron acceptors and/or donors in order to increase microbial activity and stimulate reactive mineral formation before spiking with PCE or TCE; or "killed" (K), which were amended and preincubated as described above, then treated by boiling water bath and antibiotics to kill bacteria

prior to addition of PCE or TCE. Details about the heat/antibiotic treatment as well as the effect of heat treatment on the concentrations of abiotic mineral fractions are discussed in Appendix B.

Except for those that were unamended, microcosms were set up to stimulate iron reduction (IR), sulfate reduction (SR), or methanogenesis (Meth). Electron donors and acceptors were added to the microcosms to increase both the concentrations of potentially reactive biogenic minerals and microbial activity. Duck Pond and Landfill aquifer microcosms were amended with amorphous Fe(III) gel (50 mM) (Cornell and Schwertmann, 2003), $FeSO_4$ (30 mM), or no electron acceptor in order to establish iron reducing, sulfate reducing, or methanogenic conditions, respectively. For AAFB microcosms, only sulfate reducing conditions were stimulated, since this most closely represented site conditions, where dissolved sulfate in the ground water is high (1.4-12.5 mM). Acetate (20 mM), lactate (40 mM), and ethanol (15 mM) were added as electron donors for iron reducing, sulfate reducing, and methanogenic conditions, respectively. While it is possible that the use of different electron donors affected the rate and/or extent of dechlorination in the microcosms, the choice of each electron donor was made to be certain to stimulate microorganisms known to be capable of iron reduction, sulfate reduction, or methanogenesis, respectively.

In order to prevent methanogenic bacteria present in soil and sediment samples from competing for electron donors and preventing the establishment of iron or sulfate reduction, 1 mM 2-bromo-ethanosulfonic acid was added to the sulfate and iron reducing microcosms before adding electron acceptors and/or donors. This concentration was chosen because it was lower than concentrations reported to inhibit dechlorinating bacteria (2-3 mM) (Loffler et al., 1997; Chiu and Lee, 2001), but was

still sufficient to inhibit methane production. After addition of these amendments, microcosms were preincubated until terminal electron acceptors were consumed in the sulfate and iron reducing microcosms or formation of methane leveled off in the methanogenic microcosms. Then, the solid phase geochemistry was analyzed, microcosms were spiked with PCE or TCE, and monitored for abiotic and microbial transformation. Experiments with PCE were done for all microcosm conditions; experiments with TCE were done for selected conditions (Table 3.1). Sediments from one microcosm (DP-SR-pH 8.2) were imaged by scanning electron microscopy (SEM) to visualize the morphology and surface conditions of biogenic minerals. The images (Figure B1 in Appendix B), show rod-shaped bacteria (Figure B1(a) and (b)) and nano- to micrometer scale crystalline precipitates (Figure B1(b)) that could be FeS, Fe_3S_4, and/or FeS_2. Additional details on microcosm setup and analytical techniques are given in Appendix B. A summary of all experimental conditions and their abbreviations is given in Table B1 in Appendix B. As an example, the abbreviation "DP-Meth-pH 8.2-TCE" is used hereafter for Duck Pond sediments preincubated under methanogenic conditions at pH 8.2 and spiked with TCE.

3.3. Results and Discussion

3.3.1. Equilibrium among the Aqueous, Solid, and Gas Phases in Microcosms

Microcosms contained three phases: gas, aqueous, and solid. Concentrations discussed below and used in calculations ("total concentrations") are equal to the sum of the aqueous, solid, and gas phase masses divided by the aqueous volume. Kinetic parameters were calculated assuming rapid equilibrium of PCE or TCE among the phases relative to kinetic transformation, and kinetic transformation in the aqueous phase only; the approach is described in Appendix B.

Table 3.1. Summary of results for the microcosm experiments[a]

Microcosm ID[b]	Time (days) (PCE/TCE)	Percent remaining (%)		Abiotic product recovery (%) [c]		Microbial product recovery (%) [c]	
		PCE	TCE	PCE	TCE	PCE	TCE
Unamended Microcosms							
DP-U-pH 7.2	107/102	2.26±0.87	94.0±3.9	0	0.1	91	5
L-U-pH 7.2	107/102	90.1±2.0	98.77±0.42	0	0	8	1
AAFB-8-U-pH 7.2	59	0	—[d]	NC[e]	—	119	—
AAFB-9-U-pH 7.2	74	0	—	NC	—	112	—
AAFB-10-U-pH 7.2	77	0	—	NC	—	123	—
AAFB-12-U-pH 7.2	75	0	—	NC	—	105	—
AAFB-14-U-pH 7.2	54	0	—	NC	—	99	—
Amended Microcosms							
DP-IR-pH 7.2	27	0	—	1	—	89	—
DP-IR-pH 8.2	98/79	104.7±5.7	0.607±0.030	1	0.5	0.5	98
DP-SR-pH 7.2	33	0	—	0.1	—	102	—
DP-SR-pH 8.2	79/31	67.3±1.6	0	0.2	0.1	12	111
DP-Meth-pH 7.2	35	0.88±0.63	—	0	—	97	—
DP-Meth-pH 8.2	96/83	83±12	4.72	0.2	0.5	2	106
L-IR-pH 7.2	98	86±16	—	1	—	17	—
L-IR-pH 8.2	98/102	81.6±8.1	98.4±2.5	1	2	2	0.6
L-SR-pH 7.2	107	72±12	—	1	—	8	—
L-SR-pH 8.2	98/102	85±35	104.8±6.5	1	1	21	1.9
L-Meth-pH 7.2	93	2.9±3.5	—	0	—	73	—
L-Meth-pH 8.2	93/102	1.9±2.3	74.9±19.9	0	1	104	8
AAFB-8-SR-pH 7.2	17	0	—	NC	—	67	—
AAFB-9-SR-pH 7.2	51	0	—	NC	—	89	—
AAFB-10-SR-pH 7.2	54	0	—	NC	—	105	—
AAFB-12-SR-pH 7.2	74	0	—	NC	—	NC	—
AAFB-14-SR-pH 7.2	70	0	—	NC	—	NC	—
Killed Microcosms							
L-K-Meth-pH 7.2	53	77.9±3.2	—	0	—	0	—
L-K-Meth-pH 8.2	53	87.08±0.14	—	0	—	0	—
AAFB-8-K-U-pH 7.2	154	71.1±4.3	—	1	—	7	—
AAFB-9-K-U-pH 7.2	149	71.2±1.5	—	1	—	4	—
AAFB-10-K-U-pH 7.2	154	64.8±3.9	—	1	—	3	—
AAFB -12-K-U-pH 7.2	155	79.8±17.4	—	0.5	—	33	—
AAFB -14-K-U-pH 7.2	155	77.5±5.8	—	0.4	—	6	—

[a] Uncertainties are standard deviations of replicate microcosms; [b] Abbreviations: Duck Pond (DP), Norman Landfill (L), Altus AFB (AAFB), unamended (U), killed with heat-treatment and antibiotics (K), iron reduction (IR), sulfate reduction (SR) and methanogenesis (Meth); [c] See Appendix C for discussion of uncertainties; [d] __, samples were not set up under these conditions; [e] NC, not calculated because it was unclear if ethylene came from abiotic or microbial dechlorination.See detailed explanation in Appendix B5.2.

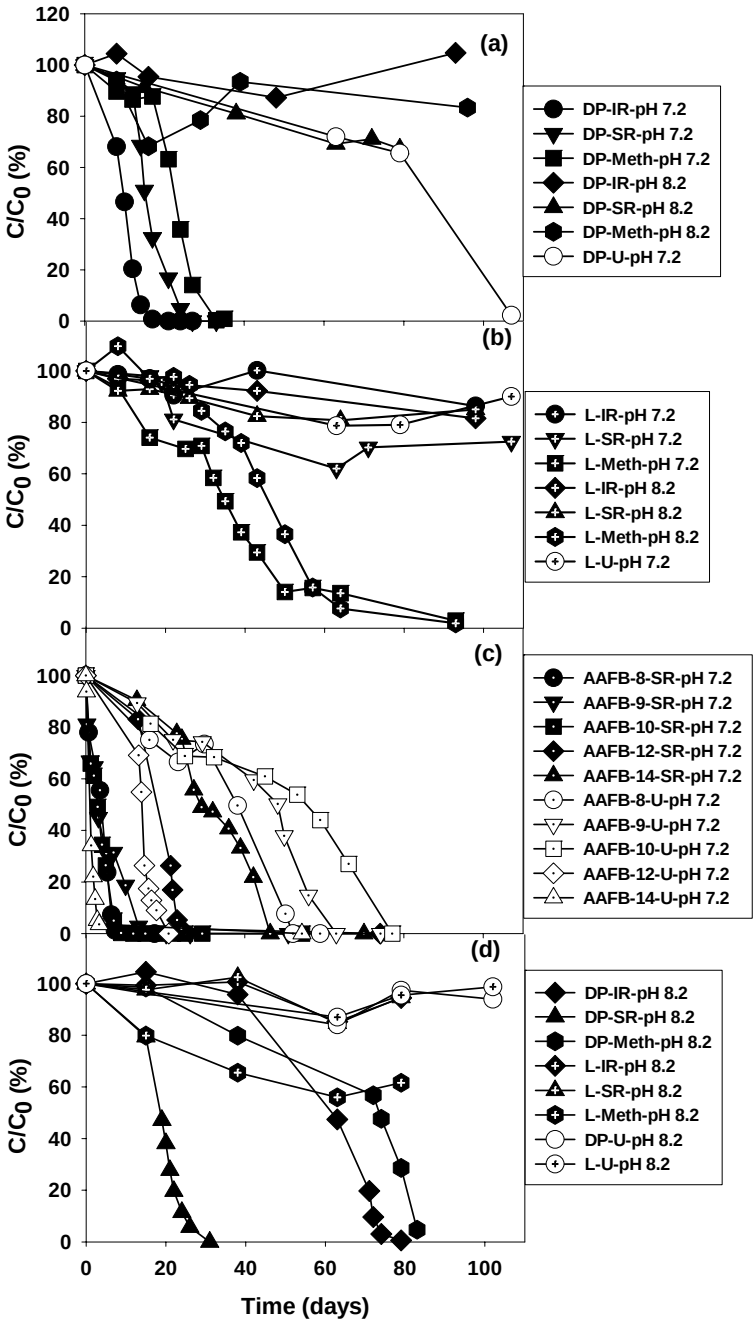

Figure 3.1. PCE reductive dechlorination in the Duck Pond (DP) (a), Landfill (L) (b), and Altus AFB (AAFB) (c) microcosms and TCE reductive dechlorination in selected DP and L microcosms (d), under iron reducing (IR), sulfate reducing (SR), and methanogenic (Meth) conditions. U=Unamended. Data points are averages of samples from duplicate or triplicate microcosms

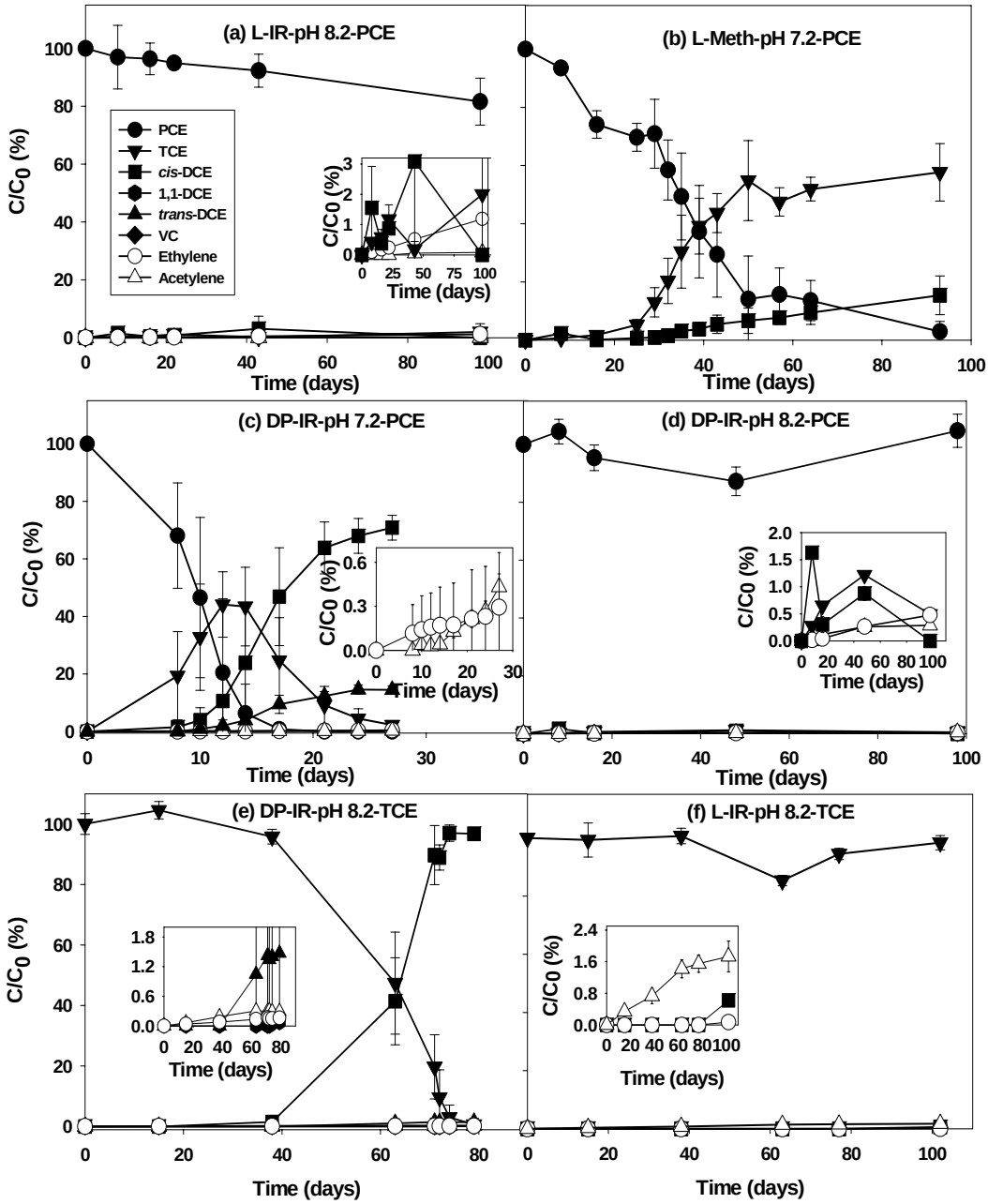

Figure 3.2. Normalized concentrations of PCE (a-d), TCE (e-f), and reaction products in representative microcosms. Reactants and products were normalized by dividing the concentration at any time by the concentration of the reactant at time zero. The insets show reaction products with low concentrations. Error bars are standard deviations of triplicate microcosms. To better show the data points, parts of the error bars were cut off in the insets for (a) and (e). In the inset for (e), the symbols for 1,1-DCE (closed hexagons) are partially covered with ethylene (open circles) and acetylene (open triangles).

3.3.2. Relative Importance of Abiotic and Microbial Reductive Dechlorination

Normalized concentrations of PCE and TCE versus time have been plotted for all the microcosm conditions (Figure 3.1) and time courses for representative microcosms, which also show normalized concentrations of detected reaction products, were also plotted (Figure 3.2). Normalized concentrations for antibiotic/heat killed microcosms along with their live counterparts prepared under the same conditions, as well as time courses for all live AAFB microcosms, are shown in Appendix B (Figures B2 and B3, respectively). Evidence from these figures indicates that in most cases, reductive dechlorination of PCE and TCE in the microcosms took place primarily by microbial transformation by indigenous dechlorinating bacteria rather than abiotic transformation by reactive minerals. This evidence includes: (1) slow rates and a small extent of PCE transformation in killed microcosms compared to the amended and unamended microcosms prepared under the same conditions (Figure B2); (2) a lag time followed by a rapid pseudo-zero-order (i.e., straight line or constant slope) disappearance of PCE or TCE that is characteristic of microbial transformations, rather than an initial pseudo-first-order reaction characteristic of abiotic reactions (Figures 3.1,3.2, B2, and B3); (3) near quantitative accumulation of PCE and TCE hydrogenolysis products, such as TCE (for PCE), cis 1,2-DCE, and VC, for all microcosms where there was significant transformation of PCE or TCE (Figure 3.2) (two possible exceptions to this trend, AAFB-12-SR-pH 7.2-PCE and AAFB-14-SR-pH 7.2-PCE, are discussed further below); and (4) the rapid transformation of PCE or TCE after the initial lag period, compared to the relatively slow abiotic transformation of these compounds. For instance, using previously reported mass-normalized rate constants for PCE and TCE transformation by

FeS that were corrected for partitioning among the gas, aqueous, and solid phases (Section B5, Table B4 in Appendix B), we estimated that the half lives for PCE or TCE transformation by the FeS present in our microcosms would be 900-5,000 days (PCE) or 500-1,000 days (TCE) at the highest FeS mass loading (approx. 0.9 g/L) and a median fraction organic carbon (f_{oc}) value of 0.002 (Table B2) (Longer half lives are for pH ≈ 7; shorter half lives are for pH ≈ 8). While other reactive minerals could have also contributed to abiotic PCE and TCE transformation in the microcosms, their mass loadings and reactivity are likely to be at least the same order of magnitude as those for FeS, so abiotic reactions alone cannot account for the rapid transformation of PCE and TCE following the lag period (Figures 3.1, 3.2, and B3).

To quantify the extent of microbial and abiotic PCE and TCE transformation, we calculated product recoveries for both processes by dividing the summed total concentrations of abiotic or microbial dechlorination products at the last sampling time (see Table 3.1, column 2) by the initial total concentration of PCE or TCE, and multiplying by 100 % (Lee and Batchelor, 2002). Calculation details are in Appendix B and abiotic and microbial product recoveries are reported in Table 3.1. While product recoveries are not constant with time, their calculation allows comparison of the relative importance of abiotic versus microbial PCE and TCE transformation among microcosms sampled at approximately the same time. For some live AAFB microcosms, we were not able to distinguish whether the ethylene detected in the microcosms came from microbial hydrogenolysis of VC or from abiotic hydrogenation of acetylene (Jeong et al., 2007); in these cases, product recoveries were not calculated. Details are in Appendix B.

Table 3.1 shows that abiotic product recoveries were never significantly higher

than 1 %. Considering only live microcosms, there were two conditions where the abiotic product recovery exceeded the microbial product recovery, one for PCE transformation (DP-IR-pH 8.2; Figure 3.2d, Table 3.1), and one for TCE transformation (L-IR-pH 8.2; Figure 3.2f, Table 3.1). For these microcosms, both abiotic and microbial transformation were slow (close to 100% of the PCE or TCE remained after approximately 100 days (Table 3.1)), but abiotic products accumulated to a greater extent than did microbial products, suggesting that abiotic processes could be more important for PCE or TCE transformation in subsurface environments under conditions where dechlorinating bacteria are not active. The high pH (8.2) of these microcosms may have inhibited the activity of dechlorinating bacteria. In five other live microcosms (DP-Meth-pH 8.2-PCE; L-IR-pH 8.2-PCE; L-SR-pH 7.2-PCE; L-SR-pH 8.2-TCE; and L-Meth-pH 8.2-TCE), the abiotic and microbial product recoveries were relatively close to each other (within a factor of 10). Four of these five were incubated at pH 8.2, providing additional evidence that, at least in some cases, higher pH values may not be optimal for growth of dechlorinating bacteria. In all other samples, microbial product recoveries were much higher than abiotic product recoveries.

We considered the possibilities that our low abiotic product recoveries could be due to microbial transformation of abiotic dechlorination products (e.g., acetylene). To test this possibility, we spiked acetylene into the Duck Pond and Landfill microcosms at a total concentration of approximately 2 μM, which was close to the highest concentration of acetylene observed in our microcosms. Figure B4 shows that acetylene was transformed within approximately 2-4 days in the Duck Pond microcosms, but remained essentially constant after more than 40 days in all the Landfill microcosms. We then

treated the three Duck Pond microcosms showing the fastest acetylene transformation in a boiling water bath for 15 min and respiked them with acetylene. Following this, no acetylene transformation was observed, indicating that acetylene transformation was microbial, not abiotic. Microbial fermentation of acetylene has been reported previously (Schink, 1985). Despite the loss of abiotically-generated acetylene via microbial transformation in the Duck Pond microcosms, however, there are still several lines of evidence (discussed above) indicating the greater involvement of microbial versus abiotic transformation of PCE and TCE in the microcosms. Consumption of acetylene by indigenous microorganisms cannot account for the low abiotic product recoveries observed for almost every microcosm condition (Table 3.1), including the Landfill microcosms, where acetylene transformation was not observed (Figure B4).

Two possible exceptions to the trend of higher microbial versus abiotic product recoveries are AAFB-12-SR-pH 7.2-PCE and AAFB-14-SR-pH 7.2-PCE (Table 3.1, Figures B3(d) and (e)). In neither case could we determine if the abundant ethylene in these microcosms came from abiotic or microbial processes, or some combination of both. The existence of a lag phase before the onset of pseudo-zero-order PCE disappearance (Figures B3(d) and (e)) and the inhibition of PCE disappearance in killed controls (Figure B2), however, are consistent with a greater role for microbial PCE dechlorination in these microcosms.

3.3.3. Isotope Fractionation during Reductive Dechlorination

Stable carbon isotope fractionation is another tool that may provide information about the predominant process for PCE or TCE transformation, i.e., abiotic or microbial.

Several recent articles describe in detail the principles of isotope analysis for environmental applications (Elsner et al., 2005). While a range of ε_{bulk} values has been reported for both abiotic and microbial transformation of PCE and TCE, the range of reported ε_{bulk} values for abiotic PCE transformation in batch systems is generally more negative than that for microbial PCE transformation (Bloom et al., 2000; Slater et al., 2001, 2002, 2003; Schüth et al., 2003; Zwank, 2004; Nijenhuis et al., 2005; Liang et al., 2007; Cichocka et al., 2007, 2008; Lee et al., 2007). Thus, very large (in magnitude), negative ε_{bulk} values are suggestive of abiotic PCE transformation while very small (in magnitude), negative ε_{bulk} values are suggestive of microbial PCE transformation. The limitation of this approach lies in the exceptions; specifically, negative ε_{bulk} values that are intermediate in magnitude have been reported for both abiotic and microbial PCE transformation. As just one example, an ε_{bulk} value of -14.7 ‰ was reported for abiotic transformation of PCE by FeS (Zwank, 2004), while a more negative value of -16.7 ‰ was reported for microbial transformation of PCE (Cichocka et al., 2008). Thus, intermediate ε_{bulk} values such as these are of less value in assessing the predominant reaction pathway for PCE transformation (abiotic or microbial), than are very large or small (in magnitude) values. Also, interpretation of ε_{bulk} values must always be done with caution and in conjunction with other lines of evidence such as those described above (e.g., analysis of reaction order and reaction products). Finally, ε_{bulk} values for abiotic and microbial transformation of TCE are typically closer together than are those for PCE (Zwank, 2004; Liang et al., 2007), making isotope fractionation less useful for differentiating abiotic and microbial transformation of TCE versus PCE.

Plots of $\delta^{13}C$ versus fraction PCE or TCE remaining (C/C_0) for all microcosms for

which significant PCE or TCE transformation took place are plotted in Figure 3.3. ε_{bulk} values were calculated using the Rayleigh equation (Mariotti et al., 1981). For PCE, ε_{bulk} values for the Duck Pond and all but one AAFB microcosm showed weak isotope fractionation (these ε_{bulk} values ranged from -0.71 to -3.1 ‰), which is typical of microbial reductive dechlorination of PCE (Bloom et al., 2000; Slater et al., 2001;

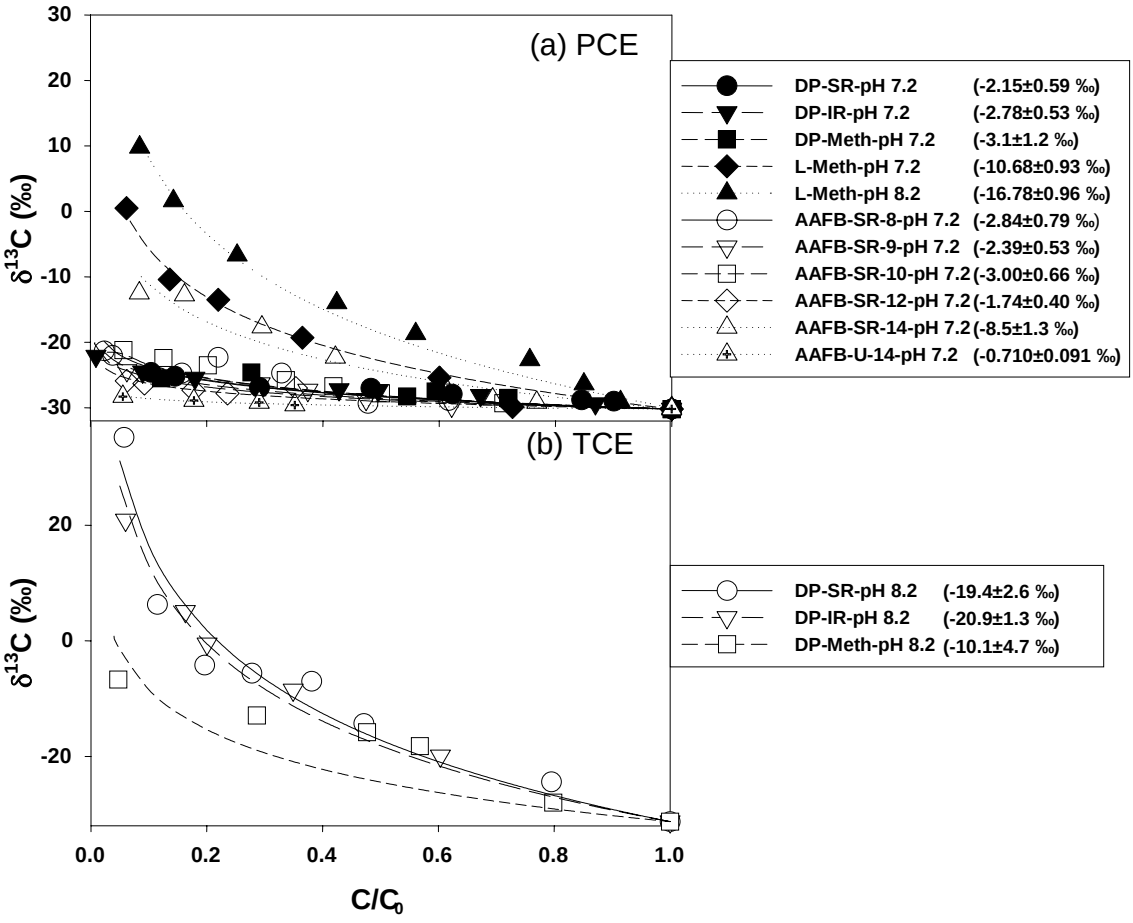

Figure 3.3. Isotope fractionation of PCE (a) and TCE (b) in the microcosms where PCE and TCE were below detection limits at the end of experiment. The values in parentheses are bulk enrichment factors (ε_{bulk} values). Data points are experimentally measured values, and lines represent a fit to the Rayleigh model. Uncertainties are 95 % confidence intervals.

Nijenhuis et al., 2005; Liang et al., 2007; Cichocka et al., 2007, 2008; Lee et al., 2007), and therefore consistent with the other evidence for microbial dechlorination discussed above. Significantly stronger isotope fractionation was measured in the remaining AAFB microcosm (AAFB-14-SR-pH 7.2-PCE; ε_{bulk} = -8.5 ‰) and the Landfill microcosms incubated under methanogenic conditions (ε_{bulk} = -10.68 and -16.78 ‰ for pH 7.2 and 8.2, respectively); thus the isotope data from these microcosms is less useful in distinguishing abiotic from microbial dechlorination. While the first two of these ε_{bulk} values are less negative than previously reported ranges for abiotic PCE dechlorination, and therefore presumably due to microbial dechlorination, the third value (for L-Meth-pH 8.2-PCE (ε_{bulk} = -16.78 ‰) is close to reported values for both microbial PCE transformation (ε_{bulk} = -16.7 ‰)(Cichocka et al., 2007) and abiotic PCE transformation (ε_{bulk} = -14.7 ‰) (Zwank, 2004). The remaining evidence (discussed above) is, however, consistent with microbial reductive dechlorination for these microcosms.

For TCE, ε_{bulk} values for Duck Pond microcosms incubated with different terminal electron acceptors at pH 8.2 equaled -10.1, -19.4, and -20.9 ‰ for methanogenic, sulfate reducing, and iron reducing conditions, respectively. The first of these values is within the range of previously reported values for microbial TCE reductive dechlorination (Hunkeler et al., 1999; Sherwood Lollar et al., 1999; Bloom et al., 2000; Slater et al., 2001; Zwank, 2004; Liang et al., 2007; Lee et al., 2007). The second two are more negative than previously reported ε_{bulk} values for microbial dechlorination of TCE, but they are close to the value of -18.9 ‰ recently reported by Cichocka et al. (2007). We are reluctant, therefore to interpret these second two ε_{bulk} values as indicative of abiotic reductive dechlorination of TCE. In addition, the remaining evidence for these

microcosms (low abiotic and high biotic product recoveries (Table 3.1) and a lag period before the start of TCE degradation (Figures 3.1d and 3.2e)) is consistent with microbial and not abiotic reductive dechlorination.

3.3.4. Influence of Geochemical Parameters on Abiotic Reductive Dechlorination

Dechlorinating enzymes are responsible for microbial degradation of PCE and TCE, and the half lives ranges from several days to one month (Liang et al., 2007). In contrast, 50% of PCE and TCE degradation by minerals takes at least months (Liang et al., 2007, 2009). While microbial transformation of PCE and TCE was typically faster than abiotic transformation in our microcosms, it is possible that abiotic dechlorination may ultimately transform more PCE and TCE under certain conditions, for example where the activity of dechlorinating bacteria is low (e.g., Figures 3.2a, d, and f), for microbial communities that do not completely dechlorinate PCE or TCE, or for soils or sediments that are amended to generate significantly higher mass loadings of reactive minerals or significantly higher pH values as part of a remediation strategy. For this reason, we analyzed our kinetic and geochemical data to see if there was a relationship between the concentration of one or more geochemical parameters and abiotic product recoveries. Because a number of studies indicate that abiotic reductive dechlorination is a surface and not aqueous phase process (Erbs et al., 1999; Kenneke and Weber, 2003), we considered only solid-associated geochemical species in this analysis. Geochemical data are reported in Table B2 and illustrated in Figure 4. The arrows in Figure 4 indicate those microcosms where no abiotic PCE or TCE reaction products were detected; this occurred under only three conditions (L-U-pH 7.2, DP-Meth-pH 7.2, and L-Meth-pH 7.2).

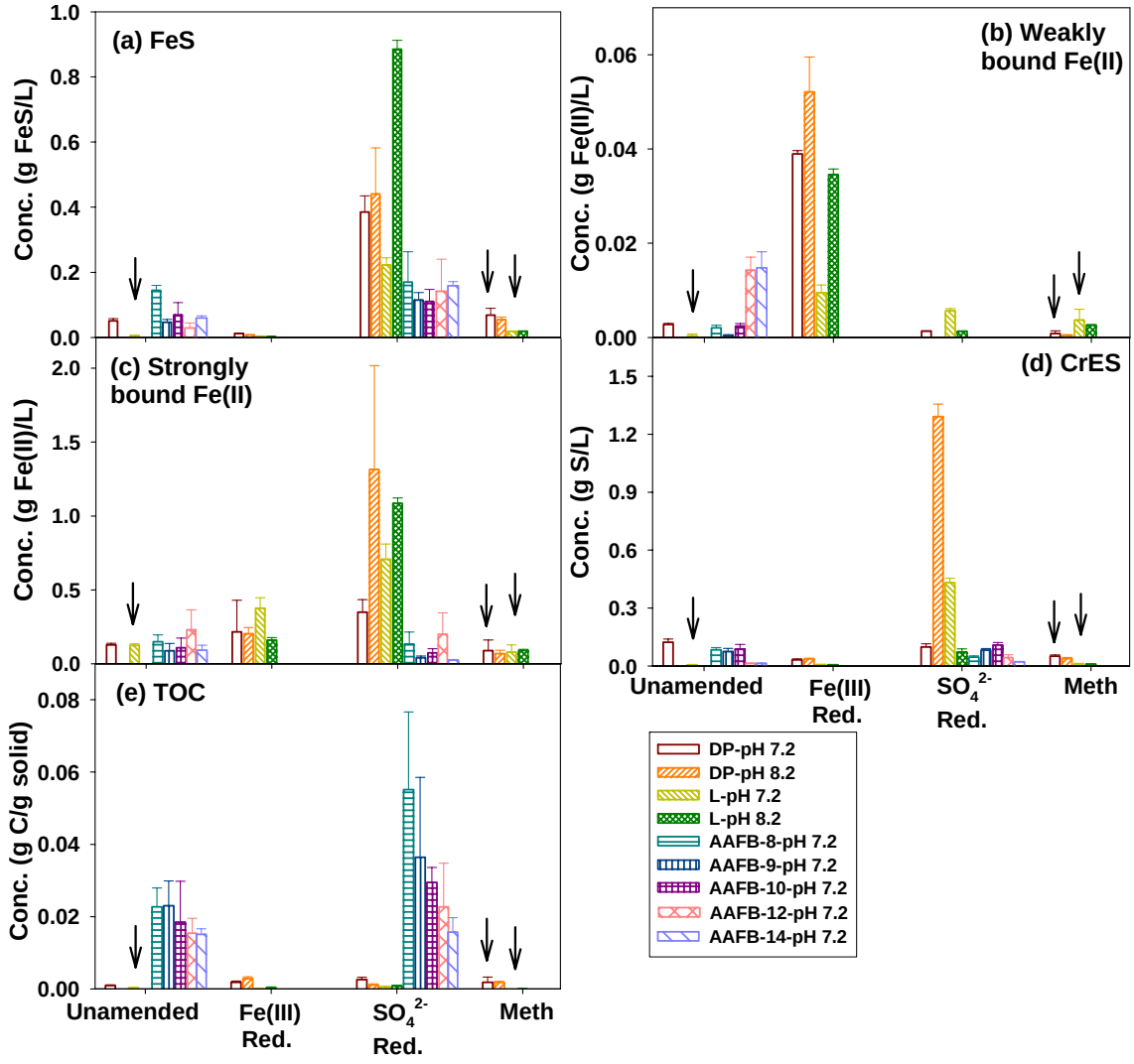

Figure 3.4. Geochemical analyses of the microcosms, including FeS (a), weakly bound Fe(II) (b), strongly bound Fe(II) (c), chromium extractable sulfur (CrES) (d) and TOC (e), under unamended, iron reducing (Fe(III) Red.), sulfate reducing (SO_4^{2-} Red.) or methanogenic (Meth) conditions. Arrows indicate the microcosms where neither PCE nor TCE abiotic reductive dechlorination products were detected. Error bars are standard deviations of triplicate samples from the same microcosm. See Appendix B for methods used to quantify the geochemical species shown in this Figure.

These three conditions were either unamended (no electron donors or acceptors added),

or amended to produce methanogenic conditions (Figure 4.4). Table B2 and Figure 4

show that such microcosms typically had lower concentrations of potentially reactive Fe(II) and S(-II) mineral fractions (presumably due to the absence of iron and sulfate reduction that leads to formation of Fe(II) and S(-II) minerals) than did microcosms incubated under iron reducing or sulfate reducing conditions, suggesting the importance of freshly precipitated Fe(II) and S(-II) minerals in abiotic PCE and TCE dechlorination. It is not possible from Table B2 and Figure 4.4 to identify which mineral fraction is most reactive with respect to PCE and TCE abiotic reductive dechlorination, but Table 3.1 shows similar abiotic product recoveries for microcosms incubated under both iron reducing and sulfate reducing conditions, indicating that both non-sulfur-bearing and sulfur-bearing Fe(II) mineral fractions likely contribute to the slow abiotic reductive dechlorination of PCE and TCE observed in most microcosms.

3.4. Environmental Significance

Abiotic transformation of PCE and TCE in the microcosms was typically much slower than microbial reductive dechlorination due to the very slow abiotic transformation of PCE and TCE by reactive minerals that were present at concentrations typically below 1 g/L. The microcosms in this study contained 20 g wet soil, 100 mL water, and 50 mL headspace. Assuming a soil water content of 15% and a total volume of wet soil plus water equal to 110 mL, this equals a soil mass loading of 154 g soil/L. Increasing the soil mass loading to a value typical of an aquifer (e.g., 2,000 g soil/L) would have the effect of both increasing the fraction of total PCE or TCE in the sorbed phase and, assuming that the loadings of the soil and its reactive mineral components increased proportionally, increasing the mass loadings of potentially reactive soil

minerals. These two phenomena would have opposite effects on apparent rate constants or half lives for abiotic transformation of PCE or TCE by soil minerals. The effect of increasing soil mass loading on rate constants or half lives for microbial PCE or TCE transformation would depend on the fraction of dechlorinating bacteria associated with aquifer solids and would likely result in a commensurate increase in the rate constant. Shen and Wilson (2007) assessed the relative contributions of abiotic and microbial transformation of TCE in a system with a higher mass loading, in which groundwater flowed through laboratory columns constructed from OU1 biowall materials (samples AAFB-8, -9, and -10 were obtained from the OU1 biowall, see Appendix B) and concluded that the predominant TCE transformation process was abiotic. Further testing will be needed to assess the relative contribution of abiotic and microbial reductive dechlorination under field conditions.

Bacteria capable of dechlorinating PCE or TCE were present under almost all microcosm conditions, and microbial PCE and TCE dechlorination had a typical half life (after the lag phase) of 10 days (Figure 3.1). Such half lives are shorter than those reported in most studies of abiotic transformation of PCE and TCE by minerals (Sivavec and Horney, 1996, 1997; Butler et al., 1999, 2001; Lee and Batchelor et al., 2002a, 2002b), even for conditions where mass loadings of reactive minerals were much higher than those in the microcosms studied here (Table B2). From this we conclude that microbial processes have the potential for the most rapid transformation of PCE and TCE in the field and should be exploited for this purpose where appropriate. Abiotic processes also have the potential to contribute to the transformation of PCE and TCE in cases where significantly higher mass loadings of reactive minerals are generated in situ as part

of a remediation technology or where the activity of dechlorinating bacteria is low (e.g., Figures 3.2a, 3.2d and 3.2f). Abiotic processes can also play a significant role in cases where complete microbial degradation of PCE or TCE to ethene does not occur (e.g., Figure 3.2b), since mineral-mediated dechlorination of cis-DCE and VC to ethane, ethylene, and/or acetylene has been shown (Lee and Batchelor et al., 2002a, 2002b). Under these conditions, although slow, abiotic processes may still contribute to the complete transformation of PCE and TCE to benign products at contaminated sites.

CHAPTER 4

Effects of Natural Organic Matter on the Degradation of Carbon Tetrachloride by Chloride Green Rust

4.1. Introduction

Iron minerals play an important role in the natural attenuation of carbon tetrachloride (CT) in subsurface environments (Kriegman-King and Reinhard, 1992, 1994; Erbs et al., 1999; Amonette et al., 2000; Butler and Hayes, 2000; O'Loughlin et al., 2003b; Danielsen and Hayes, 2004; Elsner et al., 2004; McCormick and Adriaens, 2004; Maithreepala and Doong, 2005; Zwank et al., 2005; Hanoch et al., 2006; Vikesland et al., 2007; Shao and Butler, 2007; Shao and Butler, 2009). Among these minerals, green rusts (GRs) are layered double hydroxides (LDHs) with positively charged Fe(II)/Fe(III) hydroxide sheets which alternate with interlayered water molecules and anions (Figure 4.1) (Brindley et al., 1976; McGill et al., 1976; Hensen et al., 1996; Abdelmoula et al., 1998; Refait et al., 1998). A general formula of GRs is $[Fe^{II}_{(1-x)}Fe^{III}_{x}(OH)_2]^{x+} \cdot [(x/n)(A^{n-})\cdot(m/n)H_2O]^{x-}$ where A is an anion (e.g., SO_4^{2-}, Cl^-, or CO_3^{2-}) (Abdelmoula et al., 1998). GRs are the intermediates formed during the corrosion of iron (McGill et al., 1976; Refait et al., 1998) and bioreduction of iron oxides (Fredrickson, et al., 1998; Glasauer et al., 2002; Ona-Nguema et al., 2002; Berthelin et al., 2006; O'Loughlin et al., 2007) as well as microbial oxidation of Fe (II) (Lack et al., 2002). They have been identified in anoxic soils (Abdelmoula et al., 1998; Feder et al., 2005) and iron permeable reactive barriers (PRBs) (Ritter et al., 2002).

GRs are strong natural reductants and they are capable of degrading a variety of

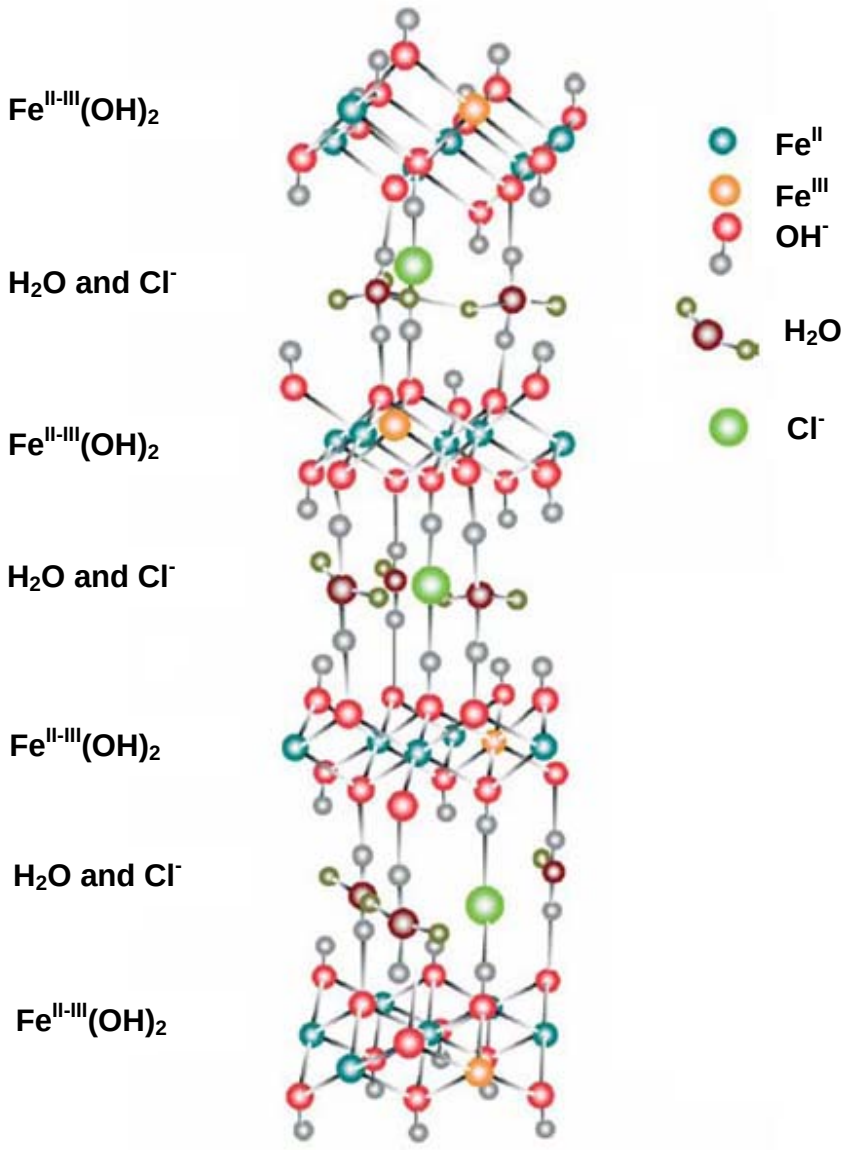

Figure 4.1. Layered crystal structure of GR-Cl with an interlayer thickness of 0.559 nm (Refait et al., 1998). Figure copied from Gẻnin and Ruby (2004).

groundwater contaminants including carbon tetrachloride (Erbs et al., 1999; O'Loughlin et al., 2003b), chlorinated ethanes (O'Loughlin and Burris, 2004), chloronitrobenzene (Elsner et al., 2004), chlorinated ethylenes (Lee and Batchelor, 2002; Maithreepala and

Doong, 2005; Liang et al., 2009), nitrate (Hansen and Koch, 1998), chromate (Williams and Scherer, 2001; Bond and Fendorf, 2003), uranium (VI) (O'Loughlin et al., 2003a), selenate (Myneni et al., 1997), and hexahydro-1,3,5-trinitro-1,3,5-triazine (RDX) (Larese-Casanova and Scherer, 2008).

There is little information about which reactive sites (external vs. interlayer) of GR-Cl are responsible for CT reduction. Hansen and Koch (1998) examined the reduction of $NaNO_3$ and $Ba(NO_3)_2$ by GR-SO_4. They found that the interlayer spacing did not change during the reduction of $NaNO_3$ by GR-SO_4 while the interlayer spacing decreased from 1.09 nm to 0.77 nm during the reaction of $Ba(NO_3)_2$ with the same mineral, suggesting that SO_4^{2-} was removed from the interlayers of the mineral. The intercalation of NO_3^- was facilitated by the precipitation of $BaSO_4$. In addition, 40-fold greater reaction rate of $Ba(NO_3)_2$ than $NaNO_3$ indicates that the reduction of $Ba(NO_3)_2$ occurred on both external and interlayer reactive sites, which was consistent with the ratio of 32 between total surface area (both external and interlayer surface) and external surface area. In a related study, Erbs et al. (1999) argued that CT might not penetrate GR-SO_4 interlayers and CT reduction may only occur on the external surface sites as CT reduction rate was very close to the reduction rate of $NaNO_3$ by GR-SO_4 in Hansen and Koch (1998). The affinity of LDHs for anions increases with the electric charge of the anion while decreasing with the radius of the anion (Miyata, 1983; Parker et al, 1983). Since CT is a highly nonpolar molecule without any electric charge and the radius of CT molecule is much greater than Cl^-, CT would not tend to extract Cl^- and have access to the reactive sites located in GR-Cl interlayers.

Natural organic matter (NOM) is widespread in groundwater and soil

environments (Larson and Weber, 1994; Kappler and Haderlein, 2003). NOM can be adsorbed on the surface of soil minerals (Tipping, 1981; McKnight et al., 1992; Gu et al., 1995; Kappler and Haderlein, 2003), and affect the fate and transport of contaminants. For example, increasing quantities of sorbed humic substances on hematite and kaolinite increased the sorption of anthracene, dibenzothiophene, and carbazole (Murphy et al., 1990). Degradation of CT, tetrachloroethylene, and trichloroethylene by zero-valent iron was inhibited in the presence of NOM (Tratnyek et al., 2001; Doong and Lai, 2005) due to competitive adsorption between the contaminant and NOM on the reactive sites of iron surface. Although little information exists on the adsorption of NOM on GRs, previous studies examined NOM adsorption on other LDHs (e.g., hydrotalcite $Mg_6Al_2(OH)_{16}CO_3.4H_2O$) which have a similar crystal structure found in GRs. Two major adsorption mechanisms were proposed including surface complex-ligand exchange and anion intercalation in interlayers via ion exchange (Seida and Nakano, 2000; Vreysen and Maes, 2008; Gasser et al., 2008). Adsorption of large NOM molecules may be inhibited as they cannot enter into the interlayers due to limited interlayer spacing of LDHs (Seida and Nakano, 2000).

Previous studies showed that the diffusion of anions into the interlayers of LDHs is typically completed in hours. In Barriga et al. (2002), the equilibrium time was 2 hours for 2, 4, 6-trinitrophenol (TNP) adsorption on MgFeCl type LDH. The combined thickness of Mg(II)-Fe(III) hydroxide layer and interlayer (C_0) increased from 0.78 nm to 1.36 nm, suggesting the presence of TNP anions in the interlayer. You et al. (2002) investigated the adsorption of large anionic surfactants on MgAlCl type LDH, including sodium octylsulfate, sodium dodecylsulfate, sodium 4-octylbenzenesulfonate, sodium

dodecylbenzenesulfonate. After mixing surfactants with the mineral suspension for 16 hours, the combined thickness (C_0) expanded from 0.79 nm to 2.27-3.08 nm, depending on the intercalated surfactant in the interlayers.

For groundwater remediation, LDHs show promise as adsorbents for the removal of harmful oxyanions such as arsenate, chromate, and phosphate (Goh et al., 2008) as well as benzenecarboxylates (Sato and Okuwak, 1991). These findings suggest that GRs may also have strong adsorption capacity for NOM since NOM is present as anions under neutral conditions and green rusts are common LDHs. The hypothesis of our research was that competitive adsorption between CT and NOM on the surface reactive sites of GRs would decrease the degradation rate of CT. Our research objectives were (1) to investigate the effects of different functional groups on NOM adsorption; (2) to quantify the relative contributions of ligand exchange and intercalation to NOM adsorption; and (3) to measure the reaction kinetics of CT by GRs in the absence/presence of NOM. We chose small organic acids (Figure 4.2) as model NOM compounds, which are composed of some functional groups (e.g., carboxylic, hydroxyl, and phenolic groups) typically present in the molecular structure of NOM (Greenland and Hayes, 1978; Simpson et al., 2001). We selected GR-Cl because it is more reactive than GR-SO_4 with chlorinated hydrocarbons (Liang et al., 2009) and it is more stable than GR-CO_3 (Bond and Fendorf, 2003) (Our preliminary experiments showed GR-CO_3 quickly decomposed to magnetite at pH 8 within 24 hours under anaerobic conditions) . To our knowledge, previous studies investigated the effects of NOM on the degradation of CT only in the following systems: FeS (Schwarzenbach et al., 1990), aqueous solutions of Fe^{+2} and HS^- (Curtis and Reinhard, 1994), zero valent iron (Tratnyek et al., 2001), and FeS coated goethite

(Hanoch et al., 2006).

4.2. Experimental Section

4.2.1. Materials

The following chemicals were obtained from Sigma-Aldrich: $FeCl_2 \cdot 4H_2O$ (99%), CT (99.9%), chloroform (CF) (99.9%), benzoic acid, benzene-1,2-dicarboxylic acid (phthalic acid), benzene-1,3,5-tricarboxylic acid (trimesic acid), benzene-1,2,4,5-tetracarboxylic acid (pyromellitic acid), benzene hexacarboxylic acid (mellitic acid), 4-hydroxy-benzoic acid, 3,5-dihydroxybenzoic acid (α-resorcylic acid), 3, 4-dihydroxycinnamic acid (caffeic acid), phenylacetic acid, and 4-phenylbutanoic acid.

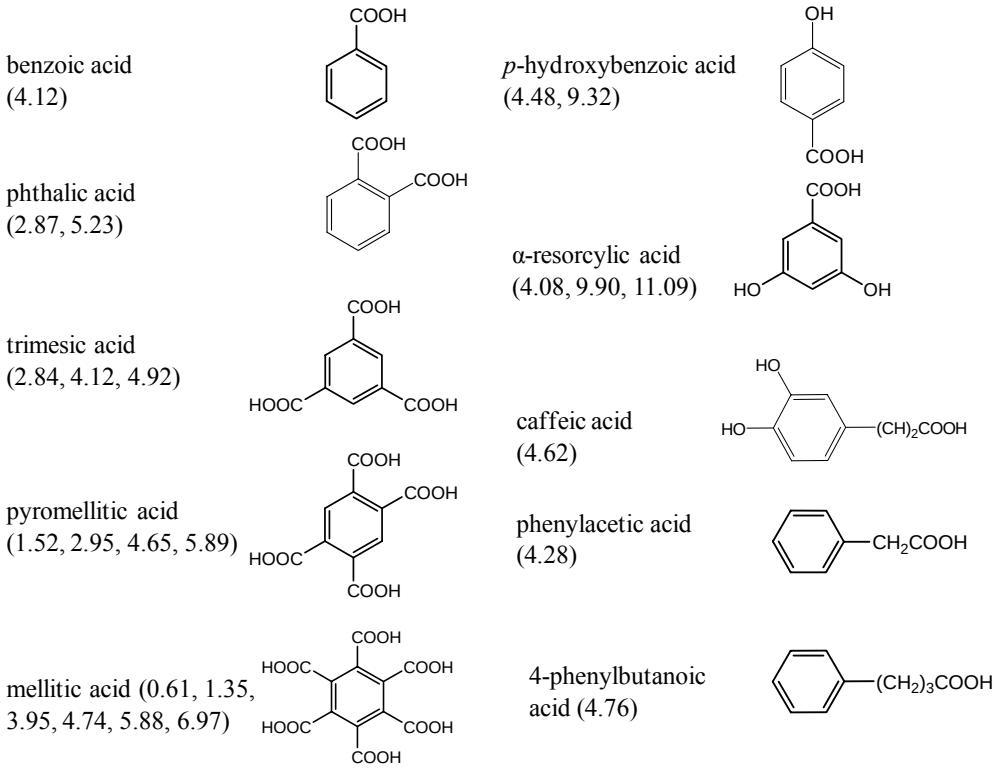

Figure 4.2. Molecular structure and pK_a values of model NOM compounds (Martell and Smith, 1974).

Methanol, hydrochloric acid, and sodium hydroxide were purchased from Fisher Scientific (Pittsburgh, PA). All aqueous solutions were prepared with Nanopure water (18.0 MΩ cm resistivity, Barnstead Ultrapure Water System, IA). GR-Cl was synthesized according to Refait et al. (1998) and characterized by X-ray diffraction (XRD) (Rigaku DMAX X-ray Diffractometer) after freeze-drying. The specific surface area (SSA) was 19.1 ± 1.5 m^2/g (the uncertainty represents one 95% confidence interval of the mean of two measurements), determined by BET surface analysis (Autosorb-1, Quantachrome Instruments, Boynton Beach, FL).

We concluded that the SSA of GR-Cl (19.1 ± 1.5 m^2/g) means the external surface area of the mineral due to several lines of evidence as below: (1) Rives (2001) calculated the external surface area of hydrotalcite (S_{ext}) using the equation:

$$S_{ext} = \frac{6}{D \times \delta} \tag{4.1}$$

where D is the average particle diameter (assuming spherical particles) and δ is the density of the mineral (Rives, 2001). The calculated S_{ext} value was 20 m^2/g, which is similar to the S_{ext} (21 m^2/g) determined by BET using N_2 adsorption (Labajos et al., 2002); (2) Most isotherms recorded during the process of BET surface area measurement for LDHs don't indicate the presence of micropores (Rives, 2001), despite the fact that the interlayer space can be seen as a pore; and (3) The ratio of Mg^{+2}/Al^{+3} that controls the occupancy of interlayer region by CO_3^{2-}, had no effect on the external surface area of the samples (Rives, 2001).

4.2.2. Adsorption Isotherms

Previous studies showed that the adsorption behavior of NOM on LDHs can be

described by Langmuir equation (Crepaldi et al., 2002; Gasser et al., 2008; Vreysen and Maes., 2008), which is expressed below:

$$q_e = \frac{q_{\text{max-Langmuir}} K C_e}{1 + K C_e} \tag{4.2}$$

Where C_e is the adsorbate concentration in the solution at equilibrium (mmol/L), q_e is the amount of adsorbate adsorbed on the solid at equilibrium (mmol adsorbate/ g adsorbent), $q_{\text{max-Langmuir}}$ is the maximum adsorption capacity at monolayer coverage (mmol adsorbate/ g adsorbent) and K is the adsorption equilibrium constant (L/mmol) that represents the affinity of adsorbent for adsorbate. Langmuir adsorption isotherm of mellitic acid using an initial concentration range from 0.1 mM to 5 mM (Figure 4.3) showed that four data points are on the plateau of the isotherm. Thus the remaining adsorption experiments were conducted using the maximum initial concentration less than 5 mM in order to collect more data points for isotherms at low coverage. Vials were prepared in an anaerobic chamber. An appropriate amount of GR-Cl was added to deoxygenated water, and 3 ml of the resulting GR-Cl slurry was added to each vial with an automatic pipet while the slurry was mixed vigorously on a magnetic stir plate. Vials were then spiked with deoxygenated NOM stock solution. The pH was adjusted to 8 using NaOH or HCl, and the ionic strength in all adsorption experiments was adjusted to 50 mM by adding NaCl. After preparation, vials were crimp sealed and placed on the continuous rotation shakers (Labquake, 8 rotations per min) in a constant temperature incubator at 25 °C with an equilibrium time of 24 hours, since preliminary tests showed that C_e did not change after 4 hours.

After equilibration, vials were centrifuged at 2016 relative centrifuge force (RCF)

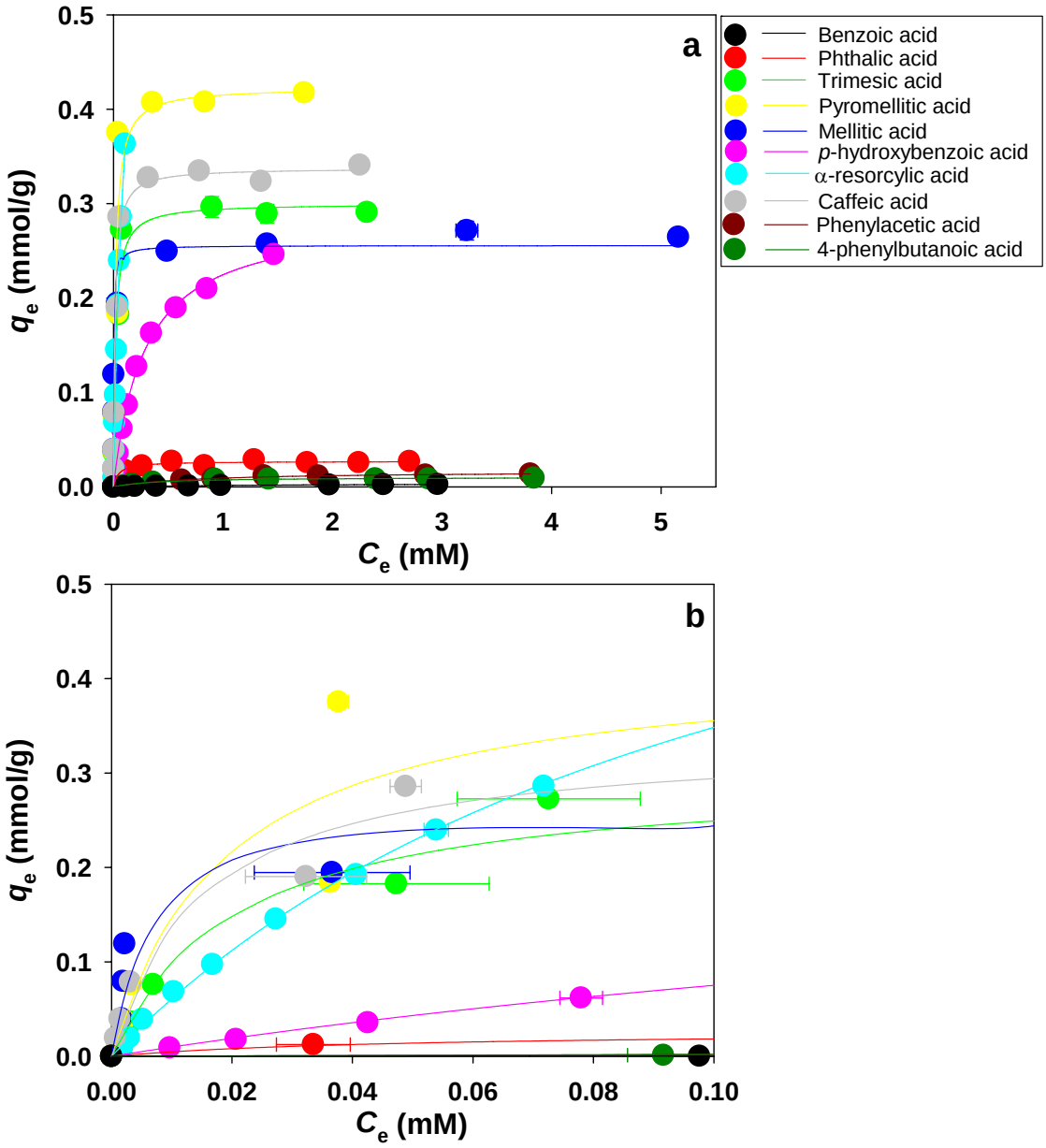

Figure 4.3. Adsorption isotherms of model NOM compounds (a) for Ce ranging from 0 to 5 mM; (b) for Ce ranging from 0 to 0.1 mM.

for 30 minutes (IEC Clinical Centrifuge-7R, International Equipment Co.), and the supernatant was transferred to 5 ml vials in the anaerobic chamber. The supernatant was acidified by adding 2 ml of 0.1 M HCl to avoid the oxidation of dissolved Fe (II) in

equilibrium with GR-Cl and precipitation as Fe(III) during the period of NOM measurement. Standards were similarly acidified in the same way as samples. Final pH was approximately 1.3. Then 5ml vials were taken out of the chamber, and UV absorbance spectra for each sample and standard were recorded between wavelengths of 200 and 400 nm at 0.5 nm intervals using a Shimadzu UV-1601 spectrophotometer. The aqueous concentrations of NOM model compounds were determined using multiwavelength analysis (Hari et al., 2005). Briefly, this method used 250-300 separate linear standard curves associated with each individual wavelength, covering a subset of scanned wavelengths where UV absorbance was observed for model NOM compounds. Total absorbance in samples at each wavelength was the sum of absorbance from each component in solution (NOM, Fe (II), and HCl). An aqueous concentration of a model NOM compound was obtained when the best fit was achieved between sample spectrum and predicted spectrum, which was generated by applying standard curves to a hypothetical concentration of the model NOM compound. The whole set of adsorption samples for each isotherm was done in triplicate, and standards were done in duplicate. Background of UV absorption in nano-pure water was corrected before measuring samples and standards.

4.2.3. Reductive Dechlorination of CT by GR in the Presence of NOM

When adding 2.5 mM of model NOM compounds to 10 g/L GR-Cl suspension, adsorption fractions of NOM ($q_e/q_{max\text{-}Langmuir}$) ranged from 5% to 97% on the basis of our calculations using the isotherm parameters given in Table 4.1. A wide range of adsorption fraction was desirable in order to discover the relationship between NOM

adsorption and CT degradation rate. For batch kinetic experiments, therefore, GR-Cl suspension (10g/L) containing a model NOM compound (2.5 mM) was stirred for 24 hours in the anaerobic chamber. Then the pH and ionic strength were subsequently adjusted to the same conditions to those for adsorption experiments (pH=8 and I=0.05 M). Eight mL of GR slurry was added to 8-ml serum vials in the same way to adsorption experiments, followed by spiking 80 μL of a 3.0×10^{-3} M CT stock solution (prepared in N_2-sparged methanol). The resulting initial concentration of CT was approximately 3.0×10^{-5} M. Vials were crimp sealed immediately in the anaerobic chamber and placed on the continuous rotation shakers at 25°C. Vials were free of headspace, and the initial aqueous concentration of CT was approximately 3.0×10^{-5} M. At regular intervals, vials were centrifuged at 2016 RCF for 10 minutes, decapped, and sampled. The values of pH were measured again for selected samples when kinetic experiments were complete, and pH ranged from 7.6-7.9.

CT and CF were quantified by gas chromatography (GC) with electron capture detection according to Hanoch et al. (2006). Briefly, CT and CF were extracted from aqueous phase to isooctane by adding 100 μL of the aqueous supernatant to 1000 μL of isooctane in 2 mL GC autosampler vials. One μL of the isooctane phase was injected in the splitless mode and analyzed using a Shimadzu GC-17A gas chromatograph (GC) with an Agilent J&W DB-624 capillary column (30 m × 0.53 mm × 3 μm) and electron capture detector (ECD). The injector temperature was 200 °C and the detector temperature was 250 °C. The oven temperature was initially 75 °C, and then ramped to 200 °C at 18 °C/min. External calibration standards were prepared in isooctane and analyzed daily as well as blank samples of isooctane. Relative standard deviations for

duplicate injections using this method were typically less than 1 %. Each GC vial was analyzed in duplicate and the peak areas averaged. Relative standard deviations for CT and CF between duplicate vials (measured for selected samples only) were typically less than 1%, which was considered acceptable.

4.3. Results and Discussion

4.3.1. Adsorption Isotherms

Evanko and Dzomback (1998) reported that humic and fulvic acid adsorption to goethite can be best modeled by compounds with structures common to pyromellitic acid (Figure 4.2) and 2,3-dihydroxybenzoic acid: adjacent phenolic groups, adjacent carboxylic groups, and highly acidic carboxylic groups. Accordingly, we selected the following NOM model compounds that have adjacent carboxylic groups, or adjacent phenolic groups: phthalic acid, pyromellitic acid, mellitic acid, and caffeic acid (Figure 4.2). In addition, Sato and Okuwaki (1991) found that the adsorption of benzenecarboxylate anions onto the interlayers of hydrotalcite increased with increasing charge density of the anions. Charge density means the specific electric charge per unit area of anions. Therefore, in order to study the role of interlayers in NOM adsorption, we also selected the remaining 7 compounds (Figure 4.3) with either different number of carboxylic groups and phenolic groups or aliphatic chains that result in different molecular size. These 7 compounds would have different charge densities in aqueous solution at pH 8.

According to the pK_a values reported in Figure 4.2 (Martell and Smith, 1974), all model NOM compounds were present as anions in the solution at pH 8. Plots of q_e

versus C_e for NOM adsorption on GR-Cl are shown in Figure 4.3, and adsorption isotherms fitted Langmuir equation very well. K is proportional to the slope of the isotherm at low coverage (Figure 4.3). K and $q_{max\text{-}Langmuir}$ were quantified by non-linear regression of q_e versus C_e data using SigmaPlot version 9. The adsorption parameters are listed in Table 4.1.

Compounds benzoic acid, phthalic acid, trimesic acid, pyromellitic acid, and mellitic acid, which each have more carboxylic acid groups than previous compounds (see Figure 4.2), had successively higher K values (see Table 4.1). Adsorption of benzoic acid was negligible while mellitic acid containing 6 carboxylic groups has the greatest K value (218 ± 127 L/mmol) among all model NOM compounds shown in Figure 4.2. As in previous studies (Sato and Okuwaki, 1991; Edwards et al., 1996; Evanko and Dzombak, 1998), the number of carboxylic functional groups strongly influenced the tendency for NOM adsorption to GR-Cl.

A variety of surface complexes can be formed between carboxylic groups and surface iron atoms of goethite, depending on the number and position of carboxylic groups present in NOM (Evanko and Dzombak, 1998). Similar surface complexes may be also formed during NOM adsorption on the surface of GR-Cl. In addition, ion exchange between NOM anions and Cl^- in the interlayers of GR-Cl may also lead to the adsorption of NOM on GR-Cl. Ulibarri et al. (1995) discovered the presence of trinitrophenol in the interlayers of chloride hydrotalcite using XRD analysis. The ion exchange equilibrium constants for hydrotalcites follow the order $SO_4^{2-} > F^- > HPO_4^{2-} > Cl^- > B(OH)_4^- > NO_3^-$ as anions with higher negative charges and smaller radii are preferable to be intercalated in the interlayers (Parker et al., 1983). For NOM model

Table 4.1. Langmuir adsorption constants, maximum adsorption capacity, anion occupation area, theoretical maximum coverage, rate constants, and chloroform (CF) yields.

NOM	K [a] (L/mmol)	$q_{max\text{-}Langmuir}$ [a] (mmol/g)	Anion occupation area (nm^2) [b]	$q_{max\text{-}BET}$ (mmol/g) [c]	k_{SA} (L m^{-2} h^{-1}) [c]	CF Yield [c] (%)
no NOM	N/A[d]	N/A	N/A	N/A	$(6.23 \pm 0.76)\times10^{-3}$	93.6 ± 4.8
benzoic acid	0.58 ± 0.13	$(4.18 \pm 0.44)\times10^{-3}$	0.29	$(11.1 \pm 0.89)\times10^{-2}$	$(5.34 \pm 0.58)\times10^{-3}$	89.7 ± 5.6
phthalic acid	21 ± 11	$(2.7 \pm 0.19)\times10^{-2}$	0.36	$(8.91 \pm 0.71)\times10^{-2}$	$(2.11 \pm 0.19)\times10^{-3}$	97.6 ± 5.3
trimesic acid	49 ± 23	$(3.00 \pm 0.25)\times10^{-1}$	0.61	$(5.23 \pm 0.42)\times10^{-2}$	$(3.26 \pm 0.35)\times10^{-3}$	100.8 ± 6.4
pyromellitic acid	53 ± 49	$(4.23 \pm 0.74)\times10^{-1}$	0.61	$(5.23 \pm 0.42)\times10^{-2}$	$(3.59 \pm 0.35)\times10^{-3}$	95.8 ± 5.1
mellitic acid	218 ± 127	$(2.56 \pm 0.25)\times10^{-1}$	0.61	$(5.23 \pm 0.42)\times10^{-2}$	$(2.31 \pm 0.25)\times10^{-4}$	94.2 ± 6.1
p-hydroxybenzoic acid	3.52 ± 0.38	$(2.88 \pm 0.11)\times10^{-1}$	0.27	$(11.80 \pm 0.94)\times10^{-2}$	$(3.68 \pm 0.38)\times10^{-3}$	99.0 ± 4.8
α-resorcylic acid	9.0 ± 1.2	$(7.36 \pm 0.60)\times10^{-1}$	0.61	$(5.23 \pm 0.42)\times10^{-2}$	$(3.79 \pm 0.41)\times10^{-3}$	97.3 ± 5.5
caffeic acid	68 ± 32	$(3.38 \pm 0.24)\times10^{-1}$	0.52	$(6.09 \pm 0.49)\times10^{-2}$	$(2.30 \pm 0.22)\times10^{-2}$	70.8 ± 4.5
phenylacetic acid	1.31 ± 0.47	$(1.65 \pm 0.19)\times10^{-2}$	0.31	$(10.24 \pm 0.82)\times10^{-2}$	$(2.57 \pm 0.27)\times10^{-3}$	104.8 ± 4.1
4-phenybutanoic acid	2.5 ± 1.1	$(1.03 \pm 0.11)\times10^{-2}$	0.43	$(7.43 \pm 0.59)\times10^{-2}$	$(2.96 \pm 0.28)\times10^{-3}$	95.6 ± 6.9

[a] Uncertainties are 95% confidence intervals calculated by nonlinear regression; [b] See Appendix C for calculation method of anion occupation area; [c] Uncertainties are 95% confidence intervals calculated by propagation of error; [d] NA: not applicable.

compounds with similar molecular size, the one containing multiple carboxylic groups may be easier to replace Cl^- ions and enter into the interlayers of GR-Cl.

In addition to carboxylic groups, phenolic groups are often present in NOM. For *p*-hydroxybenzoic acid, α-resorcylic acid, and caffeic acid (Figure 4.2), we observed much greater *K* value for caffeic acid than for other phenolic compounds (Table 4.1), suggesting that the adsorption behavior of caffeic acid was different from *p*-hydroxybenzoic acid and α-resorcylic acid. The *pK*a values of these compounds (Table 4.1) indicate that they all have one negative charge at pH 8. The difference in the positions of functional groups may play an important role in the adsorption of NOM. NOM with functional groups (e.g., carboxylic or phenolic groups) in *ortho*- positions are more adsorbed than one with single group or multiple groups in *meta*- and *para*- positions (Davis, 1982). Caffeic acid has two adjacent phenolic groups, which may lead to the formation of bidentate organic ligand on the surface of goethite (Evanko and Dzombak, 1998). This may be the reason for much greater *K* value of caffeic acid relative to *p*-hydroxybenzoic acid and α-resorcylic acid. Next, we considered the influence of aliphatic chain length on the tendency to adsorb to the surface. Similar *K* values between phenylacetic acid and 4-phenybutanoic acid (Table 4.1) indicates that small differences in aliphatic chains length have negligible effects on the adsorption of NOM on GR-Cl.

Previous studies proposed that two major adsorption mechanisms are responsible for the adsorption of NOM on LDHs: (1) adsorption on the external surface via ligand exchange, and (2) adsorption in the interlayers via anion intercalation (Seida and Nakano, 2000; Vreysen and Maes, 2008; Gasser et al., 2008). Assuming that terephthalate anions would be adsorbed in a flat position in relation to hydrotalcite, Crepaldi et al. (2002) calculated the theoretical maximum amount (q_{max}-

$_{BET}$) that can be adsorbed on the external surface of hydrotalcite according to the BET external surface area of the mineral and the cross section area of the terephthalate anion. The value of $q_{max\text{-}BET}$ (0.47 mmol/g) was close to the maximum adsorption capacity $q_{max\text{-}Langmuir}$ (0.52 mmol/g) obtained from Langmuir isotherm, suggesting that terephthalate anions were only adsorbed on the external surface of hydrotalcite. This was supported by XRD patterns of the hydrotalcite, which demonstrated no structural change of the mineral during adsorption process. If terephthalate anions were intercalated in the interlayers, changes in the basal repeat distance of hydrotalcite crystal structure, which can be determined by XRD analysis, would be expected. The same approach was used to calculate the theoretical maximum amount ($q_{max\text{-}BET}$) for NOM adsorption on external surface of GR-Cl by using BET specific surface area of the mineral and the occupation area of NOM anions, which were estimated on the basis of the values of bond lengths and the bonding angles (Sato and Okuwaki, 1991). Calculated $q_{max\text{-}BET}$ values and occupation areas of anion are given in Table 4.1.

Since the size of NOM compound is comparable (Figure 4.2), the electric charge of the anions may be more related with the adsorption behavior of NOM. Benzoic acid, phthalic acid, phenylacetic acid, and 4-phenybutanoic acid have one negative charge when the reaction solution is at pH 8, which may lead to the difficulty in the intercalation of these compounds into GR-Cl interlayers. Our calculated results that $q_{max\text{-}Langmuir} < q_{max\text{-}BET}$ for these four compounds (Table 4.1), suggests the possibility that adsorption on the external surface might be a preferable adsorption behavior. Some NOM compounds (Figure 4.2) show high electric charges when they are present at pH 8, including trimesic acid, pyromellitic acid, and mellitic acid. High electric charges would facilitate NOM anions adsorbed in the

interlayers since the electrostatics is the major factor holding anions in the interlayers. For these NOM compounds, $q_{\text{max-Langmuir}} > q_{\text{max-BET}}$ (Table 4.1), which suggests the possibility that part of NOM is adsorbed in the interlayers of GR-Cl via anion intercalation in addition to the adsorption on the external surface. Interestingly, our calculated results shows that $q_{\text{max-Langmuir}} > q_{\text{max-BET}}$ for compounds like *p*-hydroxybenzoic acid and α-resorcylic acid, which have the same electric charge as benzoic acid at pH 8. The different relationship of $q_{\text{max-Langmuir}}$ and $q_{\text{max-BET}}$ among these compounds indicates other factors (e.g., functional groups of NOM) also play a role in NOM adsorption on GR-Cl.

4.3.2. Effects of NOM Adsorption on CT Reduction

Figure 4.4 shows that CT degradation by GR-Cl followed pseudo-first order kinetics at pH 8 in the absence/presence of 2.5 mM of model NOM compounds. Surface area normalized pseudo-first-order rate constants (k_{SA}) are calculated by using observed rate constants divided by mineral surface area loading. All k_{SA} values are reported in Table 4.1. The relatively small uncertainties associated with k_{SA} values provide the evidence for good pseudo-first-order fits. CF yields were calculated using the concentration of CF divided by the concentration of CT transformed at the end of the reaction, and given in Table 4.1. CF yields in this study ranged from 70.8% to 104.8%. The reduction of CT has been shown to be coupled with the oxidation of GR-SO_4, resulting in the formation of chloroform (CF) and magnetite (Erbs et al., 1999). Similar reaction may take place in this study. The k_{SA} for CT reduction by GR-Cl without NOM in our system ($(6.23\pm 0.76)\times10^{-3}$ L/m^2 h) is approximately 7-fold greater than the rate constant for CT removal by GR-SO_4 (8.6×10^{-4} L/m^2 h) reported by O'Loughlin et al. (2003b). The difference might be explained by a larger ratio of

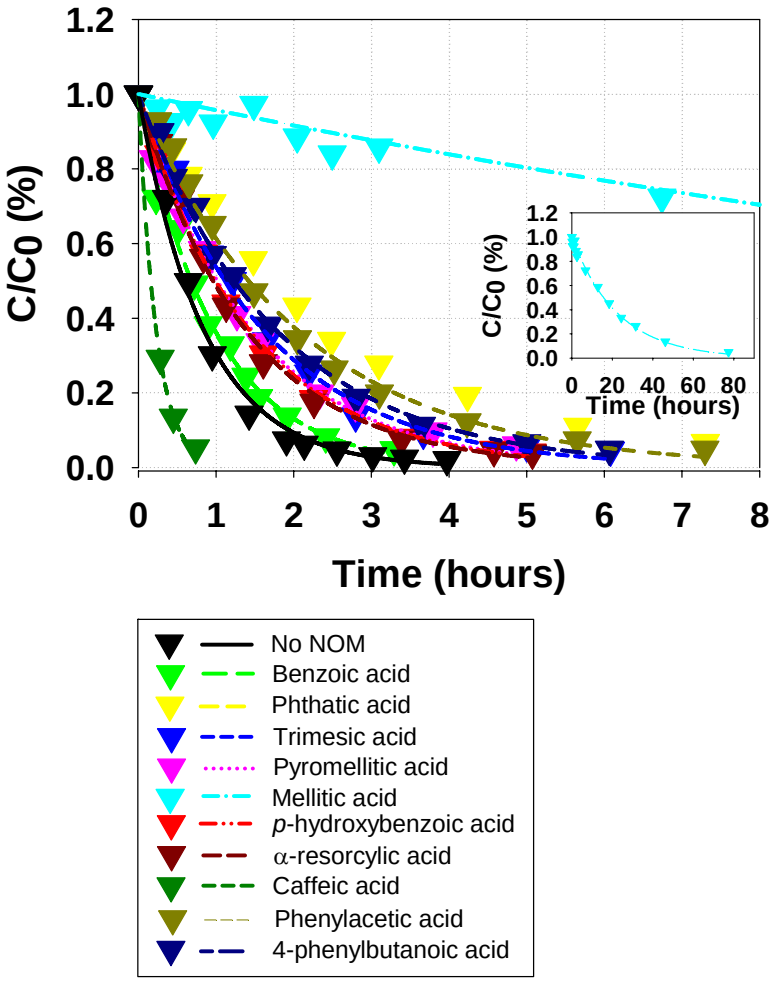

Figure 4.4. Effects of NOM on the reductive dechlorination of CT by GR-Cl at pH 8. Lines represents a pseudo-first-order model fit. The inset shows the reduction of CT by GR-Cl in the presence of mellitic acid.

Fe (II) to Fe (III) for GR-Cl than for GR-SO_4.

Most model NOM compounds significantly decreased the rate constants of CT degradation (Figure 4.4, Table 4.1). Mellitic acid had the largest effect on inhibiting CT degradation with the reaction rate one order of magnitude smaller than for CT degradation by GR-Cl alone (no NOM). Similar inhibitory effect of NOM on CT reduction was also noticed for CT reduction by zero valent iron in the presence of several humic acids (Tratnyek et al., 2001). Competitive adsorption between NOM and CT may be the reason for the inhibitory effect of NOM. Another interesting

observation is that caffeic acid significantly accelerated the rate constant for CT by a factor of 4, compared to the case when no NOM was present (Table 4.1). This might be attributed to the increased concentration of surface bound Fe(II) resulting from the reduction of Fe(III) by caffeic acid (Deiana et al., 1992, 1995). This speculation is in agreement with enhanced reduction of CT by surface bound Fe(II) on iron minerals reported by Elsner et al. (2004). Similar to caffeic acid, the reduction of soil Fe and Mn oxides was observed in the presence of the following phenolic acids: vanillic, ferulic, syringic, and sinapic acids (Lehmann et al., 1987). In addition, NOM can act as oxidizing agents. Schwarzenback et al. (1990) observed the reduction of NOM and the formation of highly reactive reduced intermediates in the presence of FeS.

4.4. Environmental Significance

Since reaction rates for abiotic and microbial reductive dechlorination of CT are comparable (Shao and Butler, 2009b), both dechlorination processes should be considered for *in-situ* CT remediation. The rate constant for CT reduction by GR-Cl in this study is generally larger than those for CT reduction with other minerals under similar conditions (magnetite and GR-SO_4), except poorly crystalline mackinawite (Butler and Hayes, 2000; McCormick et al., 2002; O'Loughlin et al., 2003; Danielsen and Hayes, 2004). Hence, GR-Cl may have a potential to contribute to the natural attenuation of CT in iron-rich subsurface environments. In addition, GR-Cl may occur on iron PRBs during the corrosion process (Refait et al., 1998), and may influence treatment capacity of the PRBs.

Effects of NOM adsorption on the reduction of CT are compound-dependent. Since NOM can be best represented by the compounds with adjacent phenolic groups, adjacent carboxylic groups, and highly acidic carboxylic groups (Evanko

and Dzomback, 1998), the influence of NOM on the degradation of CT by GR-Cl at field sites could be modeled by CT reaction with GR-Cl in the presence of pyromellitic acid. Another issue environmental regulators and engineers should pay attention to is that CT is primarily transformed to chloroform, the least desirable reaction product, during GR-Cl mediated dechlorination (both alone and with the addition of NOM).

CHAPTER 5

Conclusions and Recommendations

5.1. Conclusions

This dissertation investigated reductive dechlorination of PCE, TCE, and CT in the abiotic systems. In Chapter 2, kinetic and isotope analyses of PCE and TCE degradation by iron minerals were examined. In Chapter 3, we evaluated the relative contribution of abiotic and microbial processes to the degradation of PCE and TCE in well-defined anaerobic microcosms. In Chapter 4, we demonstrated the effects of NOM on the degradation of CT by GR-Cl. Our major findings are summarized below:

1. Three minerals are reactive for both PCE and TCE abiotic transformation, including FeS, GR-Cl, and pyrite, in which FeS is the most reactive mineral. In contrast, magnetite, GR-SO_4, Fe(II) and S(-II) treated goethite have poor reactivities for both PCE and TCE.
2. Mineral mediated dechlorination of PCE and TCE was associated with very negative ε_{bulk} (in ‰) values ranging from -24.6 ± 1.1 to -30.2 ± 4.3 for PCE and, -21.7 ± 1.0 to -33.4 ± 1.5 for TCE. ε_{bulk} (in ‰) values for abiotic PCE and TCE transformation are generally more negative than those for PCE and TCE biodegradation.
3. Abiotic reductive dechlorination of PCE and TCE was dominant under the iron-reducing conditions at pH 8.2 for Duck Pond microcosms and for Landfill microcosms, which suggests that abiotic transformation could outweigh biodegradation under iron reducing condition with high pH for *in-situ* degradation of PCE and TCE. Comparable abiotic and biotic transformation was observed in five microcosms, among which four microcosms were conduct at pH 8.2. This

provides additional evidence that at least in some cases high pH (8.2) may inhibit the growth of dechlorinating bacteria. In addition, no abiotic reaction products were detected in the three microcosms that typically had lower concentrations of Fe(II) or S(-II) species than did microcosms preincubated under iron or sulfate reducing conditions. This suggests that Fe(II) and S(-II) species are play a great role in abiotic transformation of PCE and TCE.

4. The number and positions of carboxylic and phenolic groups can considerably affect the adsorption of NOM on GR-Cl, and adjacent carboxylic or phenolic groups are mainly responsible for strong adsorption of NOM on the mineral.
5. NOM may be either solely adsorbed on the external surface of GR-Cl or adsorbed on both external and interlayer sites, partly depending on the electric charge density of NOM.
6. The degradation of CT by GR-Cl was inhibited with the addition of model NOM compounds except caffeic acid, partly due to competitive adsorption on reactive sites between NOM and CT.

5.2. Recommendations for Practice

1. Very large negative ε_{bulk} values for abiotic PCE and TCE transformation can be used as one line of evidence to evaluate abiotic degradation at field sites. Other lines of evidence (e.g., identification and isotope analysis of reaction products) are also needed in order to make the better assessment of contaminants fate.
2. Conclusion 3 suggests that stimulation of the formation of biogenic reactive minerals under iron-reducing condition at high pH could promote abiotic natural attenuation of PCE and TCE, which lead primarily to the environmental benign degradation product, acetylene.

5.3. Recommendations for Future Research

1. Previous studies reported that all PCE was transformed to TCE by Ag modified green rust. In contrast, PCE was completely converted to ethane without detecting any TCE in the presence of Cu modified green rust. Isotope analyses for these experiments would be helpful to determine ε_{bulk} values resulting from each individual pathway (hydrogenolysis or reductive β-elimination) during abiotic reductive dechlorination of PCE. Measurements of ε_{bulk} values from each individual pathway can give us a clue on the relative contributions of each pathway to isotope fractionation during abiotic PCE transformation. Thus isotope fractionation associated with each individual pathway can be determined on the basis of ε_{bulk} values for PCE from batch experiments, which simulate actual field conditions at contaminated sites. Given this information, environmental regulators and engineers can assess the amount of PCE that is degraded to acetylene via reductive β-elimination, or TCE via hydrogenolysis. This will facilitate more accurate application of natural attenuation as a remediation measure for PCE contaminated sites since traditional methods have trouble in quantifying acetylene at field sites and acetylene may be transformed to ethylene by bacteria or minerals.
2. The point of zero charge (PZC) is a key parameter for minerals, which can provide useful information on whether anions or cations can be adsorbed on the mineral surface at a certain pH. Similarly, the total surface area of green rusts (both external surface and interlayer surface) can give us a clue on theoretical maximum amount of anionic contaminants that can be adsorbed on both external and interlayers sites. Given these two parameters, one can better understand the adsorption of NOM and anionic contaminants like arsenic and chromate on green

rusts. This is critical to assess green rusts associated degradation at contaminated sites. Accordingly, further work to measure the point of zero charge and the total surface area for green rusts are needed.

3. Stable isotope analyses have been performed extensively for abiotic and biotic dechlorination of chlorinated hydrocarbons. However, only two or three papers reported the isotope fractionation of explosive contaminants like RDX (hexahydro-1,3,5-trinitro-1,3,5 trizaine) and TNT(trinitrotoluene). To our knowledge, no studies on isotope fractionation during abiotic transformation of these explosives have been performed. Zero valent iron and iron minerals like magnetite and green rusts are capable of degrading them with great reaction rates. For instance, to reach 95% of RDX degradation, mineral mediated degradation takes a couple of hours while biodegradation takes a couple of days and even several months in some cases. Based on the reaction rates, abiotic transformation may be more important than biodegradation to natural attenuation of RDX. Quantification of isotope fractionation of RDX during abiotic transformation is essential for application of isotope analysis in the assessment of natural attenuation of RDX, since abiotic degradation could be a dominant process responsible for the natural attenuation of RDX. In addition, abiotic reactions take place on the mineral surface. In contrast, biodegradation processes are more complex and involve many steps (see equation 1.3). Some steps may dilute or mask intrinsic isotope effects resulting from bond cleavage and cause the observed isotope fractionation to be different from those for abiotic transformation. Isotope analyses may be used as a tool to distinguish abiotic transformation from biodegradation of RDX or other explosive contaminants. Consequently, future efforts to quantify the isotope fractionation during abiotic transformation of explosive contaminants are desirable.

Batch experiments can be conducted in laboratory to determine typical ε_{bulk} values for RDX reduction by naturally occurring Fe(II)-bearing minerals (e.g., FeS, pyrite, green rusts, magnetite). Then we can compare them with ε_{bulk} values observed from RDX biodegradation. If we discover an apparent gap in ε_{bulk} values between abiotic and biotic degradation of RDX, isotope analyses in field samples may tell us: (1) which degradation process is dominant (abiotic versus biotic), and (2) the extent of RDX degradation at sites by using an open system Rayleigh equation which assesses both degradation and dispersion/dilution contribution to natural attenuation of contaminants.

REFERENCES

Abdelmoula, M., Trolard, F., Bourrie, G., Génin, J. M. R., 1998. Evidence for the Fe(II)-Fe(III) green rust "Fougerite" mineral occurrence in a hydromorphic soil and its transformation with depth. Hyperfine Interact. 112, 235-238.

Abe, Y., Hunkeler, D., 2006. Does the Rayleigh equation apply to evaluate field isotope data in contaminant hydrogeology? Environ. Sci. Technol. 40, 1588-1596.

Alvarez, P.J.J., Illman, W.A., 2006. Bioremediation and Natural attenuation: Process Fundamentals and Mathematical Models. John Wiley&Son Inc., New Jersey.

Amonette, J. E., Workman, D. J., Kennedy, D. W., Fruchter, J. S.,Gorby, Y. A., 2000. Dechlorination of carbon tetrachloride by Fe(II) associated with goethite. Environ. Sci. Technol. 34, 4606-4613.

Arnold, W. A., Ball, W. P., Roberts, A. L., 1999. Polychlorinated ethane reactions with zero-valent zinc: pathways and rate control. J. Contam. Hydrol. 40, 183-200.

Arnold, W. A., Roberts, A. L., 2000. Pathways and kinetics of chlorinated ethylene and chlorinated acetylene reaction with Fe(0) particles. Environ. Sci. Technol. 34, 1794-1805.

Assaf-Anid, N., Lin, K., 2002. Carbon tetrachloride reduction by Fe^{2+}, S^{2-}, and FeS with vitamin B12 as organic amendment. J. Environ. Engin. 128, 94-99.

Atkinson, R. J., Posner, A. M., Quirk, J. P., 1967. Adsorption of potential determining ions at the ferric oxide-aqueous electrolyte interface. J. Phys. Chem-US. 71, 550-558.

Baciocchi, E., 1983.1,2-Dehalogenations and Related Reactions, in Patai, S., Rappoport, Z Eds., *The Chemistry of Halides, Pseudo-Halides and Azides, Supplement D to the Chemistry of Functional Groups*, Wiley: New York, pp. 161-201.

Bagley, D. M., Gossett, J. M., 1990. Tetrachloroethylene transformation to trichloroethylene and cis-1,2-dichloroethylene by sulfate-reducing enrichment cultures. Appl. Environ. Microbiol. 56, 2511-2516

Barbash, J. E., Reinhard, M., 1989. Abiotic dehalogenation of 1, 2-dichloroethane and 1, 2-dibromoethane in aqueous solution containing hydrogen sulfide. Environ. Sci. Technol. 23, 1349-1358.

Barth, J. A. C., Slater, G. F., Schüth, C., Bill, M., Downey, A., Larkin, M. J., Kalin, R. M., 2002. Carbon isotope fractionation during aerobic biodegradation of trichloroethene by Burkholderia Cepacia G4: a tool to map degradation mechanisms, Appl. Environ. Microbiol. 68, 1728-1734.

Bekins, B., Rittmann, B. E., MacDonald, J. A., 2001. Natural attenuation strategy for groundwater cleanup focuses on demonstrating cause and effect. EOS, Transactions, American Geophysical Union 82.

Beneteau, K. M., Aravena, R., Frape, S. K., 1999. Isotopic characterization of chlorinated solvents- laboratory and field results, Org. Geochem. 30, 739-753.

Benjamin, M. Chang, Y.-J. Li, C. -W., Korshin, G., 1993. NOM adsorption onto iron-oxide coated sand. American Water Works Association Research Foundation, Denver, CO.

Benning, L. G., Wilkin, R. T., Barnes, H. L., 2000. Reaction pathways in the Fe-S system below 100 ºC. Chem. Geol. 167, 25-51.

Berner, R. A., 1967. Thermodynamic stability of sedimentary iron sulphides. Am. J. Sci. 265, 773-785.

Berthelin, J., Ona-Nguema, G., Stemmler, S., Quantin, C., Abdelmoula, M., Jorand, F., 2006. Bioreduction of ferric species and biogenesis of green rusts in soils. Comptes Rendus Geoscience, 338, 447-455.

Bhatt, P., Kumar, M. S., Mudliar, S., Chakrabarti, T., 2007. Biodegradation of chlorinated compounds-a review. Crit. Rev. Environ. Sci. Technol. 37, 165-198.

Bierwagen, B. G., Keller, A. A., 2001. Measurement of Henry's law constant for methyl tert-butyl ether using solid-phase microextraction. Environ. Toxicol. Chem. 20, 1625-1629.

Bjerg, P. L., Rügge, K., Cortsen, J., Nielsen, P. H., and Christensen, T. H., 1999. Degradation of aromatic and chlorinated aliphatic hydrocarbons in the anaerobic part of the grindsted landfill leachate plume: In situ microcosm and laboratory batch experiments. Ground Water 37, 113-121.

Bloom, Y., Aravena, R., Hunkeler, D., Edwards, E., Frape, S. K., 2000. Carbon isotope fractionation during microbial dechlorination of trichloroethene, cis-1,2-dichloroethene, and vinyl chloride: implications for assessment of natural attenuation. Environ. Sci. Technol. 34, 2768-2772.

Bond, D.L., Fendorf, S., 2003. Kinetics and structure constraints of chromate reduction by green rusts. Environ. Sci. Technol. 37, 2750-2757.

Boopathy, R., Peters, R., 2001. Enhanced biotransformation of trichloroethylene under mixed electron acceptor conditions. Curr. Microbiol. 42, 134-138.

Bouwer, E. J., McCarty, P. L., 1983. Transformation of halogenated organic compounds under denitrification conditions. Appl. Environ. Microbiol. 45, 1295-1299.

Bouwer, E. J., Wright, J. P., 1988. Transformations of trace halogenated aliphatics in anoxic biofilm columns. J. Contam. Hydrol. 2, 155-169.

Bradley, P. M., 2003. History and ecology of chloroethene biodegradation: a review. Biorem. J. 7, 81-109.

Brindley, G. W., Bish, D. L., Mackay, A. L., 1976. Green rust: Apyroauritetype structure. Nature 263, 353-354.

Brown, R.A., Hines, R., Leahy, M. C., J. Cho., J. 2006. Abiotic and biotic pathways in chlorinated solvent natural attenuation. In *Remediation of Chlorinated and Recalcitrant Compounds*. Proceedings of the Fifth International Conference on Remediation of Chlorinated and Recalcitrant Compounds, Monterey, CA. May 2006. Battelle Press. Columbus, OH, CD-ROM, 8 pp.

Brungard, K. L., Munakata-Marr, J., Johnson, C. A., Mandernack, K. W., 2003. Stable carbon isotope fractionation of trans-1,2- dichloroethylene during co-metabolic degradation by methanotrophic bacteria. Chem. Geol. 195, 59-67.

Burris, D.R., Antworth, C.P., 1992. In situ modification of an aquifer material by a cationic surfactant to enhance retardation of organic contaminants. J. Contam. Hydrol. 10, 325-337.

Burris, D. R., Delcomyn, C. A., Smith, M. H., Roberts, A. L., 1996. Reductive dechlorination of tetrachloroethylene and trichloroethylene catalyzed by vitamin B_{12} in homogeneous and heterogeneous systems. Environ. Sci. Technol. 30, 3047-3052.

Butler, E. C., Hayes, K. F., 1998. Effects of solution composition and pH on the reductive dechlorination of hexachloroethane by iron sulfide. Environ. Sci. Technol. 32, 1276-1284.

Butler, E. C., Hayes, K. F., 1999. Kinetics of the transformation of trichloroethylene and tetrachloroethylene by iron sulfide. Environ. Sci. Technol. 33, 2021-2027.

Butler, E. C., Hayes, K. F., 2000. Kinetics of the transformation of halogenated aliphatic compounds by iron sulfide. Environ. Sci. Technol. 34, 422–429.

Butler, E. C., Hayes, K. F., 2001. Factors influencing rates and products in the transformation of trichloroethylene by iron sulfide and iron metal. Environ. Sci. Technol. 35, 3884-3891.

Canfield, D. E., Raiswell, R., Westrich, J. T., Reaves, C. M., Berner, R. A., 1986. The use of chromium reduction in the analysis of reduced inorganic sulfur in sediments and shales. Chem. Geol. 54, 149-155.

Carlson, D. L., McGuire, M. M., Roberts, A. L., Fairbrother, D. H., 2003. Influence of surface composition on the kinetics of alachlor reduction by iron pyrite. Environ. Sci. Technol. 37, 2394-2399.

Charlet, L., Silvester, E., Liger, E., 1998. N-compounds reduction and actinide immobilization in surficial fluids by Fe(II): the surface ≡FeIIIOFeIIOH° species, as major reductant. Chem. Geol. 151, 85-93.

Chartrand, M.M.G., Waller, A., Mattes, T.E., Elsner, M., Lacrampe-Couloume, G. Gossett, J.M., Edwards, E.A., Sherwood Lollar, B., 2005. Carbon isotopic fractionation during aerobic vinyl chloride degradation, Environ. Sci. Technol. 39, 1064–1070.

Chefetz, B., Tarchitzky, J., Deshmukh, A.P., Hatcher, P.G., Chen, Y., 2002. Structural characterization of soil organic matter and humic acids in particle-size fractions of an agricultural soil. Soil Sci. Soc. Am. J. 66, 129-141.

Chiu, P. C., Lee, M., 2001. 2-bromoethanesulfonate affects bacteria in a trichloroethene-dechlorinating culture. Appl. Environ. Microbiol. 67, 2371-2374.

Chu, K. H., Mahendra, S., Song, D. L., Conrad, M. E., Alvarez-Cohen, L., 2004. Stable carbon isotope fractionation during aerobic biodegradation of chlorinated ethenes. Environ. Sci. Technol.38, 3126-3130.

Cichocka, D., Siegert, M., Imfeld, G., Andert, J., Beck, K., Diekert, G., Richnow, H.-H., Nijenhuis, I., 2007. Factors controlling the carbon isotope fractionation of tetra- and trichloroethene during reductive dechlorination by Sulfurospirillum sp. and Desulfitobacterium sp. strain PCE-S. FEMS Microbiol. Ecol. 62, 98-107.

Cichocka, D., Imfeld, G., Richnow, H.-H., Nijenhuis, I., 2008. Variability in microbial carbon isotope fractionation of tetra- and trichloroethene upon reductive dechlorination. Chemosphere 71, 639-648.

Cobb, G. D., Bouwer, E. J., 199. Effects of electron acceptors on halogenated organic compound biotransformations in a biofilm column. Environ. Sci. Technol. 25, 1068-1074.

Cornell, R. M., Schwertmann, U., 2003. *The Iron Oxides Structure, Properties, Reactions, Occurrences, and Uses*. 2nd ed., Wiley-VCH Verlag GmbH & Co. KGaA: Weinheim, New York, pp 525-540.

Cozzarelli, J. M., Suflita, J. M., Ulrich, G. A., Harris, S. H., Scholl, M. A., Schlottmann, J. L., Christenson, S., 2000. Geochemical and microbiological methods for evaluating anaerobic processes in an aquifer contaminated by landfill leachate. Environ. Sci. Technol. 34, 4025-4033.

Criddle, C. S., Dewitt, J. T., Grbic-Galic, D., McCarty, P. L., 1990. Transformation of carbon tetrachloride by Pseudomonas sp. strain KC under denitrification conditions. Appl. Environ. Microbiol. 56, 3240-3246.

Criddle, C. S., McCarty, P. L., 1991. Electrolytic model system for reductive dehalogenation in aqueous environments. Environ. Sci. Technol. 25, 973-978.

Crepaldi, E. L., Tronto, J., Cardoso, L. P., Valim, J. B., 2002. Sorption of terephthalate anions by calcined and uncalcined hydrotalcite-like compounds. Colloids Surf. A, 211, 103-114.

Curtis, G. P., Reinhard, M., 1994. Reductive dehalogenation of hexachloroethane, carbon tetrachloride, and bromoform by anthrahydroquinone disulfonate and humic acid. Environ. Sci. Technol. 28, 2393-2402.

Danielsen, K. M., Hayes, K. F., 2004. pH dependence of carbon tetrachloride reductive dechlorination by magnetite. Environ. Sci. Technol. 38, 4745–4752.

Danielsen, K. M., Gland, J. L., Hayes, K. F., 2005. Influence of amine buffers on carbon tetrachloride reductive dechlorination by the iron oxide magnetite. Environ. Sci. Technol. 39, 756-763.

Davis, J.A., 1982. Adsorption of natural dissolved organic matter at the oxide/water interface. Geochim. Cosmochim. Acta 46, 2381-2393.

Davis, J. A., Kent, D. B., 1990. Surface complexation modeling in aqueous geochemistry. In: Hochella, M. F., White, A. F. (Eds.), 1990. *Mineral-Water Interface Geochemistry*. Rev. Mineral. 23, pp 177-259.

Dayan, H., Abrajano, T., Sturchio, N. C., Winsor, L., 1999. Carbon isotopic fractionation during reductive dehalogenation of chlorinated ethenes by metallic iron. Org. Geochem. 30, 755-763.

Deiana, S., Gessa, C., Marchetti, M., Usai, M., 1992. Mechanism and stoichiometry of the redox reaction between Fe(III) and caffeic acid. Plant Soil 145, 287-294.

Deiana, S., Gessa, C., Marchetti, M., Usai, M., 1995. Phenolic acid redox properties: pH influence on iron (III) reduction by caffeic acid. Soil Sci. Soc. Am. J. 59, 1301-1307.

Devlin, J. F., Müller, D., 1999. Field and laboratory studies of carbon tetrachloride transformation in a sandy aquifer under sulfate reducing conditions. Environ. Sci. Technol. 33, 1021-1027.

Doherty, R.E., 2000. A history of the production and use of carbon tetrachloride, tetrachloroethylene, trichloroethylene and 1,1,1-trichloroethane in the United States: Part 1-historical background; carbon tetrachloride and tetrachloroethylene. J. of Environ. Forensics 1, 69-81.

Doong R. and Lai Y., 2005. Dechlorination of tetrachloroethylene by palladized iron in the presence of humic acid. Wat. Res. 39, 2309-2318.

Doucette, W. J., 2000. Soil and sediment sorption coefficients. In *Handbook of Property Estimation Methods for Chemicals: Environmental and Health Sciences*, Boethling, R. S., Mackay, D., Eds, CRC Press LLC: Boca Raton, FL, pp 141-188.

Dunnivant, F.M., Schwarzenbach, R.P., Macalady, D.L., 1992. Reduction of substituted nitrobenzenes in aqueous solutions containing natural organic matter. Environ. Sci. Technol. 26, 2133–2141.

Edwards, M., Benjamin, M. M., Ryan, J. N., 1996. Role of organic acidity in sorption of natural organic matter (NOM) to oxide surfaces. Colloids Surf. A 107, 297-307.

Egli, C., Tschan, T., Scholtz, R., Cook, A. M., Leisinger, T., 1988. Transformation of tetrachloromethane to dichloromethane and carbon dioxide by Acetobacterium woodii. Appl. Environ. Microbiol. 54, 2819-2824.

Elsner, M., Haderlein, S. B., Kellerhals, T. Luzi S., Zwank, L., Angst, W., Schwarzenbach, R. P., 2004. Mechanisms and products of surface-mediated reductive dehalogenation of carbon tetrachloride by Fe(II) on goethite. Environ. Sci. Technol. 38, 2058–2066.

Elsner, M., Schwarzenbach, R. P., Haderlein, S. R., 2004. Reactivity of Fe (II)-bearing minerals toward reductive transformation of organic contaminants. Environ. Sci. Technol. 38, 799-807.

Elsner, M., Zwank, L., Hunkeler, D., Schwarzenbach, R. P., 2005. A new concept

linking observable stable isotope fractionation to transformation pathways of organic pollutants. Environ. Sci. Technol. 39, 6896-6916.

Elsner, M., Cwiertny, D. M., Roberts, A. L., Sherwood Lollar, B., 2007. 1,1,2,2-Tetrachlorethane reactions with OH-, Cr(II), granular iron, and a copper-iron bimetal: Insights from product formation and associated carbon isotope fractionation. Environ. Sci. Technol. 41, 4111-4117.

Elsner, M., Chartrand, M., Vanstone, N., Lacrampe Couloume, G., Sherwood Lollar, B., 2008. Identifying abiotic chlorinated ethane degradation: Characteristic isotope patterns in reaction products with nanoscale zero-valent iron. Environ. Sci. Technol. 42, 5963-5970.

Erbs, M., Hansen, H.C.B., Olsen, C.E., 1999. Reductive dechlorination of carbon tetrachloride using iron(II)iron(III)-hydroxide-sulphate (green rust). Environ. Sci. Technol. 33, 307-311.

Erbs, M., 2004. Ph.D dissertation. Formation and redox reactions of green rusts under geochemical conditions found in natural soils and sediments. Swiss Federal Institute of Technology (ETH), Zurich, Switzerland.

Evanko, C. R., Dzombak, D. A., 1998. Influence of structural features on sorption of NOM-analogue organic acids to goethite. Environ. Sci. Technol. 32, 2846-2855.

Everett, J. L., Kennedy, L. G., Gonzales, J., 2006. Natural attenuation assessment using mineral data. Pract. Periodical Hazard., Toxic, Radioact. Waste Manage. 10, 256-263.

Feder, F., Trolard, F., Klingelhofer, G., Bourrie, G., 2005. In situ Mössbauer spectroscopy: Evidence for green rust (fougerite) in a gleysol and its mineralogical transformations with time and depth. Geochim. Cosmochim. Acta. 69, 4463-4483.

Ferrey, M., Norris, B., 2003. Editor's perspective-Guest column: Monitored natural attenuation: Its application and the formation of a panel for discussions. Remediat. J. 13,1-5

Fredrickson, J.K., Zachara, J.M., Kennedy, D.W., Dong, H., Onstott, T.C., Hinman, N.W., Li, S., 1998. Biogenic iron mineralization accompanying the dissimilatory reduction of hydrous ferric oxide by a groundwater bacterium. Geochim. Cosmochim. Acta. 62, 3239-3257.

Fredrickson, J. K., Kostandarithes, H. M., Li, S. W., Plymale, A. E., Daly M. J., 2000. Reduction of Fe(III), Cr(VI),U(VI), and Tc(VII) by Deinococcous radiodurans R1.Appl. Environ. Microbiol. 66, 2006-2011.

Gasser, M. S., Mohsen, H. T., Aly, H. F., 2008. Humic acid adsorption onto Mg/Fe layered double hydroxide. Colloids Surf. A 331, 195-201.

Génin, J.-M. R., Bourrié, G., Trolard, F., Abdelmoula, M., Jaffrezic,A., Refait, P., Maitre, V., Humbert, B., Herbillon, A.,1998. Thermodynamic equilibria in aqueous suspensions of synthetic and natural Fe(II)-Fe(III) green rusts: Occurrences of the mineral in hydromorphic. Environ. Sci. Technol. 32, 1058-1068.

Gẻnin, J-M. R., Ruby, C., 2004. Anion and cation distributions in Fe(II–III) hydroxysalt green rusts from XRD and Mössbauer analysis (carbonate, chloride, sulphate, …); the "fougerite" mineral. Solid State Sci. 6, 705-718.

Gibbs, R. J., 1973. Mechanisms of trace metal transport in rivers. Science 180, 71-73.

Glasauer, S., Langley, S., Beveridge, T.J., 2002. Intracellular iron minerals in a dissimilatory iron-reducing bacterium. J. Sci. 295, 117-119.

Greenland, D.J., Hayes, M.H.B., 1978. *The Chemistry of Soil Constituents*. Wiley, New York.

Gu, B., Schmitt, J., Chen, Z., Liang, L., McCarthy, J.F., 1995. Adsorption and desorption of different organic matter fractions on iron oxide. Geochim. Cosmochim. Acta 59, 219-229.

Goh, K., Lim, T., Dong, Z., 2008. Application of layered double hydroxides for removal of oxyanions: a review. Wat. Res. 42, 1349-1368.

Glod, G., Brodmann, U., Angst, W., Holliger, C., Schwarzenbach, R. P., 1997. Gobalamin-mediated reduction of cis- and trans-dichloroethene, 1,1-dichloroethene, and vinyl chloride in homogeneous aqueous solution: Reaction kinetics and mechanistic considerations. Environ. Sci. Technol. 31, 3154-3160.

Haggblom, M. M., Bossert, I. D., 2003. Dehalogenation: microbial processes and environmental applications. Kluwer Academic Publisher, Boston.

Hanoch, R. J., Shao, H., Butler, E. C., 2006. Transformation of carbon tetrachloride by bisulfide treated goethite, hematite, magnetite, and kaolinite. Chemosphere 63, 323–334.

Hansen, H.C.B., Koch, C.B., 1998. Reduction of nitrate to ammonium by sulphate green rust: activation energy and reaction mechanism. Clay Miner. 33, 87-101.

Hari, A.C., Paruchuri, R.A., Sabatini, D.A., Kibbey, T.C.G., 2005. Effects of pH and cationic and nonionic surfactants on the adsorption of pharmaceuticals to a natural aquifer material. Environ. Sci. Technol. 39, 2592–2598.

Hayes, M.H.B., Swift, R.S. 1978, The chemistry of soil organic colloids. In *The Chemistry of Soil Constituents*. Greenland, D.J., Hayes, M.H.B. Eds., Wiley, New York, pp 179-230.

He, Y., Wilson, J. T., Wilkin, R.T., 2008. Transformation of reactive iron minerals in a permeable reactive barrier (biowall) used to treat TCE in groundwater. Environ. Sci. Technol. 42, 6690-6696.

Herbert, R. B., Jr., Benner, S. G., Pratt, A. R., Blowes, D. W., 1998. Surface chemistry and morphology of poorly crystalline iron sulfides precipitated in media containing sulfate-reducing bacteria. Chem. Geol. 144, 87-97.

Heron, G., Crouzet, C., Bourg, A. C. M., Christensen, T. H., 1994. Speciation of Fe(II) and Fe(III) in contaminated aquifer sediments using chemical extraction techniques. Environ. Sci. Technol. 28, 1698-1705.

Hirschorn, S. K., Dinglasan, M. J., Elsner, M., Mancini, S. A., Lacrampe-Couloume, G., Edwards, E. A., Sherwood Lollar, B., 2004. Pathway dependent isotopic fractionation during aerobic biodegradation of 1,2-dichloroethane. Environ. Sci. Technol. 38, 4775-4781.

Hoefs, J., 1997. Stable isotope geochemistry, Springer-Verlag: Berlin.

Hofstetter, T. B., Schwarzenbach, R. P., Haderlein, S. B., 2003. Reactivity of Fe(II) species associated with clay minerals. Environ. Sci. Technol. 37, 519-528.

Holliger, C., Gaspard, S., Glod, G., Heijman, C., Schumacher, W., Schwarzenbach, R. P., Vazquez, F., 1997. Contaminated environments in the subsurface and bioremediation: organic contaminants. FEMS Microbiol. Rev. 20, 517-523.

Howard, P. H., Meylan, W. M., 1997. *Handbook of Physical Properties of Organic Chemicals*. CRC Press, Inc., Boca Raton, FL.

Huerta-Diaz, M. A., Carignan, R., Tessier, A., 1993. Measurement of trace metals associated with acid volatile sulfides and pyrite in organic freshwater sediments. Environ. Sci. Technol. 27, 2367-2372.

Hunkeler, D., Aravena, R., Butler, B. J., 1999. Monitoring microbial dechlorination of tetrachloroethene (PCE) in groundwater using compound-specific stable carbon isotope ratios: microcosm and field studies. Environ. Sci. Technol. 33, 2733-2738.

Hunkeler, D., Aravena, R., 2000. Evidence of substantial carbon isotope fractionation among substrate, inorganic carbon and biomass during aerobic mineralization of 1, 2-dichloroethane by *Xanthobacter* autotrophicus. Appl. Environ. Microbiol. 66, 4870-4876.

Hunkeler, D., Butler, B. J., Aravena, R., Barker, J. F., 2001. Monitoring biodegradation of methyl tert-Butyl Ether (MTBE) using compound-specific carbon isotope analysis, Environ. Sci. Technol. 35, 676-681.

Hunkeler, D., Aravena, R., and Cox, E., 2002. Carbon isotopes as a tool to evaluate the origin and fate of vinyl chloride: Laboratory experiments and modeling of isotope evolution. Environ. Sci. Technol. 36, 3378-3384.

Huskey, W. P., 1991. In *Enzyme mechanism from isotope effects*, Cook, P.F., Ed., CRC Press: Boca Raton, FL, pp 37-69.

Hwang, I., Batchelor, B., 2000. Reductive dechlorination of tetrachloroethylene by Fe(II) in cement slurries. Environ. Sci. Technol. 34, 5017-5022

Jenkins, R., Snyder , R., 1996. *Introduction to X-ray Powder Diffractometry*. John Wiley & Sons, Inc.: New York, NY, Vol. 138, pp 335-339.

Johnson, T. M., Fish, W., Gorby, Y. A., Tratnyek, P.G., 1998. Degradation of carbon tetrachloride by iron metal: Complexation effects on the oxide surface. J. Contam. Hydrol. 29, 379-398.

JCPDS, 1990. Powder Diffraction File, Inorganic Volume, Swarthmore, PA.

Jeong, H. Y., Kim, H., Hayes, K. F., 2007. Reductive dechlorination pathways of tetrachloroethylene and trichloroethylene and subsequent transformation of their dechlorination products by mackinawite (FeS) in the presence of metals. Environ. Sci. Technol. 41, 7736-7743.

Kang, Y. S., Risbud, S., Rabolt, J. F., Stroeve, P., 1996. Synthesis and characterization of nanometer-size Fe3O4 and γ-Fe2O3 particles. Chem. Mater. 8, 2209-2211.

Karickhoff, S. W., Brown, D. S., Scott, T. A., 1979. Sorption of hydrophobic pollutants on natural sediments. Wat. Res. 13, 241-248.

Kappler, A., Haderleein. S.B., 2003. Natural organic matter as reductant for chlorinated aliphatic pollutants. Environ. Sci. Technol. 37, 2714-2719.

Kennedy, L. G., Everett, J. W., Gonzales, J., 2006. Assessment of biogeochemical natural attenuation and treatment of chlorinated solvents, Altus Air Force Base, Altus, Oklahoma. J. Contam. Hydrol. 83, 221-236.

Kennedy, L. G., Everett, J. W., Becvar, E., DeFeo, D., 2006. Field-scale demonstration of induced biogeochemical reductive dechlorination at Dover Air Force Base, Dover, Delaware. J. Contam. Hydrol. 88, 119-136

Kenneke, J. F., Weber, E. J., 2003. Reductive dehalogenation of halomethanes in iron- and sulfate-reducing sediments. 1. reactivity pattern analysis. Environ. Sci. Technol. 37, 713-720.

Kim, S., Picardal, F. W., 1999. Enhanced anaerobic biotransformation of carbon tetrachloride in the presence of reduced iron oxides. Environ. Toxicol. Chem. 18, 2142-2150.

Kirtland, B.C., Aelion, C.M., Stone, P.A., Hunkeler, D., 2003. Isotopic and geochemical assessment of biodegradation of chlorinated hydrocarbons, Environ. Sci. Technol. 37, 4205-4212.

Kriegman-King, M. R., Reinhard, M., 1992. Transformation of carbon tetrachloride in the presence of sulfide, biotite, and vermiculite. Environ. Sci. Technol. 26, 2198-2206.

Kriegman-King, M. R., Reinhard, M., 1994. Transformation of carbon tetrachloride by pyrite in aqueous solution. Environ. Sci. Technol. 28, 692–700.

Krone, U. E., Laufer, K., Thauer, R. K., Hogenkamp, H. P. C., 1989. Coenzyme F430 as a possible catalyst for the reductive dehalogenation of chlorinated C1 hydrocarbons in methanogenic bacteria. Biochemistry 28, 10061-10065.

Kuder, T., Wilson, J. T., Kaiser, P., Kolhatkar, R., Philp, P., Allen, J., 2005. Enrichment of stable carbon and hydrogen isotopes during anaerobic biodegradation of MTBE: microcosm and field evidence. Environ. Sci. Technol. 39, 213-220

Lack, J.G., Chaudhuri, S.K., Chakraborty, R., Achenbach, L.A., Coates, J.D., 2002. Anaerobic biooxidation of Fe(II) by *Dechlorosoma suillum*. Microbial Ecol. 43, 424-431.

Labajos, F. M., Rives, V., Ulibarri, M.A., 1992. Effect of hydrothermal and thermal treatments on the physicochemical properties of Mg-Al hydrotalcite-like materials. J. Mater. Sci. 27, 1546-1552.

Larese-Casanova, P., Scherer, M. M., 2008. Abiotic transformation of hexahydro-1,3,5-trinitro-1,3,5-trizaine (RDX) by green rusts. Environ. Sci. Technol. 42, 3975-3981.

Larson, R.A., Weber, E.J., 1994. *Reaction mechanisms in environmental organic chemistry*. Lewis Publishers, Boca Raton, Florida.

Lee, W., Batchelor, B., 2002a. Abiotic reductive dechlorination of chlorinated ethylenes by iron-bearing soil minerals. 1. Pyrite and magnetite. Environ. Sci. Technol. 36, 5147-5154.

Lee, W., Batchelor, B., 2002b. Abiotic reductive dechlorination of chlorinated ethylenes by iron-bearing soil minerals. 2. Green rust. Environ. Sci. Technol. 36, 5348-5354.

Lee, P. K. H., Conrad, M. E., Alvarez-Cohen, L., 2007. Stable carbon isotope fractionation of chloroethenes by dehalorespiring Isolates. Environ. Sci. Technol. 41, 4277-4285.

Legrouri, A., Lakraimi, M., Barroug, A., Roy A. D., Besse, J. P., 2005. Removal of the herbicide 2,4-dichlorophenoxyacetate from water to zinc-aluminum-chloride layered double hydroxides. Wat. Res. 39, 3441-3448.

Lehmann, R. G., Cheng, H. H., Harsh, J. B., 1987. Oxidation of phenolic acids by soil iron and manganese oxides. Soil Soc. Am. J. 51, 352-356.

Lewis, D. G., 1997. Factors influencing the stability and properties of green rusts. Advances in GeoEcology 30, 345-372.

Liang, X., Dong, Y., Kuder, T., Krumholz, L. R., Philp, R. P., Butler, E. C., 2007. Distinguishing abiotic and biotic transformation of tetrachloroethylene and trichloroethylene by stable carbon isotope fractionation. Environ. Sci. Technol. 41, 7094-7100.

Liang, X., Philp, R. P., Butler, E. C., 2009. Kinetic and isotope analyses of tetrachloroethylene and trichloroethylene degradation by model Fe(II)-bearing minerals. Chemosphere 75, 63-69.

Liger, E., Charlet, L., Cappellen, P.V., 1999. Surface catalysis of uranium(VI) reduction by iron(II). Geochim. Cosmochim. Acta 63, 2939-2955.

Lindsay, W. L., 1979. Chemical Equilibria in Soils. John Wiley & Sons, Inc., NY, p. 129.

Liu, X.M., Peng, P., Fu, J.M., Huang, W.L., 2003. Effects of FeS on the transformation kinetics of γ-hexachlorocyclohexane. Environ. Sci. Technol. 37, 1822–1828.

Lloyd J. R., Sole V. A., Van Praagh, C. V. G., Lovely, D. R., 2000. Direct and Fe(II)-mediated reduction of technetium by Fe(III)-reducing bacteria. Appl. Environ. Microbiol. 66, 3743–3749.

Lovely, D. R., Phillips, E. J. P., 1987. Rapid assay for microbially reducible ferric iron in aquatic sediments. Appl. Environ. Microbiol. 53, 1536-1540.

Lovely, D. R., Phillips, E. J. P., Lonergan, D. J., 1991. Enzymatic versus nonenzymatic mechanism for Fe(III) reduction in aquatic sediments. Environ. Sci. Technol. 25, 1062-1067.

Loyaux-Lawniczak, S., Refait, P., Lecomte, P., Ehrhardt, J.-J., Génin, J. M. R., 1999. The reduction of chromate ions by Fe(II) layered hydroxides. Hydrol. Earth Syst. Sci. 3, 593-599.

Loyaux-Lawniczak, S., Refait, P., Ehrhardt, J. J., Lecomte, P., Génin, J. R., 2000. Trapping of Cr formation of ferrihydrite during the reduction of chromate ions by Fe(II)-Fe(III) hydroxysalt green rusts. Environ. Sci. Technol. 34, 438-443.

Loffler, F. E., Ritalahti, K. M., Tiedje, J. M., 1997. Dechlorination of chloroethenes is inhibited by 2-bromoethanesulfonate in the absence of methanogens. Appl. Environ. Microbiol. 63, 4982-4985.

Lu, G.P., Clement, T.P., Zheng, C.M., Wiedemeier, T.H., 1999. Natural attenuation BTEX compounds: model development and field-scale application. Ground Water 37, 707-717.

Lu, X., Wilson, J. T., Shen, H., Henry, B. M., Kampbell, D. H., 2008. Remediation of TCE-contaminated groundwater by a permeable reactive barrier filled with plant mulch (Biowall). J. Environ. Sci. Health, Part A: Environ. Sci. Eng. 43, 24-35.

Luther III, G.W., 1991. Pyrite synthesis via polysulfide compounds. Geochim. Cosmochim. Acta 55, 2839-2849.

Mackay, D., Shiu, W. Y., 1981. A critical review of Henry's Law constants for chemicals of environmental interest. J. Phys. Chem. Ref. Data 10, 1175-1199.

Mackay, D., Shiu, W. Y., Ma, K.-C., Lee, S. C., 2006. Handbook of Physical-Chemical Properties and Environmental Fate for Organic Chemicals. 2nd ed., CRC Press LLC: Boca Raton, FL, Vol. II, p 1063-1115.

Maithreepala, R. A., Doong, R., 2005. Enhanced dechlorination of chlorinated methanes and ethenes by chloride green rust in the presence of copper (II). Environ. Sci. Technol. 39, 4082-4090.

Marconetto, S., Gui, L., Gillham, R.,2005. Adsorption of natural organic matter and its effects on TCE degradation by iron PRBs. IAHS-AISH 297, 389-397.

Mariotti, A., Germon, J. C., Hubert, P., Kaiser, P., Letolle, R., Tardieux, A., Tardieux, P., 1981. Experimental determination of nitrogen kinetic isotope fractionation: some principles, illustration for the denitrification and nitrification processes. Plant soil 62, 413-430.

Martell, A. E., Smith, R. M. Critical Stability Constants, Plenum Press: New York, 1974.

Masters, G. M., 1998. Introduction to Environmental Engineering and Science. Prentice Hall, N.J.

McCormick, M. L., Bouwer, E. J., Adrianes, P., 2002. Carbon tetrachloride transformation in a model iron-reducing culture: Relative kinetics of biotic and abiotic reactions. Environ. Sci. Technol. 36, 403-410.

McCormick, M. L., Adriaens, P., 2004. Carbon tetrachloride transformation on the surface of nanoscale biogenic magnetite particles. Environ. Sci. Technol. 38, 1045–1053.

McGill, I. R., McEnaney, B., Smith, D. C., 1976. Crystal structure of green rust formed by corrosion of cast iron. Nature 259, 200-201.

McKnight, D.M., Bencala, K.E., Zellweger, G.W., Aiken, G.R., Feder, G.L., Thorn, K.A., 1992. Sorption of dissolved organic carbon by hydrous aluminum and iron oxides occurring at the confluence of Deer Creek with the Snake River, Summit County, Colorado. Environ. Sci. Technol. 26, 1388-1396.

Meckenstock, R.U., Morasch, B., Griebler, C., Richnow, H.H., Stable isotope fractionation analysis as a tool to monitor biodegradation in contaminated aquifers. J. Contam. Hydrol. 75, 215-255.

Middeldorp, P. J. M., Luijten, M. L. G. C, van de Pas, B. A., van Eekert, M. H.A., Kengen, S. W. M., Schraa, G., Stams, A. J. M., 1999. Anaerobic microbial reductive dehalogenation of chlorinated ethenes. Bioremediation Journal 3, 151-169.

Miller, J. C., Miller, J. N., 1988. Statistics for Analytical Chemistry, 2nd Ed., John Wiley & Sons, New York, pp 47-50.

Miller, P. L., Vasudevan, D., Gschwend, P. M., Roberts, A. L., 1998. Transformation of hexachloroethane in a sulfidic natural water. Environ. Sci. Technol. 32, 1269-1275.

Moggi, P., Albanesi, G. 1991. Transition metal phosphomolybdates as catalysts for the gas phase hydration of acetylene to acetaldehyde and acetic acid. React. Kinet. Catal. L. 44, 375-380.

Moran, M. J., Zogorski, J. S., Squillace, P. J., 2007. Chlorinated solvents in groundwater of the United States. Environ. Sci. Technol. 41, 74-81.

Morrison, R. T., Boyd, R. N., 1983. *Organic Chemistry*, 4th Ed., Allyn and Bacon, Inc., Boston, pp. 753-754.

Morse, J. W., Millero, F. J., Cornwell, J. C., Rickard, D., 1987. The chemistry of the hydrogen sulfide and iron sulfide systems in natural waters. Earth Sci. Rev. 24, 1-42.

Murphy, E.M., Zachara, J.M., Smith, S.C., 1990. Influence of mineral-bound humic substances on the sorption of hydrophobic organic compounds. Environ. Sci. Technol. 24, 1507-1516.

Myneni, S. C. B., Tokunaga, T. K., Brown, G. E., Jr., 1997. Abiotic selenium redox transformations in the presence of Fe(II,III) oxides. Science 278, 1106-1109.

National Research Council, 1994. Alternatives for Ground-Water Cleanup. The National Academies Press, Washington, D. C.

Neal, A. L., Techkarnjanaruk, S., Dohnalkova, A., McCready, D., Peyton, B. M., Gessey, G.G., 2001. Iron sulfides and sulfur species produced at hematite surfaces in the presence of sulfate-reducing bacteria. Geochim. Cosmochim. Acta 65, 223-235.

Nijenhuis, I., Andert, J., Beck, K., Kaestner, M., Diekert, G., Richnow, H.-H., 2005. Stable isotope fractionation of tetrachloroethene during reductive dechlorination by Sulfurospirillum multivorans and Desulfitobacterium sp. strain PCE-S and abiotic reactions with cyanocobalamin. Appl. Environ. Microbiol. 71, 3413-3419.

Nirmalakhandan, N. N., Speece, R. E., 1988. QSAR model for predicting Henry's constant. Environ. Sci. Technol. 22, 1349-1357.

Novak, P. J., Daniels, L., Parkin, G. F., 1998. Enhanced dechlorination of carbon tetrachloride and chloroform in the presence of elemental iron and Methanosarcina barkeri, Methanosarcina thermophila, or Methanosaeta concillii. Environ. Sci. Technol. 32, 1438-1443.

Ona-Nguema, G., Abdelmoula, M., Jorand, F., Benali, O., Génin, A., Block, J.C., Génin, J-M.R., 2002. Iron(II,III) hydroxycarbonate green rust formation and stabilization from lepidocrocite bioreduction. Environ. Sci. Technol. 36, 16-20.

O'Loughlin, E.J., Kelly, S.D., Cook, R.E., Csencsits, R., Kemner, K.M., 2003a. Reduction of uranium (VI) by mixed iron(II)/iron(III) hydroxide (green rust): Formation of UO2 nanoparticles. Environ. Sci. Technol. 37, 721-727.

O'Loughlin, E. J., Kemner, K. M., Burris, D. R., 2003b. Effects of AgI, AuIII, and CuII on the reductive dechlorination of carbon tetrachloride by green rust. Environ. Sci. Technol. 37, 2905-2912.

O'Loughlin, E. J., Burris, D. R., 2004. Reduction of halogenated ethanes by green rust. Environ. Toxicol. Chem. 23, 41-48.

O'Loughlin, E. J., Larese-Casanova, P., Scherer, M., Cook, Russell., 2007. Green rust formation from the bioreduction of γ-FeOOH (Lepidocrocite): Comparison of several Shewanella species. Geomicrobiol. J. 24, 211-230.

O'Loughlin, E. J., Kemner, K. M., Burris, D. R., 2003. Effects of AgI, AuIII, and CuII on the reductive dechlorination of carbon tetrachloride by green rust. Environ. Sci. Technol. 37, 2905-2912.

Page, D.W., van Leeuwen, J.A., Spark, K.M., Mulcahy, D.E., 2002. Pyrolysis characterization of plant, humus and soil extracts from Australian catchments. J. Anal. Appl. Pyrolysis 65, 269-285.

Pankow, A., Cherry, J.A., 1996. Dense Chlorinated Solvents and Other DNAPLs in Groundwater. Waterloo Press: Portland, Oregon, U.S.

Parker, L. M., Milestone, N. B., Newman, R. H., 1995. The use of hydrotalcite as an anion absorbent. Ind. Eng. Chem. Res. 34, 1196-1202.

Parmar, N., Gorby, Y.A., Beveridge, T.J., Ferris, F.G., 2001. Formation of green rust and immobilization of nickel in response to bacterial reduction of hydrous ferric oxide. Geomicrobiol. J. 18, 375-385.

Parsons, J.W., 1989. Hydrolytic degradations of humic substances. In Humic substances II: In Search of Structure. Hayes, M.H.B, MacCarthy, P., Malcolm, R.L., Swift, R.S., Eds., Wiley, New York,, pp 99-120.

Parsons Corporation., 2006. Construction closeout report bark mulch trench interim corrective action for in-situ anaerobic bioremediation of chlorinated solvents in ground water Altus Air Force Base, Oklahoma. Prepared for Altus AFB Air Education and Training Command and the Air Force Center for Environmental Excellence, Brooks City-Base, Texas. Contract No. F41624-01-D-8544, Delivery Order No. 0025, Parsons, Denver, CO.

Pasakarnis, T. S., Gorski, C. A., O'Loughlin, E., Parkin, G. F., Scherer, M. M., 2006. Abiotic reduction of chlorinated ethenes in the presence of anaerobic bacteria. In Preprints of Extended Abstracts presented at the ACS National Meeting, American Chemical Society: Atlanta, GA, Vol. 46, pp 957-961.

Pecher, K., Haderlein, S. B., Schwarzenbach, R. P., 2002. Reduction of polyhalogenated methanes by surface-bound Fe(II) in aqueous suspensions of iron oxides. Environ. Sci. Technol. 36, 1734-1741.

Perlinger, J. A., Angst, W., Schwarzenbach, R. P. Kinetics of the reduction of hexachloroethane by juglone in solutions containing hydrogen sulfide," Environ. Sci. Technol. 1996, 30, 3408-3417.

Perlinger, J. A., Buschmann, J., Angst, W., Schwarzenbach, R. P., 1998. Iron porphyrin and mercaptojuglone mediated reduction of polyhalogenated methanes and ethanes in homogeneous aqueous solution. Environ. Sci. Technol. 32, 2431-2437.

Perlinger, J. A., Kalluri, V. M., Venkatapathy, R., Angst, W., 2002. Addition of hydrogen sulfide to juglone. Environ. Sci. Technol. 36, 2663-2669.

Poulson, S. R., Drever, J. I., 1999. Stable Isotope (C, Cl, and H) Fractionation during Vaporization of Trichloroethylene, Environ. Sci. Technol. 33, 3689-3694.

Pyzik, A. J., Sommer, S. E., 1981. Sedimentary iron monosulfides: Kinetics and mechanisms of formation. Geochim. Cosmochim. Acta. 45, 687-698.

Ramasamy, K., Kalyanasundaram, S. L., Shanmugam, P., 1978. Debromination of vic-dibromides using sodium hydrogen telluride reagent. Synthesis 311-312.

Randall, S. R., Sherman, D. M., Ragnarsdottir, K. V., 1999. Sorption of As (V) on green rust (Fe4(II)Fe2(III)(OH)12SO4.3H2O) and lepidocrocite (γ-FeOOH): Surface complexes from EXAFS spectroscopy. Geochim. Cosmochim. Acta 65, 1015-1023.

Rechnagel, R.O., Glende, J., Dolar, J.A., Waller, R.L., 1989. Mechanisms of carbon tetrachloride toxicity. Pharmacol. Ther. 43, 139-154.

Refait, P. H., Abdelmoula, M., Génin, J. -M. R., 1998. Mechanisms of formation and structure of green rust one in aqueous corrosion of iron in the presence of chloride ions. Corros. Sci. 40, 1547-1560.

Refait, Ph., Abdelmoula, M., Gẻnin, J-M. R., 1998. Mechanisms of formation and structure of green rust one in aqueous corrosion of iron in the presence of chloride ions. Corros. Sci. 40, 1547-1560.

Rickard, D. T., 1969. The chemistry of iron sulfide formation at low temperatures. Stockholm Contrib. Geology 20, 67–95.

Rickard, D. T., 1974. Kinetics and mechanism of the sulfidation of goethite. Am. J. Sci. 274, 941-952.

Ritter, K., Odziemkowski, M.S., Gillham, R.W., 2002. An in situ study of the role of surface films on granular iron in the permeable iron wall technology. J. Contam. Hydrol. 55, 87-111.

Rives, V. 2001. *Layered Double Hydroxides: Present and Future*. Nova Science Publishers, Inc. New York, pp 230-231.

Roberts, A. L., Totten, L. A., Arnold, W. A., Burris, D. R., Campbell, T. J., 1996. Reductive elimination of chlorinated ethylenes by zero-valent metals. Environ. Sci. Technol. 30, 2654-2659.

Sato, T., Okuwaki, A., 1991. Intercalation of benzenecarboxylate ions into the interlayer of hydrocite. Solid State Ionics 45, 43-48.

Schink, B., 1985. Fermentation of acetylene by an obligate anaerobe, Pelobacter acetylenicus sp. nov. Arch. Microbiol. 142, 295-301.

Schmidt, T. C., Zwank, L., Elsner, M., Berg, M., Meckenstock, R. U., Haderlein, S. B., 2004. Compound-specific stable isotope analysis of organic contaminants in

natural environments: a critical review of the state of the art, prospects, and future challenges. Anal. Bioanal. Chem. 378, 283-300.

Schüth, C., Bill, M., Barth, J. A. C., Slater, G. F., Kalin, R. M., 2003. Carbon isotope fractionation during reductive dechlorination of TCE in batch experiments with iron samples from reactive barriers. J. Contam. Hydrol. 66, 25-37.

Schwarzenbach, R. P., Stierli, R., Lanz, K., Zeyer, J., 1990. Quinone and iron porphyrin mediated reduction of nitroaromatic compounds in homogeneous aqueous solution. Environ. Sci. Technol. 24, 1566-1574.

Schwarzenbach, R. P., Gschwend, P. M., Imboden, D. M., 2003. *Environmental Organic Chemistry* 2nd ed., John Wiley & Sons, Inc. Hoboken, NJ, p 276-330.

Seida, Y., Nakano, Y., 2000. Removal of humic substance by layered double hydroxide containing iron. Wat. Res. 34, 1487-1494.

Shao, H., Butler, E. C., 2007. The influence of iron and sulfur mineral fractions on carbon tetrachloride transformation in model anaerobic soils and sediments. Chemosphere 68, 1807–1813.

Shao, H., Butler, E. C., 2009a. Influence of soil minerals on the rates and products of abiotic transformation of carbon tetrachloride in anaerobic soils and sediments. Environ. Sci. Technol. 43, 1996-1901.

Shao, H., Butler, E. C., 2009b. The relative importance of abiotic and biotic transformation of carbon tetrachloride in anaerobic soils and sediments. Soil Sediment Contam. in press.

Shao, H., Butler, E. C., 2007. The influence of iron and sulfur mineral fractions on carbon tetrachloride transformation in model anaerobic soils and sediments. Chemosphere 68, 1807-1813.

Shen, H., Wilson, J. T., 2007. Trichloroethylene removal from groundwater in flow-through columns simulating a permeable reactive barrier constructed with plant mulch. Environ. Sci. Technol. 41, 4077-4083.

Sheng, G.Y., Xu, S.H., Boyd, S.A., 1996. Mechanisms controlling sorption of neutral organic contaminants by surfactant-derived and natural organic matter. Environ. Sci. Technol. 30, 1553-1557.

Sherwood Lollar, B., Slater, G. F., Ahad, J., Sleep, B., Spivack, J., Brennan, M., MacKenzie, P., 1999. Contrasting carbon isotope fractionation during biodegradation of trichloroethylene and toluene: Implications for intrinsic bioremediation. Org. Geochem. 30, 813-820.

Sherwood Lollar, B., Slater, G. F., Sleep, B., Witt, M., Klecka, G. M., Harkness, M., Spivack, J., 2001. Stable carbon isotope evidence for intrinsic bioremediation of tetrachloroethene and trichloroethene at Area 6, Dover Air Force Base. Environ. Sci. Technol. 35, 261-269.

Sivavec, T. M., Horney, D. P., 1996. Reductive dechlorination of chlorinated solvents by zero-valent iron, iron oxide and iron sulfide minerals. In Book of Abstracts, 211th ACS National Meeting, New Orleans, LA.

Sivavec, T. M., Horney, D. P., 1997. Reduction of chlorinated solvents by Fe (II) minerals. In: Preprints of papers presented at the 213th ACS national meeting. American Chemical Society: San Francisco, CA, 37, pp 115-117.

Siivola, J., Schmid, R. A., 2007. List of mineral abbreviations. In *Metamorphic Rocks: A Classification and Glossary of Terms. Recommendations of the International Union of Geological Sciences Subcommission on the Systematics of Metamorphic Rocks*, Douglas, F., Desmons, J., Eds, Cambridge University Press: New York, pp 93-110.

Simpson, A.J., Burdon, J., Graham, C.L., Hayes, M.H.B., Spencer, N., Kingery, W.L., 2001. Interpretation of heteronuclear and multidimensional NMR spectroscopy of humic substances. Euro. J. Soil Sci. 52, 495-509.

Skeen, R.S., Valentine, N.B., Petersen, J.N., Hooker, B.S., 1995. Kinetics of nitrate inhibition on biological transformation of carbon tetrachloride. Biotechnol. Bioeng. 45, 279-284

Slater, G. F., Dempster, H. S., Sherwood Lollar, B. S., Ahad, J., 1999. Headspace analysis: A new application for isotopic characterization of dissolved organic contaminants. Environ. Sci. Technol. 33, 190-194.

Slater, G. F., Sherwood Lollar, B., Edwards, E., Sleep, B., Witt, M., Klecka, G. M., Harkness, M. R., Spivack, J. L., 2000. Carbon isotopic fractionation of chlorinated ethenes during biodegradation: field applications. In *Natural Attenuation Considerations and Case Studies*, Second International Conference on Remediation of Chlorinated and Recalcitrant Compounds, Monterrey, CA, May 22-25, 2000, Wickramanayake, G. B., Gavaskar, A. R., Kelley, M. E., Eds., Batelle Press: Columbus, OH, pp 17-24.

Slater, G. F., Ahad, J., Sherwood Lollar, B. S., Allen-King R., Sleep, B., 2000. Carbon isotope effects resulting from equilibrium sorption of dissolved VOCs, Anal. Chem. 72, 5669-5672.

Slater, G. F., Lollar, B. S., Sleep, B. E., Edwards, E. A., 2001. Variability in carbon isotopic fractionation during biodegradation of chlorinated ethenes: implications for field applications. Environ. Sci. Technol. 35, 901-907.

Slater, G. F., Sherwood Lollar, B., Allen King, R., O'Hannesin, S. ,2002. Isotopic fractionation during reductive dechlorination of trichloroethene by zero-valent iron: influence of surface treatment. Chemosphere 49, 587-596.

Slater, G. F., Sherwood Lollar, B., Lesage, S., Brown, S., 2003. Carbon isotope fractionation of PCE and TCE during dechlorination by vitamin B_{12}. Ground Water Monit. Rem. 23, 59-67.

Steelink, C., 1985. Implications of elemental characteristics of humic substances. In: G.R. Aiken, D.M. McKnight and R.L. Warshaw, Editors, *Humic substances in soil, sediment, and water*, Wiley, New York (1985), pp. 457–476.

Taylor, J. K., Cihon, C., 2004. Statistical techniques for data analysis, Second Edition, Chapman and Hall/CRC: New York, p 208.

Tessier, A., Campbell, P. G. C., Bisson, M., 1979. Sequential extraction procedure for the speciation of particulate trace metals. Anal. Chem. 51, 844-851.

Tipping, E., 1981. The adsorption by goethite (α-FeOOH) of humic substances from three different lakes. Chem. Geol. 33. 81-89.

Tratnyek, P.G., Scherer, M.M., Deng, B., Hu, S., 2001. Effects of natural organic matter, anthropogenic surfactants, and model quinones on the reduction of contaminants by zero-valent iron. Wat. Res. 35, 4435-4443.

Ulibarri, M.A., Pavlovic, I., Hermosin, M.C., Cornejo, J., 1995. Hydrotalcite-like compounds as potential sorbents of phenols from water. Appl. Clay Sci. 10, 131-145.

Ulrich, G. A., Krumholz, L. R., Suflita, J. M., 1997. A rapid and simple method for estimating sulfate reduction activity and quantifying inorganic sulfides. Appl. Environ. Microbiol. 63, 1627-1630.

U.S. EPA, 1997. Use of Monitored Natural Attenuation at Superfund, RCRA Corrective Action and Underground Storage Tank Sites, Draft Interim Final, U.S. EPA Office of Solid Waste and Emergency Response Directive 9200.4-17, U.S. EPA Washington, DC (http://www.epa.gov/oust/directiv/9200417z.htm.

U.S. Environmental Protection Agency (EPA), 2008. Volatile Target Compound List and Corresponding CRQLs. http://www.epa.gov/superfund/programs/clp/somvtarget.htm).

van Breukelen, B. M. 2007. Quantifying the degradation and dilution contribution to natural attenuation of contaminants by means of an open system Rayleigh equation. Environ. Sci. Technol. 41, 4980-4985.

Van Eekert, M. H. A., Schroder, T. J., Stams, A. J. M., Schraa, G., Field, J. A., 1998. Degradation and fate of carbon tetrachloride in unadapted methanogenic granular sludge. Appl. Environ. Microbiol. 64, 2350-2356.

VanStone, N. A., Focht, R. M., Mabury, S. A., Sherwood Lollar, B., 2004. Effect of iron type on kinetics and carbon isotopic enrichment of chlorinated ethylenes during abiotic reduction on Fe(0). Ground Water, 42, 268-276.

VanStone, N., Elsner, M., Lacrampe-Couloume, G., Mabury, S., Sherwood Lollar, B., 2008. Potential for identifying abiotic chlroalkane degradation mechanisms using carbon isotopic fractionation. Environ. Sci. Technol. 42, 126-132.

Vieth, A., Müller, J., Strauch, G., Kastner, M., Gehre, M., Mechenstock, R. U., Richnow, H. H., 2003. In-situ biodegradation of tetrachloroethene and trichloroethene in contaminated aquifers monitored by stable isotope fractionation. Isotope Environ. Health Stud. 39, 113-124.

Vikesland, P. J., Heathcock, A. M., Rebodos, R. L., Makus, K. E., 2007. Particle size and aggregation effects on magnetite reactivity toward carbon tetrachloride. Environ. Sci. Technol. 41, 5277-5283.

Villa, M.V., Sanchez-Martin, M.J., Sanchez-Camazano, M., 1999. Hydrotalcites and organo-hydrotalcites as sorbents for removing pesticides from water. J. Environ. Sci. Health B. 34, 509-525.

Vogel, T. M., Criddle, C.S., McCarty, P.L., 1987. Transformation of halogenated aliphatic compounds. Environ. Sci. Technol. 21, 722-736.

von Wandruszka, R., 2000. Humic acids: Their detergent qualities and potential uses in pollution remediation. Geochem. Trans. 1, 10, doi:10.1186/1467-4866-1-10

Vreysen, S., Maes, A., 2008. Adsorption mechanism of humic and fulvic acid onto Mg/Al layered double hydroxides. Appl. Clay. Sci. 38, 237-249.

Wang, Q., Morse, J. W., 1996. Pyrite formation under conditions approximating those in anoxic sediments I. Pathway and morphology. Mar. Chem. 52, 99-121.

Weerasooriya, R., Dharmasena, B., 2001. Pyrite assisted degradation of trichloroethene (TCE). Chemosphere 42, 389-396.

Wiedemeier, T. H., Rifai, H.S., Newell, C.J., Wilson, J.T., 1999. Natural Attenuation of Fuels and Chlorinated Solvents in the Subsurface. John Wiley&Sons, Inc., New York.

Williams, A.G., Scherer, M.M., 2001. Kinetics of Cr (VI) reduction by carbonate green rust. Environ. Sci. Technol. 35, 3488-3494.

Workman Jr., J., Springsteen, A., Duckworth, J., 1998. *Applied Spectroscopy: A Compact Reference for Practitioners*. Academic Press, Chestnut Hill, MA, pp. 98-104.

Wu, Q., Sowers, K. R., May, H. D., 2000. Establishment of a polychlorinated biphenyl-dechlorinating microbial consortium, specific for doubly flanked chlorines, in a defined, sediment-free medium. Appl. Environ. Microbiol. 66, 49-53.

Yalkowsky, S. H., He, Y., 2003. *Handbook of Aqueous Solubility Data*. CRC Press LLC: Boca Raton, FL, p 22-29.

Zhu, X., Castleberry, S. R., Nanny, M. A., Butler, E. C., 2005. Effects of pH and catalyst concentration on photocatalytic oxidation of aqueous ammonia and nitrite in titanium dioxide suspensions. Environ. Sci. Technol. 39, 3784-3791.

Zou S., Stensel. H. D., Ferguson, J. F., 2000. Carbon tetrachloride degradation: Effect of microbial growth substrate and vitamin B_{12} content. 34, 1751-1757.

Zwank, L., 2004. Assessment of the fate of organic groundwater contaminants using their isotopic signatures. PhD thesis, Swiss Federal Institute of Technology (ETH), Zurich, Switzerland.

Zwank, L., Elsner, M., Aeberhard, A., Schwarzenbach, R. P., Haderlein, S. B., 2005. Carbon isotope fractionation in the reduction dehalogenation of carbon tetrachloride at iron (hydr)oxide and iron sulfide minerals. Environ. Sci. Technol. 39, 5634–5641.

APPENDIX A

XRD Analyses for Iron Minerals

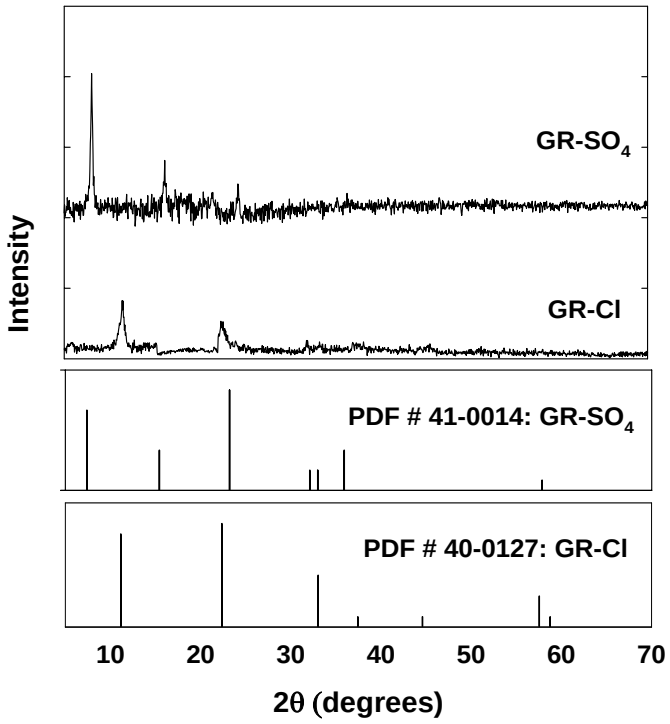

Figure A1. XRD patterns for chloride green rust (GR-Cl) and sulfate green rust (GR-SO_4). Reference patterns are from JCPDS (1990).

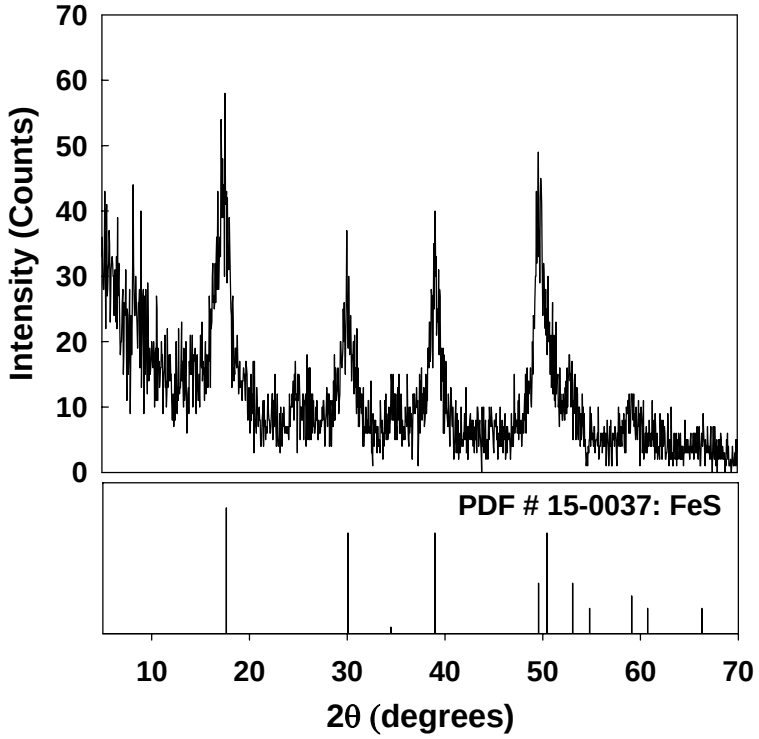

Figure A2. XRD pattern for FeS.

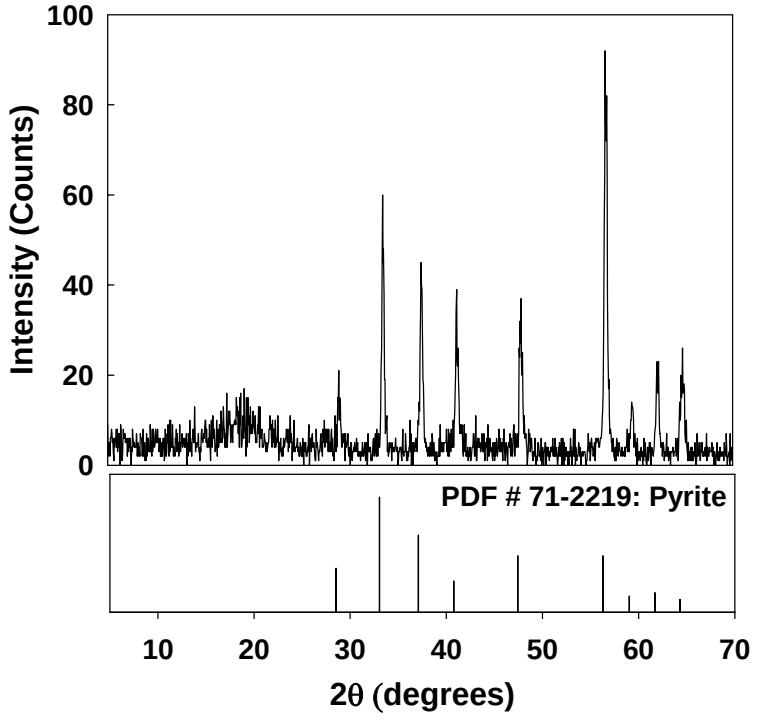

Figure A3. XRD pattern for pyrite.

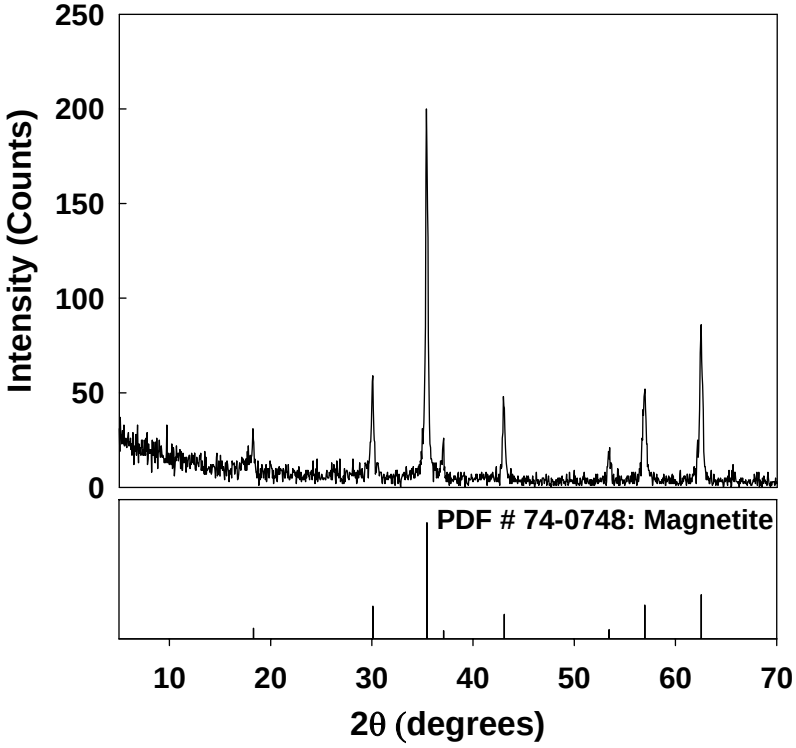

Figure A4. XRD pattern for magnetite.

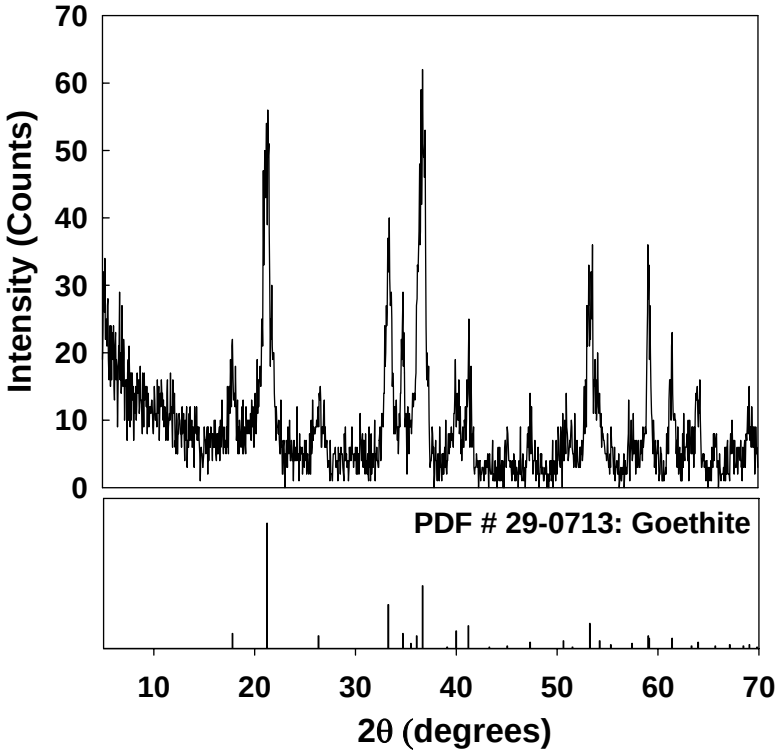

Figure A5. XRD pattern for goethite.

APPENDIX B

Supporting Information for Chapter 3

This appendix is the supporting information related to chapter 3, including experimental setup, analytical methods, and additional data.

B1. Sources of Chemical Reagents

The following chemicals were obtained from Sigma-Aldrich (St. Louis, MO): PCE (99%), TCE (99.5%), *cis*-1,2-dichlorethylene (*cis*-DCE), *trans*-1,2-dichlorethylene (*trans*-DCE), 1,1-dichlorethylene (1,1-DCE), N-(2-hydroxyethyl)-piperazine-N'-3-propanesulfonic acid (HEPES), and [(2-Hydroxy-1,1-bis(hydroxymethyl)ethyl)amino]-1-propanesulfonic acid (TAPS). Ethylene (1026 ppm in N_2), acetylene (1001 ppm in N_2), and vinyl chloride (VC) (1019 ppm in N_2) were obtained from Scott Specialty Gases (Houston, TX). Other chemicals were purchased from Fisher Scientific (Pittsburgh, PA). All aqueous solutions were prepared with nanopure water (18.0 MΩ cm resistivity, Barnstead Ultrapure Water System, IA).

B2. Sampling Locations

Norman Landfill (L) soil samples were obtained from approximately 2 m below the ground surface near the No. 35 multilevel well (Cozzarelli et al., 2000) using a Geoprobe® (Geoprobe Systems, KS) and ground water was obtained approximately 3.5 m below the ground surface from the same well using a peristaltic pump. Duck Pond (DP) sediments were taken from the top 3-8 cm of the near shore sediment with a sterile spatula. Duck Pond water was collected in autoclaved 2L

Pyrex® medium bottles at the sediment sampling site. Altus AFB (AAFB) biowall samples were obtained using a Simco earthprobe® (Simco Drilling Equipment Inc. IA) from 3.5-6.2 m deep and approximately 1.5 m south of Well MP 1 (microcosms AAFB-8, AAFB-9 and AAFB-10) inside the biowall in the OU1 area (see map in (Lu et al., 2008)) and from 2.7-5.0 m deep and about 0.9 m east of Well BB04 inside the biowall downgradient of Building 506 in the SS-17 area (microcosms AAFB-12 and AAFB-14) (see map of the area around building 506 in ref. (Kennedy et al., 2006)). In order to prevent oxidation and loss of fine particles during the sampling process, biowall samples were frozen *in-situ* with liquid nitrogen injected into the ground via a steel tube, extracted from the ground frozen, and then stored on dry ice in a cooler until transport to the laboratory. Ground water at AAFB was pumped from 4.6 m below the ground surface from Wells MP1 and BB05W. All solid and liquid samples were flushed with sterile N_2/CO_2 and stored in the dark at 4 °C before use.

B3. Microcosm Setup

After preparation, microcosms were sealed with sterilized thick butyl rubber stoppers and aluminum crimp seals, removed from the anaerobic chamber and flushed with sterile cotton filtered N_2. Microcosms (except unamended ones) were preincubated until the desired terminal electron accepting process was established. We determined this by monitoring Fe(II) (aq), sulfate, and methane, for iron reducing (IR), sulfate reducing (SR), and methanogenic (Meth) conditions, respectively. During preincubation, microcosms were stored upside down at room temperature in the dark. A summary of the microcosm conditions set up and the abbreviations used to describe them is given in Table B1.

After preincubation, some microcosms were killed by placement in a boiling water bath for 15 minutes a total of three times at three day intervals. Then, 100 μg/mL of the wide spectrum antibiotics kanamycin and chloramphenicol were added to completely inhibit microbial metabolism (Wu et al., 2000). Both sulfate reduction and methane production were inhibited in the killed microcosms for up to 155 days.

After preincubation, and, in some cases, heat/antibiotic treatment, butyl rubber septa were replaced with autoclaved Teflon-lined butyl rubber septa (West Pharmaceutical Services, Kearney, NE) inside the anaerobic chamber. Ten milliliters of saturated PCE or TCE stock solution were then spiked into the microcosms to yield total concentration (mass in the aqueous plus gas phases divided by aqueous volume) of 24-103 μM (PCE) or 92-130 μM (TCE) in standards containing no solid phase. At the same time, an additional 5 mM of electron donor was spiked into the microcosms to support microbial reductive dechlorination. After preincubation with electron donors and acceptors (or without preincubation for unamended microcosms), one microcosm for each condition was sacrificed for geochemical analysis using techniques summarized below, and the results are summarized in Table B2. Each geochemical parameter was measured in duplicate. Dissolved Fe(II), sulfate, and methane were also measured to determine whether the desired redox conditions had been established.

All amended microcosms were prepared in triplicate, and unamended and killed microcosms were prepared in duplicate. Except if noted otherwise, reported concentrations, percent remaining values, and product recoveries are means of values measured in replicate microcosms; uncertainties are standard deviations of the mean.

B4. Analytical Techniques

Concentrations of PCE, TCE, *cis*-DCE, *trans* 1,2-dichloroethylene (*trans*-DCE), 1,1-dichloroethylene (1,1-DCE), VC, ethylene, acetylene, and methane in the microcosms were quantified by gas chromatography (GC) with headspace analysis using methods given in Liang et al. (2007). No ethane was detected in the microcosms. Carbon isotope ratios were measured against a CO_2 standard with aqueous samples using an O.I. Analytical - Model 4560 purge and trap system interfaced with a Varian 3410 GC with Finnigan MAT 252 mass spectrometer. Approximately 15 % of samples were run in duplicate and the typical standard deviation for $\delta^{13}C$ values from duplicate measurements was 0.2-0.3 ‰ or better (Liang et al., 2007). Isotope analysis was also performed for two samples among duplicate or triplicate microcosms. The results were then combined to calculate ε_{bulk} values. ε_{bulk} values did not differ significantly between replicate microcosms.

Sulfate was quantified using a Dionex ion chromatograph (IC) with an Ion Pac AG 11 guard column (4 × 50 mm) and an Ion Pac AS 11 anion analytical column (4 × 250 mm), coupled with an ED 50 conductivity detector. Solid phase S(-II) was measured using a method adapted from Ulrich et al. (1997) and described in Shao and Butler (2007). FeS was assumed to be equal to the molar concentration of solid phase S(-II), measured as cited above. After S(-II) measurement, the remaining solid was reduced by 1 M Cr(II)-HCl solution for 72 hrs to quantify Cr(II) reducible or Cr(II) extractable sulfur (CrES), which includes S(0), polysulfides, and pyrite (Canfield et al., 1986; Huerta-Diaz et al., 1993).

Ferrous iron species were measured by ferrozine assay as described in Lovely and Phillips (Lovely and Phillips, 1987). For soluble Fe(II), the supernatant of the centrifuged solid/water slurry was acidified with anaerobic 0.5 N HCl at a 1:1 volume ratio prior to Fe(II) measurement. Sequential extractions were then performed to

quantify different Fe(II) species in the solid phase (Heron et al., 1994). Five milliliters of solid/water slurry was collected and extracted with 1 M $MgCl_2$ for 5 hours to quantify weakly bound Fe(II) (Gibbs, 1973; Tessier et al., 1979). Extraction with 0.5 N HCl was used to quantify total solid phase Fe(II), including FeS and non-sulfur Fe(II) (Lovley and Phillips, 1987). Non-sulfur solid phase Fe(II) species are referred to as "surface associated Fe(II)". Strongly bound Fe(II) was calculated by subtracting weakly bound Fe(II) from surface associated Fe(II) (Shao and Butler, 2007). Total organic carbon (TOC) in the solid phase was measured with a TOC-5000 analyzer (Shimadzu Corp.) with a solid-sample module (SSM-5050) following the protocols provided by the manufacturer.

To assess the effect of heat treatment on abiotic mineral species that could potentially react with PCE and TCE, the solid phase mineral fractions described above were analyzed for two microcosm conditions (DP-IR-pH 8.2 and AAFB-8-SR-pH 7.2) before and after heat treatment by boiling water bath for 20 minutes. While heat treatment did not significantly affect the concentration of FeS, strongly bound Fe(II), or CrES (as evidenced by overlapping 95% confidence intervals for the concentration of these species before and after heat treatment), it did significantly lower the concentration of weakly bound Fe(II) in the one microcosm (DP-IR-pH 8.2) for which this species was above detection limits (Table B3). Specifically, for DP-IR-pH 8.2, weakly bound Fe(II) decreased by 37% upon heat treatment. While we considered the possibility that this decrease in weakly bound Fe(II) in the killed microcosms could cause us to underestimate the abiotic contribution to PCE or TCE reductive dechlorination, our conclusions about the relative importance of abiotic and microbial reductive dechlorination are in fact based on several lines of evidence—mainly analysis of reaction kinetics and product recoveries in live microcosms. Thus,

the 37% decrease in weakly bound Fe(II) upon heat treatment in one representative microcosm (Table B3) does not change our overall conclusions.

For certain microcosms, we identified the more abundant minerals in the solid phase after preincubation by X-ray diffraction (XRD) using a Rigaku DMAX® X-ray Diffractometer (Table B2). Solid/liquid samples were centrifuged at an RCF of 1260 × g for 10 min and the solid was then freeze-dried under vacuum. Transfer to and from the freeze dryer was done in a glass tube with a custom vacuum valve to prevent exposure to the air. Freeze dried samples were then placed in the XRD sample holder inside the anaerobic chamber and mixed with petroleum jelly to retard the diffusion of oxygen to the sample. Quartz was the major mineral identified by XRD in the Landfill and Duck Pond solids and the two solid samples from AAFB that were analyzed (AAFB-12-SR-pH 7.2 and AAFB-14-SR-pH 7.2). We used the Hanawalt search/match method (Jenkins and Snyder, 1996) to identify minor mineral species by XRD. First, the peaks associated with quartz were eliminated from the sample pattern. Then the d-spacing value of the strongest peak in the remaining pattern was compared to the d-spacing values of the strongest peaks for iron minerals likely to be present in the natural environment. If a match was found, the sample pattern was searched for the other representative peaks for that mineral (i.e., the second or third strongest peaks). If these additional peaks were matched, then we concluded that that mineral was present in our sample. The whole XRD pattern associated with that mineral was then eliminated and the process restarted with the strongest peak in the remaining XRD pattern. If, however, no match was found for the original strongest peak not associated with quartz, that peak was ignored and the process restarted with the next strongest peak in the sample pattern. All minor mineral species identified in the microcosms using this approach are given in Table B2. In general, only

unreactive Fe(III) oxides were identified, with the exception of one microcosm (L-SR-pH 8.2), where mackinawite was identified and two microcosms (AAFB-SR-12-pH 7.2 and AAFB-SR-14-pH 7.2) where magnetite was identified. As stated in the manuscript, magnetite was added to the biowall area from which the solids used to construct these microcosms were obtained. Other potentially reactive minerals were below XRD detection limits.

One microcosm (DP-SR-pH 8.2) was analyzed using scanning electron microscopy (SEM) with a JEOL JSM-880 High Resolution instrument. This microcosm was chosen because of the high concentration of FeS formed under sulfate reducing reactions (Table B2). The SEM sample was prepared using the method by Herbert and coworkers (Herbert et al., 1998) except that ethanol and not acetone was used for sample dehydration.

B5. Equilibrium Partitioning among the Gas, Aqueous, and Solid Phases

B.5.1. Calculation of Total Concentrations

Aqueous concentrations of PCE, TCE, and their dechlorination products ($C_{i,aq}$) were calculated from measured gas concentrations ($C_{i,g}$) using Henry's Law:

$$C_{i,aq} = \frac{C_{i,g}}{H_i} \qquad \text{(eq. B1)}$$

where H_i is the dimensionless Henry's Law constant for species i. Henry's Law constants used in these calculations are given in Table B4. Total concentrations ($C_{i,T}$), defined here as the sum of the masses of species i in the gas, aqueous, and solid phases, divided by the volume of the aqueous phase, were calculated using the approach in (Hwang and Batchelor, 2000):

$$C_{i,T} = C_{i,aq}\left(1 + K_{i,s} + H_i \frac{V_g}{V_{aq}}\right) = C_{i,aq} F_i \qquad \text{(eq. B2)}$$

where $K_{i,s}$ is the solid-liquid partition coefficient, V_g and V_{aq} are volumes of the gas and aqueous phases (50 and 110 mL, respectively), and the partitioning factor (F_i) is defined as $\left(1 + K_{i,s} + H_i(V_g / V_{aq})\right)$. $K_{i,s}$ was calculated as follows (Hwang and Batchelor, 2000):

$$K_{i,s} = K_{i,d} \frac{m_s}{V_{aq}} \qquad \text{(eq. B3)}$$

where $K_{i,d}$ is the solid/water distribution coefficient and m_s is the mass of the solid phase in the microcosm (20 g). $K_{i,d}$ was estimated from the empirical relationship $K_{i,d} = K_{i,oc} f_{oc}$ (Karickhoff et al., 1979), where $K_{i,oc}$ is the solid phase organic matter/water distribution coefficient, and f_{oc} is the weight fraction of organic matter in the solid (i.e., TOC, Table B2). $K_{i,oc}$ was estimated using two empirical equations: (1) for chlorinated aliphatics: $LogK_{i,oc} = 0.57 LogK_{i,ow} + 0.66$ (Schwarzenbach et al., 2003), where $K_{i,ow}$ is the published octanol/water partition coefficients (Howard and Meylan, 1997; Mackay et al., 2006); (2) for ethylene and acetylene: $LogK_{i,oc} = -0.58 LogS_i + 4.24$ (Doucette, 2000), where S_i is the aqueous solubility in μM, obtained from Howard and Meylan (1997) and Yalkowsky and He (2003) (Table B4). Estimated $K_{i,oc}$ values are given in Table B4. The K_{oc} value for TCE in Table B4 is significantly higher than values measured for AAFB biowall solids (14-21 L/kg) (Shen and Wilson, 2007), meaning that we may have overestimated TCE sorption in the AAFB microcosms. We used the K_{oc} values in Table B4, however, so that we could do all calculations with a self consistent set of K_{oc} values.

B5.2. Calculation of Observed Product Recoveries

Observed abiotic and biotic product recoveries (R) (Table 3.1) were calculated by dividing the total concentrations of biotic products (i.e., TCE (for PCE), DCE isomers, VC and ethylene) or abiotic products (acetylene, and, except for AAFB microcosms, ethylene) by the total concentration of the reactant (PCE or TCE) at time zero ($C_{r,T,0}$):

$$R(\%) = \frac{\sum C_{p,T}}{C_{r,T,0}} \times 100\% = \frac{\sum C_{p,aq} F_p}{C_{r,T,0}} \times 100\% \qquad \text{(eq. B4)}$$

For the live AAFB microcosms, the kinetic data (Figure B3) indicate that, with the possible exceptions of AAFB-12-SR-pH 7.2-PCE and AAFB-14-SR-pH 7.2-PCE (Figures B3d, and e), the majority of ethylene was produced microbially, as evidenced by no co-detection of acetylene, and co-detection with VC. Therefore, we included ethylene in the biotic product recoveries (Table 3.1) for all live AAFB microcosms, except AAFB-12-SR-pH 7.2-PCE and AAFB-14-SR-pH 7.2-PCE. Because it was unclear if ethylene came from abiotic or microbial dechlorination in AAFB-12-SR-pH 7.2-PCE and AAFB-14-SR-pH 7.2-PCE, we calculated neither abiotic nor microbial product recoveries for these microcosms (Table 3.1).

For AAFB killed microcosms, low concentrations of ethylene were observed even when VC was not detected. Thus, ethylene (and, when detected, acetylene) was included in the abiotic product recoveries for killed AAFB microcosms (Table 3.1).

B5.3. Correction of Rate Constants for Partitioning among the Gas, Aqueous, and Solid Phases

Mass normalized rate constants (i.e., rate constants divided by mass loading) for PCE or TCE transformation by FeS, adjusted to or measured in a zero-headspace

system (k_m), were taken from the literature (Liang et al., 2007; Butler and Hayes, 1999, 2001; Zwank, 2004). The mass loadings of FeS in Zwank (2004) were estimated from the reported concentrations of reagents used to synthesize the FeS. Rate constants for similar pH values were averaged, yielding the following k_m values ($Lg^{-1}d^{-1}$): PCE at pH 7-7.3: 2.41×10^{-4}; PCE at pH 8-8.3: 1.22×10^{-3}; TCE at pH 7.3: 7.28×10^{-4}; and TCE at pH 8-8.3: 1.95×10^{-3}. Then, we used the approach in Hwang and Batchelor (2000) to correct rate constants to account for partitioning of PCE or TCE among the gas, aqueous, and solid phases ($k_{m,corr}$):

$$k_{m,corr} = \frac{k_m}{F_i} \qquad \text{(eq. B5)}$$

where F_i is defined after equation B2, and the subscript "*i*" corresponds to the reactant (PCE or TCE). While V_g and V_{aq} were the same in all our microcosms, $K_{i,s}$ was not, since f_{oc} varied among the microcosms. Values of $k_{m,corr}$ for the case where f_{oc}=0, and therefore $K_{i,s}$ is zero are reported in Table B4. We then multiplied the values in Table B4 by the term $(1 + H_i(V_g / V_{aq}))/F_i$ to yield $k_{m,corr}$ values appropriate for the f_{oc} values of each microcosm. These values of $k_{m,corr}$ were used to estimate half lives for abiotic PCE and TCE transformation based on FeS mass loadings in the microcosms. These values are discussed in the chapter 3.

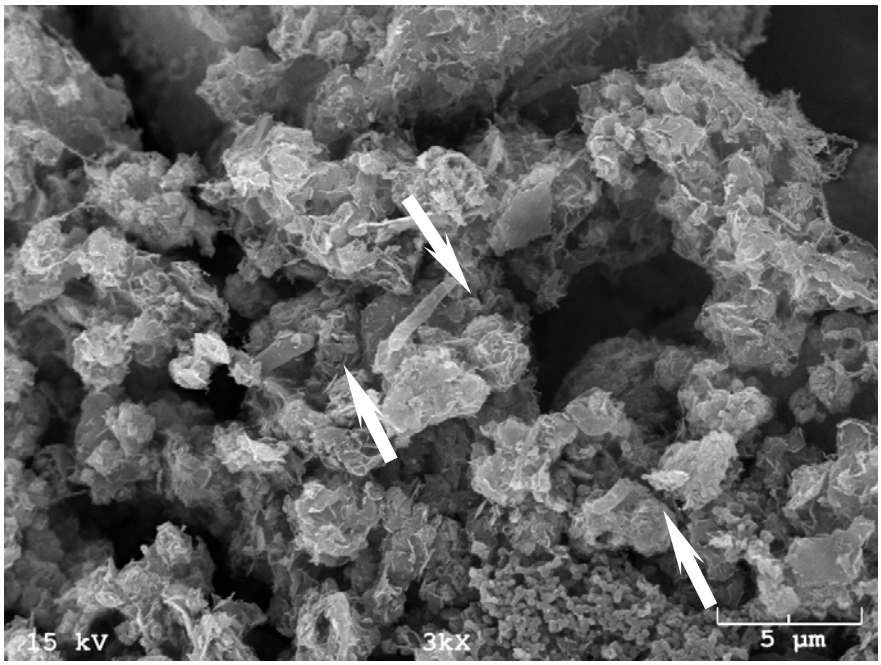

(a)

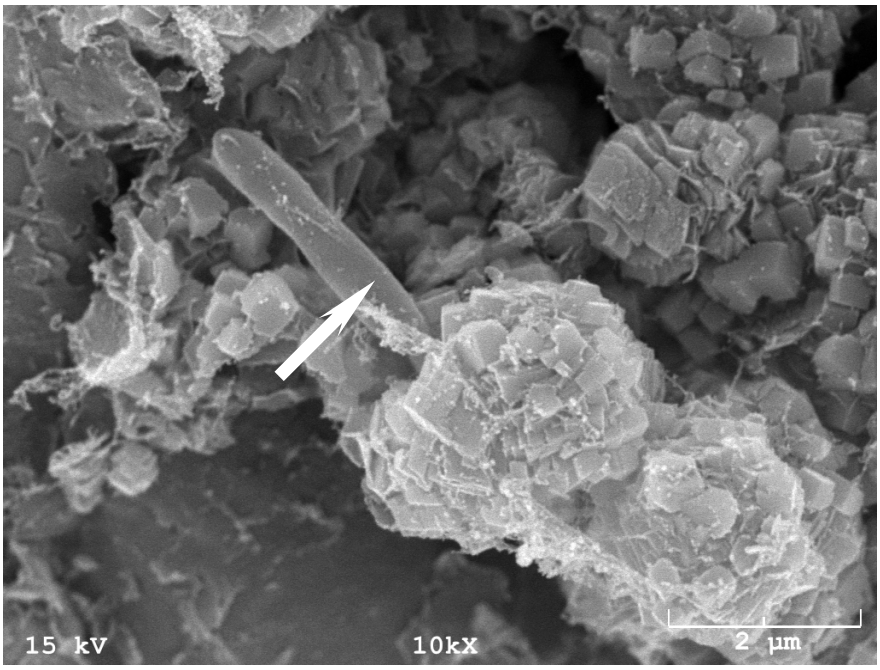

(b)

Figure B1. SEM photomicrographs of sediment from Sample DP-SR-pH 8.2. Cells attached to the surface of the minerals are indicated by arrows. Crystalline mineral precipitates are visible on the right side of panel (b).

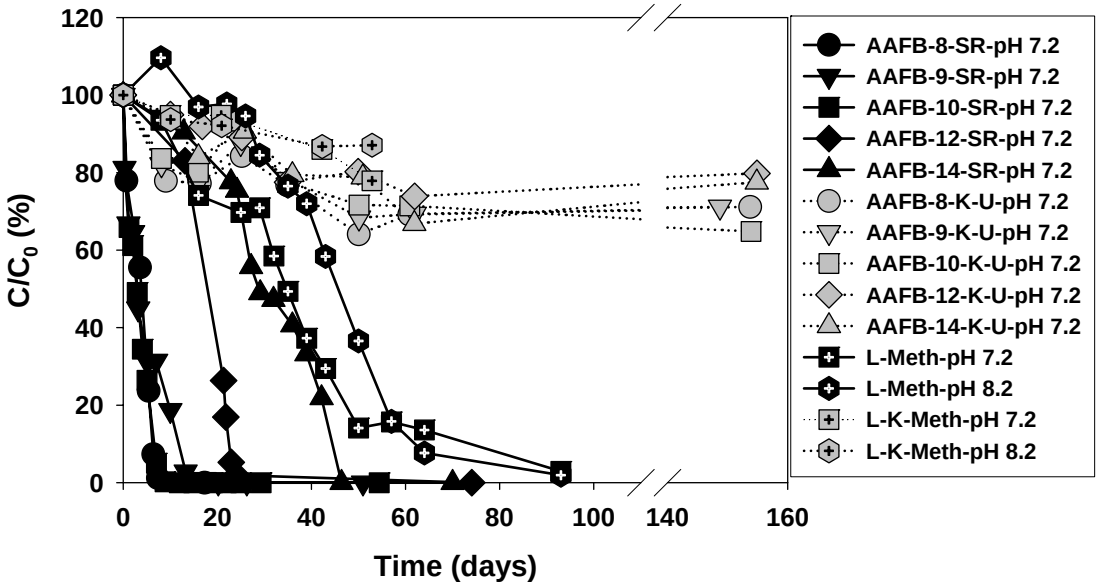

Figure B2. PCE reductive dechlorination in the microcosms with (gray symbols) and without (black symbols) antibiotic and heat treatments.

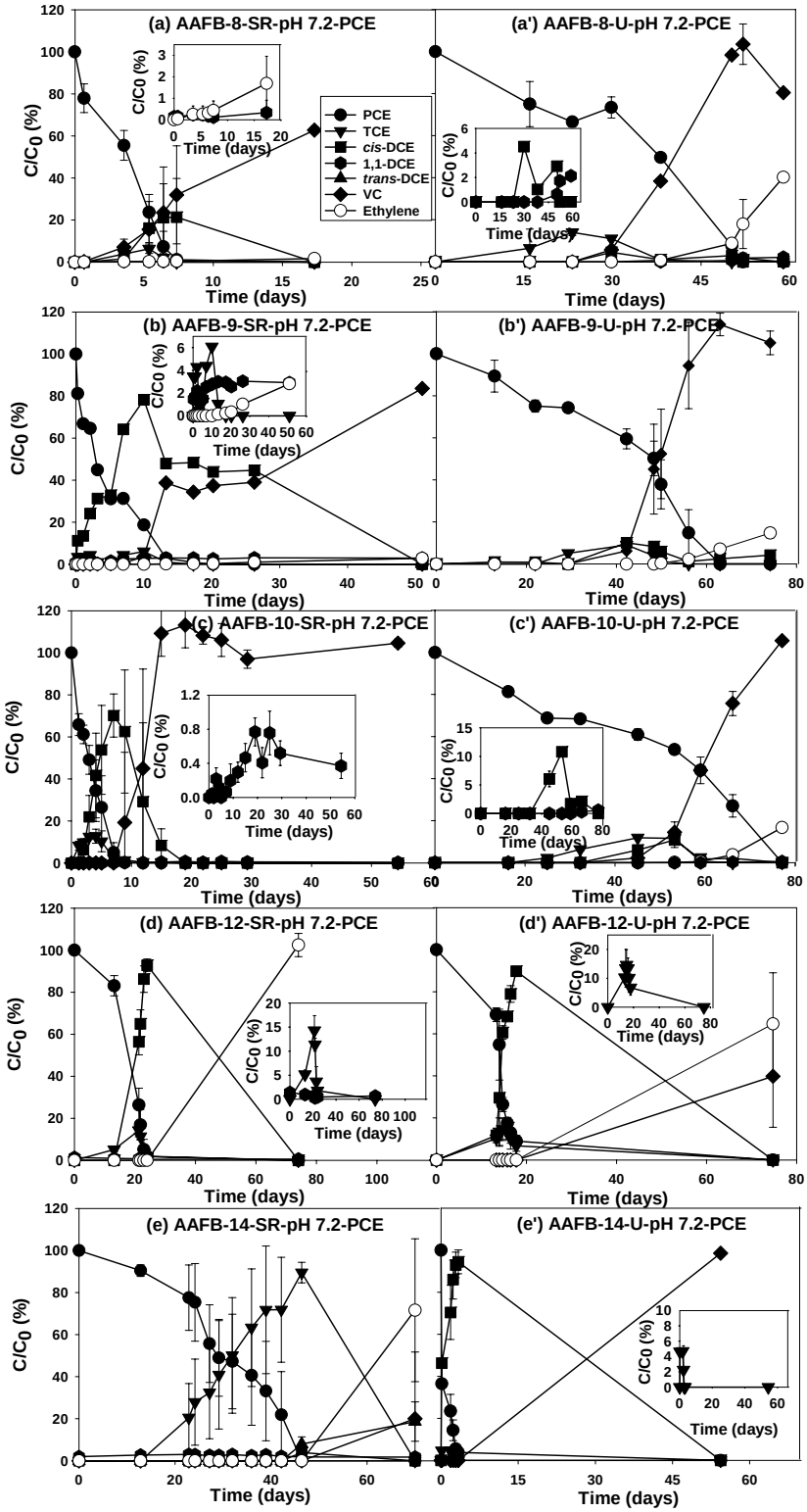

Figure B3. Normalized concentrations of PCE and reaction products in live AAFB microcosms. Reactants and products were normalized by dividing the concentration at any time by the concentration of the reactant at time zero. The insets show reaction products with low concentrations. Error bars are standard deviations of triplicate microcosms.

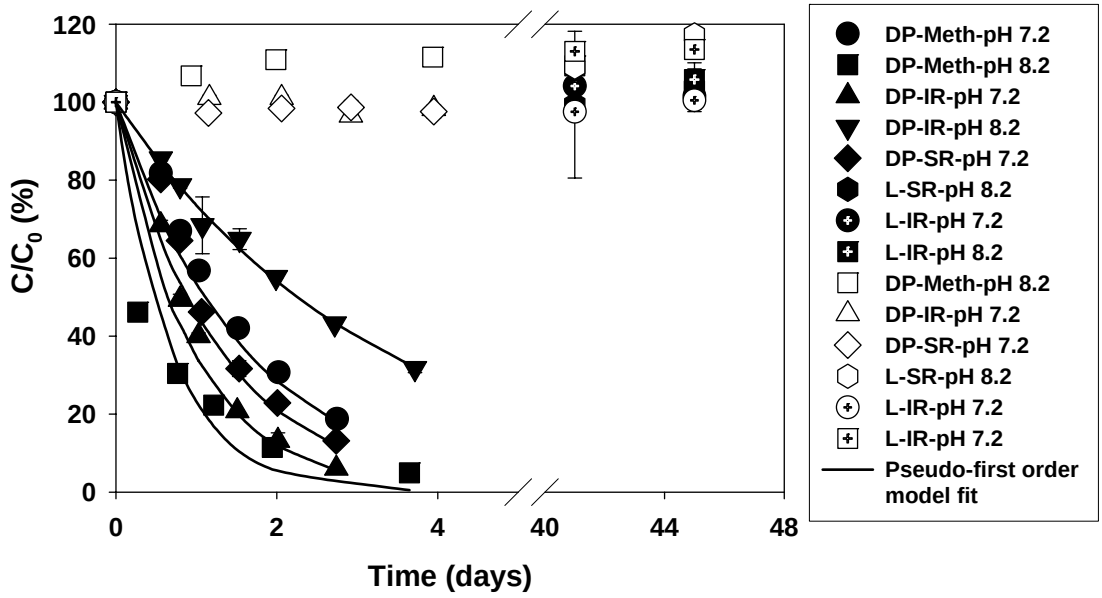

Figure B4. Acetylene transformation in the microcosms. Error bars are standard deviations of the means for duplicate measurements from the same microcosm.

Table B1. Summary of microcosm conditions and abbreviations

Treatment	Geochemical Conditions	Electron Donor	pH	Duck Pond		Norman Landfill		AAFB 8-14[a]
				PCE	TCE	PCE	TCE	PCE
Unamende	—[b]	—	7.2	DP-U-pH 7.2-PCE	DP-U-pH 7.2-TCE	L-U-pH 7.2-PCE	L-U-pH 7.2-TCE	AAFB-*i*-U-pH 7.2-PCE[c]
Amended	Iron reduction	Acetate	7.2	DP-IR-pH 7.2-PCE	—	L-IR-pH 7.2-PCE	—	—
			8.2	DP-IR-pH 8.2-PCE	DP-IR-pH 8.2-TCE	L-IR-pH 8.2-PCE	L-IR-pH 8.2-TCE	—
	Sulfate reduction	Lactate	7.2	DP-SR-pH 7.2-PCE	—	L-SR-pH 7.2-PCE	—	AAFB-*i*-SR-pH 7.2-PCE
			8.2	DP-SR-pH 8.2-PCE	DP-SR-pH 8.2-TCE	L-SR-pH 8.2-PCE	L-SR-pH 8.2-TCE	—
	Methano-genesis	Ethanol	7.2	DP-Meth-pH 7.2-PCE	—	L-Meth-pH 7.2-PCE	—	—
			8.2	DP-Meth-pH 8.2-PCE	DP-Meth-pH 8.2-TCE	L-Meth-pH 8.2-PCE	L-Meth-pH 8.2-TCE	—
Killed	Iron reduction	Acetate	7.2	—	—	—	—	—
			8.2	—	—	—	—	—
	Sulfate reduction	Lactate	7.2	—	—	—	—	AAFB-*i*-K-U-pH 7.2-PCE
			8.2	—	—	—	—	—
	Methano-genesis	Ethanol	7.2	—	—	L-K-Meth-pH 7.2-	—	—
			8.2	—	—	L-K-Meth-pH 8.2-	—	—

[a] The values "8-14" in "AAFB 8-14" refer to the five sampling locations at Altus AFB (AAFB), which were AAFB 8, 9, 10, 12, and 14. [b] — means that the microcosm was unamended or that no microcosms was prepared for this condition. [c] *i* means 8, 9, 10, 12 or 14, which corresponds to AAFB sampling locations 8, 9, 10, 12, or 14.

Table B2. Geochemical properties of microcosms [a]

Microcosm ID	FeS (g FeS/L)	Weakly bound Fe(II) (g Fe/L)	Strongly bound (g Fe/L)	CrES (g S/L)	TOC (g/g solid)	Iron Minerals Detected by XRD[b]
Unamended Microcosms						
DP-U-pH 7.2	$(5.10\pm0.68)\times10^{-2}$	$(2.76\pm0.23)\times10^{-3}$	$(1.28\pm0.11)\times10^{-1}$	$(1.23\pm0.17)\times10^{-1}$	$(9.6\pm1.7)\times10^{-4}$	—[c]
L-U-pH 7.2	$(5.23\pm0.40)\times10^{-3}$	$(3.3\pm4.0)\times10^{-4}$	$(1.25\pm0.10)\times10^{-1}$	$(6.40\pm0.72)\times10^{-3}$	$(2.6\pm1.8)\times10^{-4}$	—
AAFB-8-U-pH 7.2	$(1.45\pm0.15)\times10^{-1}$	$(2.04\pm0.57)\times10^{-3}$	$(1.49\pm0.46)\times10^{-1}$	$(8.4\pm1.1)\times10^{-2}$	$(2.27\pm0.52)\times10^{-2}$	—
AAFB-9-U-pH 7.2	$(4.66\pm0.87)\times10^{-2}$	$(4.2\pm1.9)\times10^{-4}$	$(8.8\pm5.0)\times10^{-2}$	$(7.5\pm1.6)\times10^{-2}$	$(2.30\pm0.68)\times10^{-2}$	—
AAFB-10-U-pH 7.2	$(6.9\pm3.8)\times10^{-2}$	$(2.42\pm0.54)\times10^{-3}$	$(1.08\pm0.66)\times10^{-1}$	$(8.7\pm2.5)\times10^{-2}$	$(1.9\pm1.1)\times10^{-2}$	—
AAFB-12-U-pH 7.2	$(2.9\pm1.5)\times10^{-2}$	$(1.43\pm0.28)\times10^{-2}$	$(2.3\pm1.4)\times10^{-1}$	$(1.24\pm0.27)\times10^{-2}$	$(1.54\pm0.41)\times10^{-2}$	—
AAFB-14-U-pH 7.2	$(5.95\pm0.69)\times10^{-2}$	$(1.48\pm0.34)\times10^{-2}$	$(9.2\pm3.4)\times10^{-2}$	$(1.27\pm0.31)\times10^{-2}$	$(1.51\pm0.15)\times10^{-2}$	—
Amended Microcosms						
DP-SR-pH 7.2	0.385±0.049	$(1.325\pm0.074)\times10^{-3}$	**0.349±0.084**	$(9.8\pm1.6)\times10^{-2}$	$(2.58\pm0.67)\times10^{-3}$	Ge, Lep, Fer
DP-SR-pH 8.2	0.44±0.14	$(5.1\pm1.8)\times10^{-5}$	1.31±0.70	1.291±0.065	$(1.11\pm0.28)\times10^{-3}$	Ge, Lep
DP-IR-pH 7.2	$(1.15\pm0.19)\times10^{-2}$	$(3.898\pm0.071)\times10^{-2}$	0.214±0.038	$(3.18\pm0.49)\times10^{-2}$	$(1.85\pm0.34)\times10^{-3}$	Ge
DP-IR-pH 8.2	$(7.5\pm1.1)\times10^{-3}$	$(5.21\pm0.71)\times10^{-2}$	0.203±0.042	$(3.70\pm0.30)\times10^{-2}$	$(2.86\pm0.53)\times10^{-3}$	Ge, Lep
DP-Meth-pH 7.2	$(6.9\pm2.1)\times10^{-2}$	$(8.2\pm5.9)\times10^{-4}$	$(8.9\pm7.2)\times10^{-2}$	$(5.06\pm0.70)\times10^{-2}$	$(1.8\pm1.5)\times10^{-3}$	Ge, Lep, Fer
DP-Meth-pH 8.2	$(5.45\pm0.77)\times10^{-2}$	$(4.7\pm1.3)\times10^{-4}$	$(6.8\pm2.3)\times10^{-2}$	$(3.81\pm0.64)\times10^{-2}$	$(1.76\pm0.35)\times10^{-3}$	Ge
L-SR-pH 7.2	0.223±0.022	$(5.68\pm0.47)\times10^{-3}$	0.71±0.10	0.431±0.024	$(5.8\pm1.1)\times10^{-4}$	Ge
L-SR-pH 8.2	0.885±0.028	$(1.3355\pm0.0012)\times10^{-3}$	1.085±0.036	$(7.2\pm1.6)\times10^{-2}$	$(8.6\pm2.2)\times10^{-4}$	Ge, Lep, Fer, Mgh, Mk
L-IR-pH 7.2	$(3.328\pm0.095)\times10^{-3}$	$(9.5\pm1.7)\times10^{-3}$	0.375±0.071	$(6.2\pm2.6)\times10^{-3}$	$(1.32\pm0.74)\times10^{-4}$	Lep
L-IR-pH 8.2	$(2.63\pm0.26)\times10^{-3}$	$(3.46\pm0.12)\times10^{-2}$	0.158±0.018	$(6.22\pm0.19)\times10^{-3}$	$(3.2\pm2.2)\times10^{-4}$	Ge, Lep, Fer
L-Meth-pH 7.2	$(1.85\pm0.13)\times10^{-2}$	$(3.7\pm2.3)\times10^{-3}$	$(7.9\pm4.8)\times10^{-2}$	$(1.06\pm0.31)\times10^{-2}$	BDL[d]	Ge, Lep
L-Meth-pH 8.2	$(1.85\pm0.14)\times10^{-2}$	$(2.64\pm0.11)\times10^{-3}$	$(8.94\pm0.81)\times10^{-2}$	$(9.3\pm2.3)\times10^{-3}$	$(1.20\pm0.25)\times10^{-4}$	Ge, Lep
AAFB-8-SR-pH 7.2	0.170±0.093	BDL	0.132±0.082	$(4.65\pm0.57)\times10^{-2}$	$(5.5\pm2.2)\times10^{-2}$	—
AAFB-9-SR-pH 7.2	0.115±0.023	BDL	$(4.0\pm1.2)\times10^{-2}$	$(8.22\pm0.78)\times10^{-2}$	$(3.6\pm2.2)\times10^{-2}$	—
AAFB-10-SR-pH 7.2	0.111±0.037	BDL	$(7.4\pm2.8)\times10^{-2}$	$(1.08\pm0.13)\times10^{-1}$	$(2.95\pm0.41)\times10^{-2}$	—
AAFB-12-SR-pH 7.2	0.141±0.099	BDL	0.20±0.15	$(4.4\pm1.4)\times10^{-2}$	$(2.3\pm1.2)\times10^{-2}$	Mag, Mgh, Aka
AAFB-14-SR-pH 7.2	0.159±0.013	BDL	$(2.41\pm0.35)\times10^{-2}$	$(2.07\pm0.31)\times10^{-2}$	$(1.57\pm0.40)\times10^{-2}$	Mag, Mgh, Aka

[a] All measurements, except for weakly bound Fe(II), were carried out with freeze dried solids and the results were corrected by water content to yield values correct for wet solids. [b] Aka: akaganeite, Fer: ferrihydrite, Ge: goethite, Lep: lepidocrocite, Mag: Magnetite, Mgh: maghemite, Mk: mackinawite (Siivola and Schmid, 2007); [c] —, XRD analysis was not performed for this condition. [d] BDL, below detection limits of approx. 8×10^{-6} g/L. Uncertainties are standard deviations of triplicate samples from the same microcosm.

Table B3. Results of geochemical analyses before and after heat treatment

	DP-IR-pH 8.2 (g/L)		AAFB-8-SR-pH 7.2 (g/L)	
	Before[a]	**After**[a]	**Before**[a]	**After**[a]
FeS	0.112±0.014	0.1230±0.0046	0.292±0.046	0.357±0.087
Weakly bound Fe(II)	0.0199±0.0047	0.01253±0.00084	BDL[b]	BDL
Strongly bound Fe(II)	1.72±0.27	1.84±0.16	0.056±0.054	0.076±0.018
CrES	0.114±0.042	0.122±0.014	0.0247±0.0098	0.033±0.012

[a] Uncertainties are 95% confidence intervals of the mean of triplicate samples from the same microcosm.
[b] BDL means below detection limits.

Table B4. Physical-chemical and kinetic properties of reactants and products

	H_i (Dimensionless)[a,b]	$K_{i,ow}$[a,b]	Solubility (S_i, μM) [a, c]	$K_{i,oc}$ (25ºC, L/Kg)	$k_{m,corr}$ (pH~7)($Lg^{-1}day^{-1}$)[d]	$k_{m,corr}$ (pH~8) ($Lg^{-1}day^{-1}$)[d]
PCE	0.75	2.99		231.37	$(1.8\pm1.2)\times10^{-4}$	$(9.1\pm1.6)\times10^{-4}$
TCE	0.39	2.67		153.90	$(6.2\pm5.7)\times10^{-4}$	$(1.7\pm1.9)\times10^{-3}$
cis-DCE	0.34	1.86		52.33		
trans-DCE	0.40	2.08		69.62		
1,1-DCE	1.62	2.13		74.83		
VC	5.95	1.53		33.87		
Acetylene	0.93		1.86×10^{7}	4.35		
Ethylene	8.93		1.62×10^{6}	1.05		

[a] Howard and Meylan, 1997; [b] Mackay et al., 2006; [c] Yalkowsky and He, 2003; [d] Calculated for the condition where f_{oc}=0

APPENDIX C

Calculation Methods for Surface Area Normalized Rate Constants, Mass Recoveries, and Occupation Area of NOM Anions

C1. Surface Area Normalized Rate Constants

Surface area normalized rate constants (k_{SA}) was given below using an example of abiotic reductive transformation of PCE by FeS at pH 9. An observed rate constant (k_{obs}) and the corresponding standard error (SE) were obtained from non-linear regression of PCE concentration (M) in aqueous phase versus time (days) using SigmaPlot Version 9.

$$k_{obs,\,PCE} = 2.11\times 10^{-2}\ d^{-1},\ SE = 9.86\times 10^{-4}$$

The 95% confidence interval (CI) is calculated using the following equation:

$$95\%\ CI = \pm t \cdot SE \qquad (C1)$$

The value of t can be obtained from a table according to the degree of freedom. For this example, the degree of freedom is 17 and the corresponding t value is 2.12.

$$95\%\ CI\ k_{obs,\,PCE} = \pm 2.12\times 9.86\times 10^{-4} = \pm 2.09\times 10^{-3}$$

Since the headspace of our experimental system is approximately 1.25 mL, we adjust the observed rate constant to that would be measured in a headspace-free system (k_{obs}') using the following equation (Burris et al., 1996):

$$k_{obs,PCE}' = k_{obs,PCE} f_{PCE} \qquad (C2)$$

In eq. C2, f_{PCE} is defined as $(1+H_{PCE}\times (V_g/V_{aq}))$, where H_{PCE} is the dimensionless Henry's Law constant for PCE (0.764), V_g (1.25 mL) and V_{aq} (6.5 mL) are the gas and the aqueous phase volumes of our experimental system.

$$f_{PCE}=1+ 0.764\times (1.25/6.5)= 1.15$$

$$k_{obs,PCE}'=2.11\times 10^{-2}\ d^{-1}\ \times 1.15= 2.42\times 10^{-2}\ d^{-1}$$

The surface area loading (SAL) can be calculated using the specific surface area (SSA) of the mineral multiplied by the mass loading of the mineral. For this example, SSA is 2.01 m^2/g and the mass loading is 10 g/L.

$$SAL=2.01\ m^2/g \times 10\ g/L = 20.1\ m^2/L$$

$$k_{SA,PCE} = \frac{k_{obs,PCE}'}{SAL} = \frac{2.42\times10^{-2} d^{-1}}{20.1 m^2/L}$$

$$k_{SA,\,PCE} = 1.21\times10^{-3}\ L\ m^{-2}\ d^{-1}$$

$$95\%\ CI\ k_{SA,\,PCE} = 95\%\ CI\ k_{obs,\,PCE} \times f_{PCE}\ /SAL$$

$$95\%\ CI\ k_{SA,\,PCE} = \pm\ 2.09\times10^{-3} \times 1.15/20.1 = 1.19\times10^{-4}$$

C2. Mass Recoveries

Equation 2.1 in Chapter 2 is used to calculate mass recoveries of parent compound and reaction products. The following is the sample calculation of the mass recovery of the remaining PCE for abiotic transformation of PCE by GR-Cl at pH 8. At the last sampling time, the aqueous concentration of PCE ($C_{aq,\,t}$) is 1.24×10^{-5} M and 95% CI is 6.41×10^{-8}. The mmoles of PCE in the aqueous and gas phase at the last sampling time:

$$M_t = C_{aq,\,t}\ V_{aq} + C_{g,t}V_g = C_{aq,\,t}\ V_{aq} + C_{aq,\,t}\ H_{PCE}\ V_g \qquad (C3)$$

Where Vaq and Vg are the volumes of aqueous phase (6.5 mL) and gas phase (1.25 mL), $C_{g,t}$ is the PCE concentration in gas phase, and H_{PCE} is the dimensionless Henry's Law constant for PCE (0.612).

$$M_t = 1.24\times10^{-5}\times6.5 + 1.24\times10^{-5}\times0.612\times1.25 = 9.01\times10^{-5}\ mmole$$

$$95\%\ CI\ M_t = \pm\ (6.41\times10^{-8}\times6.5 + 6.41\times10^{-8}\times0.612\times1.25) = \pm\ 4.65\times10^{-7}$$

At time zero, the aqueous concentration of PCE ($C_{aq,\,0}$) is 2.20×10^{-5} M and 95% CI is 1.93×10^{-7}. The same approach is used to calculate the mmoles of PCE in the aqueous and gas phase at time zero.

$$M_0 = 2.20\times 10^{-5}\times 6.5+2.20\times 10^{-5}\times 0.612\times 1.25=1.60\times 10^{-4} \text{ mmole}$$

$$95\%\ \text{CI}\ M_0 = \pm (1.93\times 10^{-7}\times 6.5+1.93\times 10^{-7}\times 0.612\times 1.25) = \pm 1.40\times 10^{-6}$$

The mass recovery of the remaining PCE ($MR_{PCE,t}$) can be calculated using M_t divided by M_0 and then multiplied by 100%.

$$MR_{PCE,t} = M_t/M_0 = 9.01\times 10^{-5}/1.60\times 10^{-4} \times 100\% = 56.32\%$$

Since the uncertainty of $MR_{PCE,t}$ is associated with the uncertainties of both M_t and M_0, propagation of error must be used to calculate 95% CI for $MR_{PCE,t}$. If y=a/b (Both a and b are independent measured quantities), the 95% CI for y, s_y, can be obtained from the following equation (Miller and Miller, 1988):

$$s_y = y \cdot \sqrt{\left(\frac{s_a}{a}\right)^2 + \left(\frac{s_b}{b}\right)^2} \qquad \text{(C4)}$$

where S_a and S_b are 95% CI for a and b, respectively.

$$95\%\ \text{CI}\ MR_{PCE,t} = \pm 56.32\% \cdot \sqrt{\left(\frac{4.65\times 10^{-7}}{9.01\times 10^{-5}}\right)^2 + \left(\frac{1.40\times 10^{-6}}{1.60\times 10^{-4}}\right)^2}$$

$$95\%\ \text{CI}\ MR_{PCE,t} = \pm\ 0.57\%$$

The mass recoveries of acetylene, ethylene, and TCE are calculated in the same way. The total mass recovery is the sum of all the recoveries including remaining PCE and reaction products. For this example, we notice that the total mass recovery is 131.8±1.3%, which is much greater than 100%. This indicates the calculated 95% CI does not reflect the true uncertainty with the total recovery. The possible reason may be due to the inaccuracy of H_{PCE} we used. Accordingly, we don't report uncertainties of mass recovery for both parent compound and reaction products, and don't report any digit to the right of the decimal point for the mass recoveries in this case. Similar adjustments are also used in the mass recoveries in other cases (e.g., mass recoveries in Tables 2.1, 2.2, and 3.1). In addition, in some cases, we reported one digit or two

digits to the right of the decimal point for mass recoveries when they are less than 0.5 % (Tables 2.1, 2.2 and 3.1) in order to reflect the detection of those compounds during the dechlorination process.

C3. Occupation Area of NOM Anions

The occupation areas of NOM model compounds are shown by dotted lines in Figure C3, and they can be estimated by using the values of bond lengths, covalent radius, and the bonding angle. The bond lengths (nm) of C_b-C_b, C_b-H, C_b-C, C=O, C-O, and O-H are 0.14, 0.108, 0.148, 0.124, 0.129, and 0.097 (Sato and Okuwaki, 1991). C_b means a carbon atom located on a benzene ring. The covalent radius (nm) of C and O are 0.077 (r_c) and 0.066(r_o), and the bonding angle of O-C=O is approximately 120(Sato and Okuwaki, 1991)°.

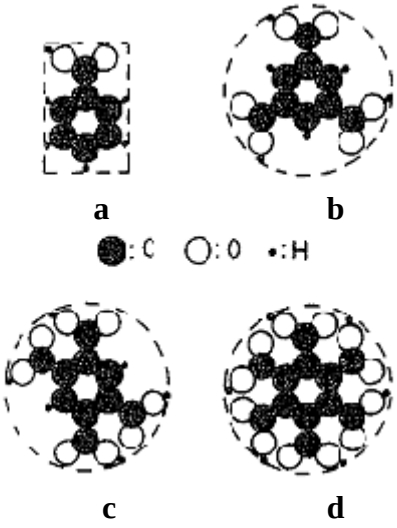

Figure C1: Occupation areas of (a) benzoic acid; (b) trimesic acid; (c) pyromellitic acid; (d) mellitic acid. (Sato and Okuwaki, 1991)

The following is the sample calculation for the occupation area of benzoic acid. The occupation area (*S*) of benzoic acid equals to the area of the rectangle shown by

dotted line in Figure C1. The length (a) and width (b) of rectangle are calculated using the bond lengths, covalent radius, and the bond angle:

$$a= [(C_b\text{-}H) + 2\times (C_b\text{-}C_b) \times Sin30^\circ + (C_b\text{-}C_b) + (C_b\text{-}C) + (C{=}O) \times Sin30^\circ + r_o]$$

$$a = [0.108 + 2\times0.14\times0.5 + 0.14 + 0.148 + 0.124\times0.5 + 0.066] = 0.664$$

$$b = [2 \times (C_b\text{-}H) \times Sin60^\circ + 2\times (C_b\text{-}C_b) \times Sin60^\circ]$$

$$b = [2\times0.108\times0.866+2\times0.14\times0.866] = 0.430$$

$$S = a\times b = 0.664\times0.430 = 0.286\ nm^2$$

APPENDIX D

UV Spectrum of *p*-hydroxybenzoic Acid

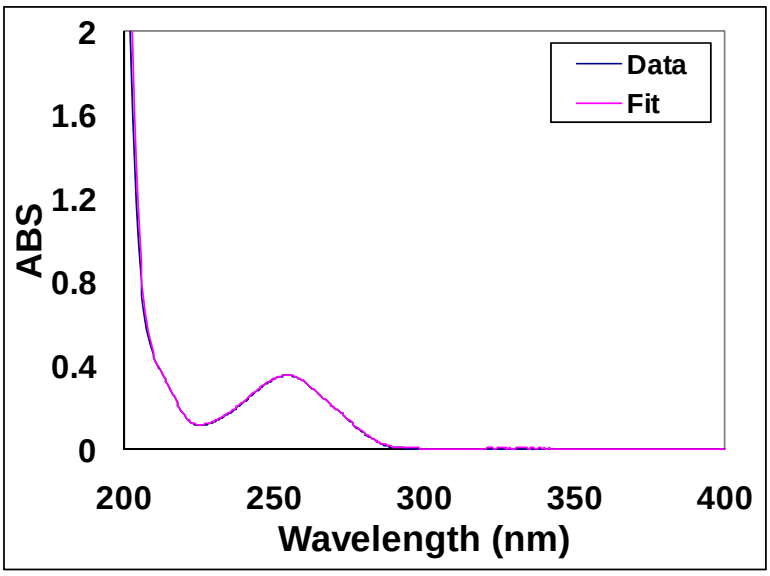

Figure D1. UV spectrum of *p*-hydroxybenzoic acid (dark blue). The line in pink represents a model fit using multiwavelength analysis.

APPENDIX E

Equilibrium Time for the Adsorption of Benzoic acid and Mellitic Acid

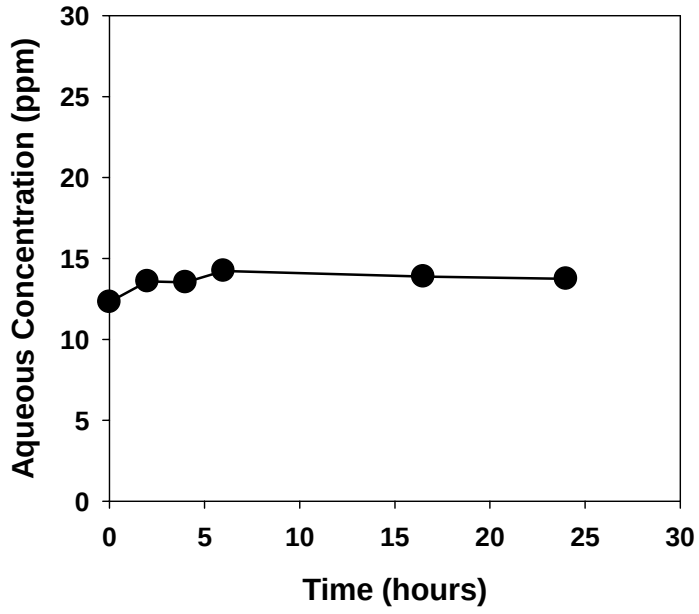

Figure E1. Equilibrium time for the adsorption of benzoic acid

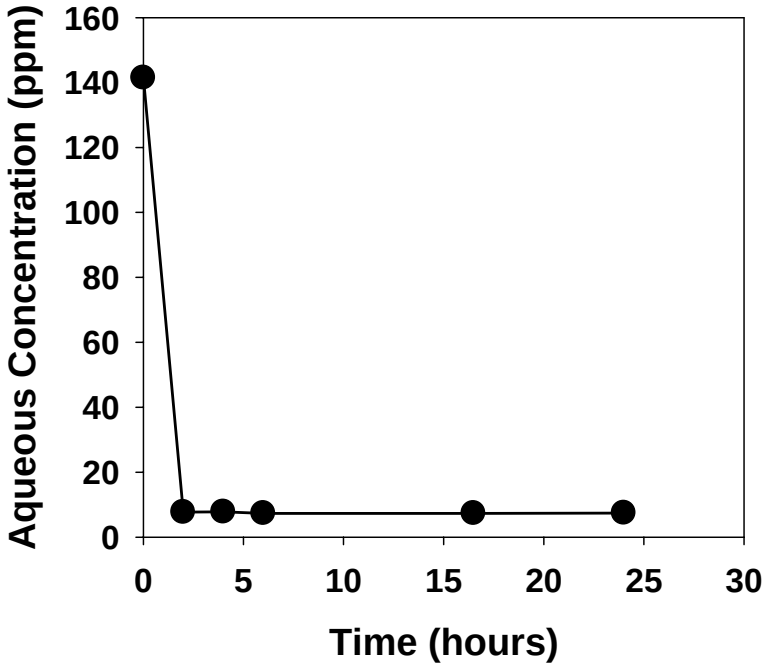

Figure E2. Equilibrium time for the adsorption of mellitic acid.